5-2012

The fabrication and integration of pillar array channels for chip based separations and analysis

Lisa Christine Taylor
ltaylo36@utk.edu

To the Graduate Council:

I am submitting herewith a dissertation written by Lisa Christine Taylor entitled "The fabrication and integration of pillar array channels for chip based separations and analysis." I have examined the final electronic copy of this dissertation for form and content and recommend that it be accepted in partial fulfillment of the requirements for the degree of Doctor of Philosophy, with a major in Chemistry.

Michael Sepaniak, Major Professor

We have read this dissertation and recommend its acceptance:

Georges Guiochon, Mark Dadmun, Jayne Wu

Accepted for the Council:
Dixie L. Thompson

Vice Provost and Dean of the Graduate School

(Original signatures are on file with official student records.)

The fabrication and integration of pillar array channels for chip based separations and analysis

A Dissertation
Presented for the
Doctor of Philosophy Degree
The University of Tennessee, Knoxville

Lisa C. Taylor
May 2012

Dedication

To my husband

for your encouragement, patience,

support, and love.

Acknowledgements

First and foremost I would like to thank God, who has guided me toward so many opportunities and blessed my wonderful life with a loving and supportive family. I would like to express my sincerest gratitude to my research advisor, Dr. Michael Sepaniak, for his continuous support. His guidance and direction provided me with the tools necessary to complete my work with skill, confidence, and enthusiasm. It has been an honor to be part of your research group. Thank you to my committee members: Dr. Guiochon, Dr. Dadmun, and Dr Wu for your willingness to take the time to serve on my committee. To the members of the Sepaniak group, past and present, I would like to thank you for assisting in the laboratory and for being a sounding board for advice about work and life.

I would also like to acknowledge the Center for Nanophase Materials Chemistry, Oak Ridge National Laboratory, as this research would not have been possible without these facilities and their staff. Specifically, I would like to recognize my collaborator, Dr. Nickolay Lavrik, for sharing his insights and expertise in the laboratory and being willing to share in this research.

I owe my deepest gratitude to my family who has encouraged me throughout my studies. I would like to thank my parents, Brian and Frances Arden, for providing me with a foundation sustained by love and a hard work ethic. Last but not least, I especially recognize my wonderful husband and best friend Adrian, and two beautiful children Anthony and Chaye. You are my heart, and your presence in my life brings me strength and happiness.

Abstract

The fundamental motivations for scaling existing technological platforms down to lab on chip dimensions are applicable in nearly all scientific disciplines. These motivations include decreasing waste, improving throughput, and decreasing time consumption. Analytical tools, such as chromatographic separation devices, can additionally benefit from system miniaturization by utilizing wafer-level fabrication technology, allowing for the rational design and precise control of variables which ultimately affect separation performance. With the use of microfabrication techniques, we have developed an original processing sequence for the fabrication of silicon oxide enclosed pillar arrays integrated within a fluidic channel. These pillar arrays create a highly uniform submicron scale architecture of solid supports for subsequent stationary phase – mobile phase interactions, while demonstrating substantial improvements in separation efficiency and permeability over traditional packed bed and monolithic columns. The general performance of these microfluidic devices is studied by optimizing the chip architecture and instrumental design to improve the stability of the pillar arrays, improve the sample injection, enhance the pillar surface characteristics, and improve the separation performance. We additionally explore simple and straightforward stationary phase modification techniques for partition based chromatography. Finally, we address the detection challenges of our design by creating the first fully integrated microfluidic chip based platform to combine separation capabilities with real time surface enhanced Raman detection.

TABLE OF CONTENTS

List of Tables

List of Figures

Nomenclature

λ	exposure wavelength
ϕ	flow resistance
η	viscosity
σ^2	band variance
A	eddie diffusion
AgNP	silver nanoparticles
B	longitudinal diffusion
BT	benzenethiol
C	resistance to mass transfer
CAD	computer aided design
CFD	computational fluid dynamics
C_m	resistance to mass transfer in the mobile phase
cm^{-1}	wavenumbers
COMOSS	collocated monolith support structures
C_s	resistance to mass transfer in the stationary phase
DART	direct analysis real time
d_{dom}	domain size
D_m	diffusion coefficient of the mobile phase
d_p	particle diameter
D_s	diffusion coefficient of the stationary phase
EK	electrokinetic
ESI	electrospray ionization

EUV	extreme ultraviolent
DRIE	deep reactive ion etching
h	reduced plate height
H	plate height
H_c	column plate height
H_{ec}	extra column plate height
HILIC	hydrophilic interaction liquid chromatography
H_{min}	minimum plate height
HPLC	high performance liquid chromatography
H_T	total plate height
k	retention factor
k'	partition coefficient
k_1	lithographic scaling parameter
K_v	column permeability
L	channel length
LC	liquid chromatography
LIF	laser induced fluorescence
LPCVD	low pressure chemical vapor deposition
MP	mobile phase
MS	mass spectrometry
N	plate number
NA	numerical aperture
PD	pressure driven

PDMS	poly(dimethylsiloxane)
PEB	post exposure bake
PECVD	plasma enhanced chemical vapor deposition
PEG	polyethylene glycol
PEG-MEM	poly ethylene glycol methyl ether methacrylate
PEO	polyethylene oxide
PPO	polypropylene oxide
R6G	rhodamine 6G
Res	chromatographic resolution
RIE	reactive ion etching
RPC	reverse phase chromatography
RSD	relative standard deviations
SEM	scanning electron microscopy
SERS	surface enhanced Raman spectroscopy
SNR	signal to noise ratio
u	linear velocity
u_{opt}	optimum velocity
UPLC	Ultra Performance Liquid Chromatography
W	lithographic resolution

Chapter 1

Introduction

Portions of Chapter 1 are an adaptation of a review article *Analytica Chimica Acta* 2011, 694, pg 6–20. The review discusses developments toward the miniaturization of pressure driven separation platforms, highlighting enabling technologies for microfluidics as well as obstacles to device integration.

1.1 Dissertation overview

This dissertation focuses on the miniaturization of separation techniques for application in pressure driven liquid chromatography, with specific concentration on the use of fabrication technology to create pillar array microfluidic devices. The structure of this dissertation is set to provide a general overview of the main historical trends toward system miniaturization and focuses on more recently developed technological approaches for on-chip integration of liquid chromatography columns (chapter1). This is followed by a discussion about various microfabrication techniques currently used in the fabrication of the pillar array separation chips (chapter 2). As the focus of work discussed in chapters 3 and 4, we first aimed to fabricate pillar arrayed channels with submicron features uncharacteristic of devices previously developed. Recognizing the fragility of such features we developed a unique processing sequence for the creation of robust and reusable fluidic chips. Then, we analyzed the chromatographic behavior of our sealed devices in terms of efficiency, permeability, and separation performance. Finally, we introduced the first fully integrated microfluidic chip to combine real time surface enhanced Raman detection with the capability of performing chemical separations (chapter 5).

1.2 Authorship

Parts of this dissertation have multiple authors, and as such those contributors are identified within this section. Much of the work was conducted in collaboration with Nickolay Lavrik at the Center for Nanophase Materials Sciences, who contributed significant portions of chapter 1 and portions of chapter 3 as well as collected data pertaining to some of the figures. Otherwise, Lisa Taylor collected nearly all of the data reported in this dissertation, and authored all sections not previously attributed to contributor above.

1.3 Nanotechnology and chip level systems for pressure driven liquid chromatography and emerging analytical separation techniques

1.3.1 Abstract

Pressure driven Liquid Chromatography (LC) is a powerful and versatile separation technique particularly suitable for differentiating species present in extremely small quantities. This chapter briefly reviews main historical trends and focuses on more recently developed technological approaches in miniaturization and on-chip integration of LC columns. We emphasizes enabling technologies as well as main technological challenges specific to pressure driven separations and highlight emerging concepts that could ultimately overcome fundamental limitations of conventional LC columns.

1.3.2 Historical trends

Over the past several decades, advances in liquid-phase chromatographic separation methods have been a major factor revolutionizing analysis of chemical and biochemical samples. The key trends in this area included miniaturization of separation columns, refinement of porous separation media and development of several hyphenated techniques, in particular by applying mass spectrometry (MS) directly to the eluent of a miniature LC column. [1] Another important trend in liquid phase analytical separations is related to techniques based on electrokinetic (EK) phenomena and establishing them as a practically viable approach in the separation, detection and species identification of many biologically active species with many applications including in genomics, proteomics[2] and drug discovery.[3] Since its first implementation by the Harrison[4] and Ramsey[5] groups, the idea of an analytical chip based on EK separation has evolved into an extremely prolific field of academic research. [6-10] On the other hand, efforts directed on the transfer of pressure driven (PD) separations from conventional liquid chromatography (LC) column formats to a chip based platform have been pursued by a small number of research groups. This can largely be explained by vastly different technical challenges involved in successful implementation of EK versus PD microfluidic chips. It is worth noting that these distinct technical challenges of EK and PD chips tend to be underemphasized in general discussions of on-chip separations. Recent breakthroughs in the area of on-chip PD LC have thus far prompted us to limit the scope of our research to PD systems. For details on microfluidic separation systems that utilize EK phenomena we, therefore, refer readers to the excellent recent reviews available on this topic.[1, 6-8, 10, 11]

The ability to analyze progressively smaller samples is among the key requirements of any analytical technique. Accordingly, analytical LC columns have followed a trend

toward miniaturization in contrast to the scaling up trend in preparative LC.[12] Since the wide acceptance of packed columns in the 70s,[13, 14] advances in analytical high performance LC (HPLC) columns have been very substantial but incremental in nature. [15-17] Figure 1.1 illustrates some historical trends and milestones in development of HPLC and on-chip LC devices. Apart from the gradual miniaturization of separation columns, advances in HPLC have relied on technological refinements of porous packing materials, in particular chemically modified monodisperse silica gel particles with well controlled sizes, surface properties and nanoscale porosity.[15-17] Early work on synthesis[13] and chemical modification[18] of porous silica particles is an excellent example of *nanotechnology* that was developed long before this term received wide acceptance. The use of packed silica capillaries with diameters down to several tens of micrometers pioneered by Tsuda and Novotny in 1978[19, 20] have subsequently led to straightforward scaling of HPLC columns down to microliter and nanoliter volumes. Soon terms, such as "nano-column" and "nano-HPLC" were coined to emphasize nanoliter volumes of capillary LC columns. Introduction of polymer rod monoliths by Svec in the early 90s[21] followed by the development of various polymeric[22] and silica[23-25] monoliths also contributed to these trends in HPLC columns. Another notable milestone was marked by the pioneering work of Regnier[26-28] whose group demonstrated for the first time on-chip chromatographic separation using collocated monolith support structures (COMOSS) created by photolithographic patterning and anisotropic dry etching on SiO_2 substrates (Figure 1.2). Although at the time COMOSS chips were evaluated exclusively with electroosmotically driven flows, they had a clear impact on the subsequent development[29, 30] of on-chip ordered stationary phases for PD LC.

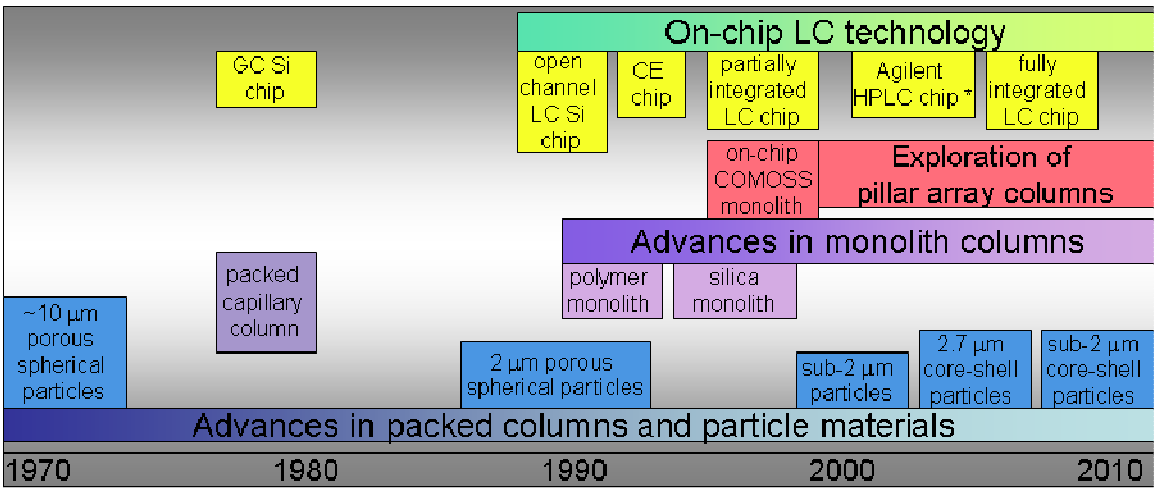

Figure 1.1 Historical trends and milestones in development of HPLC and on-chip HPLC

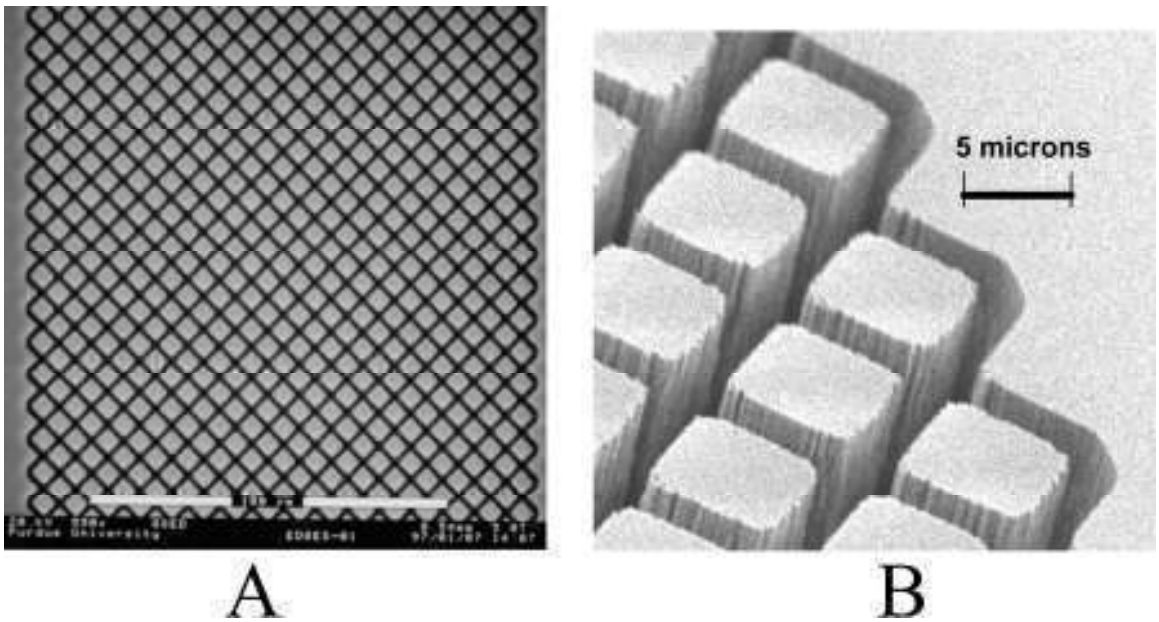

Figure 1.2 SEM images of mirofabricated COMOSS column: (A) top view of a section of the COMOSS column and (B) "bird eye" view of a fragment of the column at the column–wall interface. Reprinted with permission from reference[28]

Not only progressively smaller samples could be analyzed by capillary HPLC and HPLC-MS systems,[25, 31] but also smaller columns compared very favorably with their larger predecessors in separation performance. Transition to smaller particles (reflected in Figure 1.1) made it possible to shorten LC columns while keeping the plate count nearly the same.[16, 32] The term Ultra Performance Liquid Chromatography (UPLC^{TM}) was introduced to reflect significantly faster chromatographic analysis using shorter (30 to 80 mm) columns packed with sub 2 μm particles. [16, 17] Most, remarkably, such miniaturized columns remained basically compatible with conventional LC instrumentation that had undergone only subtle changes in their design over last few decades.

Although the sizes of the smallest LC columns that utilize packed silica capillaries are comparable to those of typical microfabricated chips, many technical challenges needed to be addressed before an LC system could be integrated on a microfluidic platform. As will discussed in the subsequent sections of this chapter, these challenges are related to the following technical aspects of a fully integrated PD LC system: (i) on-chip integration of the porous stationary phase, (ii) ultra-low volume sample injection, (iii) adequate chip sealing, (iv) on-chip pumping, and (v) on-chip detection. It is also worth noting that conventional fused silica LC columns packed with porous silica particles take advantage of technologies that have been continuously refined over the last four decades[16, 33] and, therefore, created a formidable competition for emerging technological alternatives. Nonetheless, continued advances in microfabrication and nanotechnology, as well as proliferation of wafer level processing well beyond the microelectronics industry, created an extremely fertile ground for exploration of such alternatives with high probability of upcoming breakthroughs.

1.3.3 Separation fundamentals, scaling trends and theoretical studies

One of the main performance measures of a chromatographic separation system is described by the theoretical plate theory, which defines the number of theoretical plates, *N,* that can be accommodated by the column of a certain length, *L,* and resolved by an appropriate detection scheme. The number of theoretical plates is commonly determined as a ratio of *L*/*H,* where *H* is the column plate height. Therefore, scaling down the column length results in the decreased plate number and thus adversely affects column efficiency. Therefore, column miniaturization inevitably imposes the requirement of smaller plate heights. The plate height, as introduced in the plate theory,[34] predicts a Gaussian peak profile for a sample eluted from the column. Assuming a Gaussian peak profile characterized by standard deviation, σ, the plate height is given by:

$$H = \frac{\sigma^2}{L} \tag{1}$$

Taking into account equation 1, the number of plate heights can be expressed as

$$N = \frac{L^2}{\sigma^2} \tag{2}$$

As can be seen from equation 2, the task of minimizing the band variance, σ^2 , becomes progressively more critical as the length of the column decreases.

From the standpoint of the physical processes occurring in the column, the plate height is governed by the non-equilibrium experienced by the solutes distribution between mobile and stationary phases. Analysis of the column performance and its optimization involves evaluation of both theoretical and experimental factors that cause broadening of the sample band, *i.e.* an increase in band variances, σ^2. In most cases, it is reasonable to assume

that various contributions to band variances are additive[35] and that a total plate height, H_T, can be expressed as

$$H_T = H_c + H_{ec} \tag{3}$$

where H_c and H_{ec} are, respectively, the column and extra-column plate heights. The two most significant contributions to extra-column variances arise from sample injection and detection of the eluent peak. It is important to note that, while improved performance of more advanced LC columns with smaller H_c enable column miniaturization, extra-column variances may become a larger contributing factor to the total plate height.

The on column variances are commonly analyzed using empirical correlations, reflected in the commonly used Giddings, Van Deemter and Knox equations. Each of these equations has its area of applicability and we refer readers to the available literature for in-depth discussions on this subject.[34-40] While detailed analysis of the models involved in analysis of PD LC performance is beyond the scope of this review, we would like to point out that the Van Deemter equation is considered to be most appropriate for the accurate prediction of dispersion in chromatographic systems while the Knox equation involving reduces parameters is particularly useful in evaluating the quality of a packed column. A frequently used simplified form of the Van Deemter equation is

$$H_C = A + \frac{B}{u} + Cu \tag{4}$$

where A, B, and C are variables related to various characteristics of the column and u is the mobile phase linear velocity in the column. In case of conventional packed columns the A term is influenced by packing quality, the B term is a function of a longitudinal diffusion in the column and the C term takes into account the resistance to mass transfer in both the

stationary and mobile phases. A very important finding about limitations of conventional packed and monolith LC columns was made by Knox[39] nearly a decade ago when he re-evaluated data for a number of HPLC systems using the Van Deemter equation and showed that a dominant part of band dispersion is attributable to processes in the mobile phase rather than in the static zone (stationary phase). This, in turn, led Knox to the conclusion about possible substantial improvements in separation performance as a result of more ideal pore geometries in future LC columns, in particular, by using ordered on-chip structures. [39]

Analysis of the Knox equation for a large number of various packed columns indicated that that smallest plate height is approximately two times the particle diameter, d_p, for the best packed columns.[39] Furthermore, irregularities of pores formed between spherical particles combined with large stagnant spaces in packed columns contribute substantially to band dispersion and, therefore, impose a fundamental limit as to how small a plate height can be relative to the particle diameter. It is reasonable to conclude that recently demonstrated separation efficiencies of columns packed with sub 3 μm[41, 42] and, especially, sub 2 μm superficially porous core-shell silica particles[42-44] are very close to the fundamentally limited performance and that further significant improvements in separation efficiency of packed LC columns are unlikely. These conclusions sparked strong interest in identifying alternatives to packed columns, such as monoliths and on-chip patterned 2D networks of channels[27] and lead to extensive theoretical evaluations of idealized porous media and ordered structures for PD LC.[45-51] A pioneering theoretical study in this direction reported by Gzil and coworkers[45] provided convincing evidence that perfectly ordered chromatographic beds can indeed surmount certain limitations of packed columns. Using computational fluid dynamics (CFD) modeling, this study evaluated full

convection-diffusion material balances in a rectangular channel filled with a periodic array of porous cylinders (pillars). Main variable input parameters of these simulations included pillar diameters (in the range of 1 to 3 μm), internal and external porosity, flow velocity and solute diffusivity. The band dispersion obtained as a result of these simulations was compared to those observed in the case of columns packed with spherical particles, and a significance difference in favor of perfectly ordered pillar arrays was shown. The main conclusion of this study is that columns based on perfectly ordered pillar arrays may provide a factor of ~2.5 reduction in the plate height compared to the best packed HPLC columns while also decreasing flow resistance.[45] A series of subsequent CFD studies provided more extensive analysis of various aspects of LC columns based on ordered 2-D and 3-D arrays of various geometries[46-48] and indicated their remarkable separation efficiency as well as lower separation impedances.

It should be noted that the compatibility of these CFD modeling methods for packed beds versus pillar array planar systems may not have been rigorously proven. Another approach to modeling the chromatographic behavior of pillar array systems imposed more stringent boundary conditions at the top, bottom, and side walls of the channels, and discussed the effect of macroscopic confinement on efficiency[52]. Their studies suggest that diffusion and mass transfer in uniform pillar arrays is insufficiently described solely by the Giddings and Knox equations. While both theoretical approaches recognize the advantage of uniform microstructures for chromatographic purposes, the more recent study argues that the pseudo-diffusive behavior in uniform pillar structures which replaces the eddy diffusion in packed beds can hinder separation performance.

While improvements in separation performance of porous media with smaller domain sizes are anticipated, operation of LC columns with progressively smaller pores may ultimately involve certain limitations due to the strong dependence of back pressure on pore width. Described by Darcy's law and modified for microscopic flow through a porous bed, this dependency can be written as:[38]

$$\Delta P = \frac{u_o \eta L \phi}{dp^2} \tag{7}$$

where η is viscosity and ϕ is the flow resistance parameter. Despite such an unfavorable scaling trend for the backpressure, several CFD studies clearly indicate that ordered separation beds possess lower separation impedances compared to their disordered analogs. It is worthy to note, however, that comprehensive evaluation of LC columns based on arbitrary pore geometry and packing morphology involves a complex parameter space making it challenging to perform rigorous comparative analysis of various columns and identify optimal designs. A very careful choice of reduced (dimensionless) parameters is required in order to compare columns based on different technological platforms and obtain meaningful scaling trends in case of different packing morphologies. In order to understand how separation performance is affected by various parameters beyond a simple geometrical scaling, it is convenient to use the dimensionless plate height originally introduced by Giddings.[53] This approach relies on a certain characteristic dimension, $\boldsymbol{d_{ref}}$, as a basis for parameter reduction.[39] It appears, however, that a proper selection of the characteristic dimension for columns other than a packed bed of spheres is not trivial.[47] In case of monolith columns, a skeleton size, $\boldsymbol{d_s}$, domain size $\boldsymbol{d_d}$, and pore size, $\boldsymbol{d_p}$, are possible logical choices for the characteristic dimension. According to the study by Gzil *et al.,*[47] although

the domain size is most adequate as a reduced parameter, it still does not yield an ideal overlap between the van Deemter curves for columns of different porosity in the *C* term dominated velocity range. Proper selection, justification and interpretation of reduced parameters becomes even more complicated in the case of lithographically patterned on-chip LC columns in which pore sizes, shapes and degree of porosity can be changed independently and in a wide range. Nonetheless, reduced plate heights, $\boldsymbol{h_d}$ based on domain size was shown to be very useful[48] in estimating ultimate separation performance of ordered networks of on-chip fluidic channels while taking into account high accuracy of photolithographic patterning and its ability to create ordered arrays with submicron features.[29, 54] Computational studies indicated that perfectly ordered structures can yield theoretical plate heights somewhat smaller than the domain size while theoretical plate heights 50% larger than the domain size are typical for disordered structures.[48] Furthermore, an increase in the external porosity above the values achievable in beds of packed spheres was shown to affect separation performance favorably. Assuming that solid features, $\boldsymbol{d_s}$, as small as 1 μm can be lithographically patterned, an approximately 30-fold increase in the plate number, $\boldsymbol{N}$, was predicted due to an increase of external porosity from 0.4 to 0.9.[48]

CFD studies were also carried out to assess the effect of the pillar shape in perfectly ordered chromatographic beds with lithographically patterned channels.[46, 50] It was found that chromatographic performance is improved when pillar shapes are elongated in the direction of the mobile phase flow and that diamond-shaped pillars are preferred over ellipsoids.[46] These trends can be largely explained by modeling flow velocities in channels of different geometries (Figure 1.3). Not unexpectedly, best separation performance was

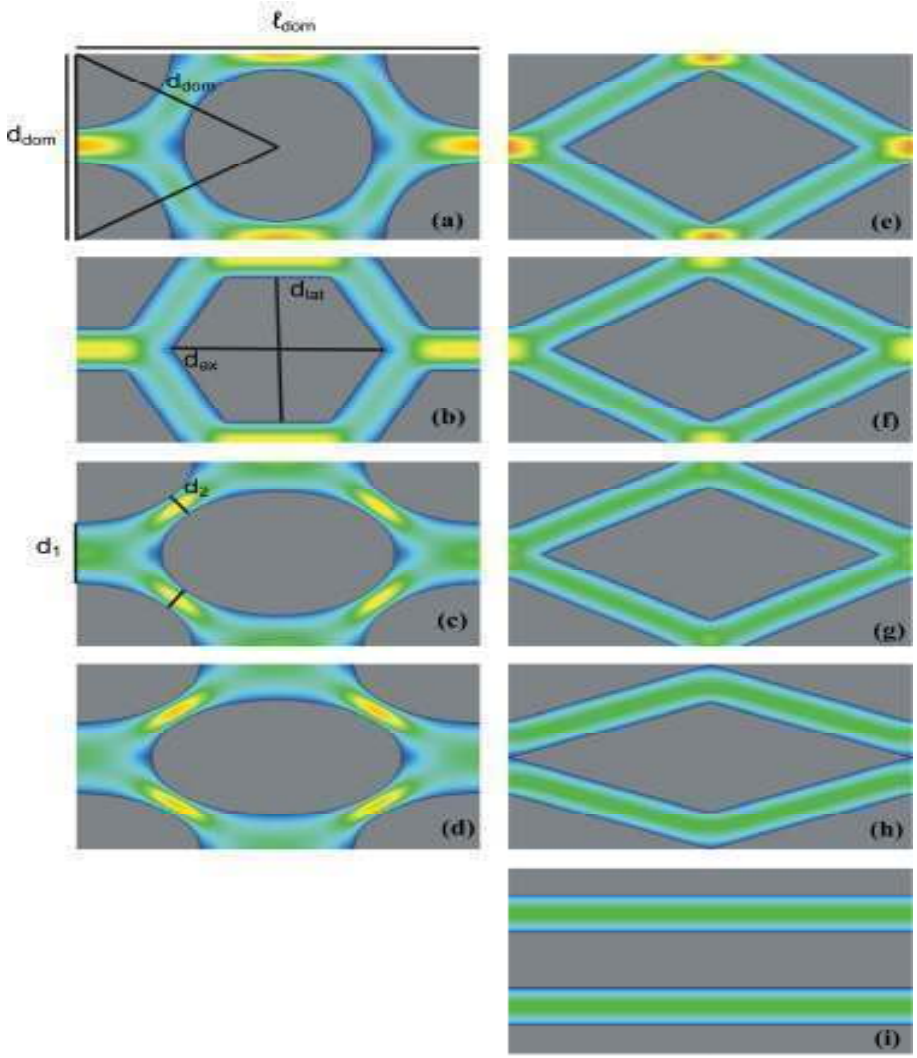

Figure 1.3 Distribution of flow velocities in an ordered 2-D network of channels formed by (a) cylinders, (b) hexagons, (c) ellipsoids with $\alpha = 0.50$, (d) ellipsoids with $\alpha = 0.73$, (e) diamonds with $\alpha = 0.50$, (f) diamonds with $\alpha = 0.73$, (g) diamonds with $\alpha = 1.0$, (h) touching diamonds with $\alpha = 1.89$, and (i) parallel plates. Desmet *et al.* [46] showed that chromatographic performance is improved when pillar shapes are elongated in the direction of the mobile phase flow, i.e. when velocity magnitude fields are more uniform. Reprinted with permission from reference[46]

found to correlate with the most uniform flow velocity.[46, 50] It was reported that perfectly ordered 2-D arrays of porous pillars with optimized geometry exhibit 5 times smaller plate heights compared to typical silica monoliths with the same domain size.[46] It was also concluded that optimized 2-D arrays of porous pillars are characterized by separation impedances that are 10 times lower in comparison to the best packed HPLC columns with similar separation performance. In a more recent CFD study, ordered 2-D networks of channels with retentive nonporous walls formed by pillars with novel shapes were evaluated.[50] It was concluded that careful refinement of pillar geometries results in additional moderate performance improvements.

In yet another CFD study by Schure and coworkers,[49] flow velocity profiles in perfectly ordered and randomly packed beds of spherical particles were investigated and separation efficiencies of such beds were compared. It was found that the velocity probability densities in the low velocity region are inversely related to the separation efficiencies. Those findings, in turn, suggested that a face centered cubic arrangement of spherical particles can provide a significantly lower plate height in comparison to both random and other possible types of ordered assemblies. However, an important practical question remains as to whether packing of spherical particles other than random[55] can be implemented in LC columns.

1.3.4 Technological approaches: Brief overview of on- and off-chip technological strategies

Implementation of on-chip microfludic devices for analytical separations has been a subject of extensive research and development efforts since the mid 90s. This trend can be explained as a logical progression of previous advances in the broader area of microfluidics. Microfluidic technology, in turn, has relied on adaptation of wafer level processes developed previously in electronics industry. Recent advances and breakthroughs in microfluidic devices, such as on-chip integration of a complete HPLC system,[56] stem from the wider availability of such processes to the research community and also from development of new techniques particularly suitable for cost efficient processing of glass, ceramic and polymeric substrates and fabrication of mechanically robust microfluidic components, such as channels, valves and ports. Comprehensive discussions of conventional wafer level technologies[57, 58] and microfabrication techniques with focus on applications in microfluidics can be found in literature.[59] Below we only briefly outline the main type of materials and technological processes most extensively used in microfluidic chip fabrication.

Single crystal Si wafers were historically among the first substrates used for on-chip separation devices[60-62] and still play a very important role in this technology, especially for proof of principle studies.[63-68] The unique role of Si is related to the fact that it is the most common material in electronic chip technology and a number of unique wafer level processes developed to process single crystal Si are not applicable to other substrates.[57] As applied to various microfluidic applications, important characteristics of Si include its chemical inertness and excellent thermal stability. Although electrical conductivity of Si makes it less suitable for separation devices that involve EK phenomena, it hardly represents a problem for PD LC chips. While single crystal Si wafers are widely used in laboratory research their brittleness and relatively high cost limits their use in practical microfluidic

devices, in which glass and polymeric laminates are more common. Glass is another important material in microfluidic technology that is widely used as a substrate as well as a chip cover. Advantages of glass include its low cost, chemical inertness, optical transparency, and wide availability in various sizes and chemical compositions, such as pyrex and fused silica that are used most extensively. Polymeric materials play an increasingly important role in microfluidic applications because of their low cost combined with excellent chemical inertness and superior mechanical qualities (absence of brittleness). A number of cost efficient scalable processing techniques, such as soft lithography,[69] have been developed to form microscale and nanoscale features in polymeric materials. Hot embossing and injection molding can be applied to various thermoplasts, such as polyolefines.[70-72] Thermosetting polymers, in particular polyimide, are used as a main material in laminated HPLC chips,[73] in which three polyimide layers are patterned using laser ablation and sandwiched to make a sealed assembly with embedded channels and valves. Elastomers, such as polydimethylsiloxanes (PDMS), are popular materials for prototyping various microfluidic chips since channels and other features can readily be replicated in PDMS by microscale and nanoscale molding.[74, 75] Elastomers have somewhat limited applicability in PD LC chips since they are prone to leaks at pressures above 100 psi. Nonetheless, thin layers of PDMS and photodefinable PDMS[76] are useful for soft bonding and sealing of PD LC chips operating at moderate pressures.[54] Other noteworthy materials useful as substrates for future PD LC chip include various ceramic materials[77] and titanium.[78, 79]

In order to create fluidic channels, porous structures and other components of an on-chip LC system, typical processing of the substrate materials involves either soft lithography[69] or conventional lithography,[57] *i.e.*. photolithography, e-beam lithography

or their combination. Soft lithography relies on a patterned master and creates morphologies complimentary to those present on the master in a single step, such as embossing and molding. By contrast, patterning of a substrate material by means of photolithography or e-beam lithography is a multi-step process that starts with defining a pattern in a thin layer of photoresist or e-beam resist that plays a role of a mask in the subsequent selective removal of the substrate material by dry or wet etching. With exception of photosensitive epoxy based polymer, such as SU-8, resist layers are removed from the final devices.

Various modifications of reactive ion etching (RIE) enable formation of channels and other structures on Si and SiO_2 substrates with excellent control of the sidewall profile and characteristic sizes ranging from tens of nanometers to the wafer scale.[57, 58] Deep RIE (DRIE) of Si based on the Bosch process is widely used in processing of LC chips to create high aspect ratio features, such as pillar arrays[27, 30, 54, 65, 80] and for through-chip port access.[54] Alternatively through-chip port holes can be formed using powder blasting[81] which is applicable to both Si and glass. Although RIE can be used to create channels and pillar arrays in glass and fused silica,[26-28, 82] wet chemical etching based on HF is often preferred for etching of glass and fused silica when vertical sidewalls are not required.[5, 83, 84] High aspect ratio structures promising for liquid phase separations can also be formed by using anisotropic KOH etch of Si substrates with appropriate crystallographic orientation.[85]

In addition to dry and wet etching processes, thin film deposition techniques play an important role in microfluidic chip fabrication. Plasma enhanced chemical vapor deposition (PECVD) tends to produce nonconformal coatings on high aspect ratio features, such as trenches and pillars, and can be used to seal channels and channel networks.[54, 67, 85, 86]

This approach is uniquely suitable to enclose and seal arrays of submicron diameter, high aspect ratio features that are too fragile to be sealed using conventional hard or soft bonding techniques. Figure 1.4 shows a cross-sectional scanning electron microscopy (SEM) image of an on-chip nanoporous monolith formed by coating a nanopillar array with a "roof" of PECVD silicon oxide.[86] In our own work, nonconformal PECVD of silicon oxide was used for chemical and geometrical modifications of high aspect ratio features etched in Si chips as shown in Figure 1.5[54, 67] Physical vapor deposition and sputtering of metals is used to create masking layers[54, 67] and electrodes.[73] Spincoating is the main technique for deposition of thin films of photoresists, e-beam resists, elastomers and sol-gel precursors.

A critical part of any microfluidic chip fabrication is a bonding technique that provides hermetic assembly and encapsulation of the chip components, such as the combination of a substrate with etched channels and a planar cover. Considerations for choosing the optimal bonding technique for practical applications include the method's tolerance of surface inhomogeneity and the systems' pressure tolerance at the bonding surface. Most microfluidic techniques can withstand operating pressures of up to 200 psi, with the most robust bonds withstanding pressures as high as a few thousand psi, comparable to typical HPLC systems. Soft bonding techniques rely on a polymeric adhesive layer between the surfaces. Examples of polymers used for soft bonding include PDMS,[54] soluble fluoropolymers[87] and thermoplastic polyimide[73] and cyclic polyolefins.[72, 88, 89] Hard bonding is accomplished through application of appropriate physical processes that result in a formation of a permanent bond between two smooth surfaces of inorganic materials. Important types of hard bonding used in microfluidic chip fabrication include anodic and fusion bonding.[58]

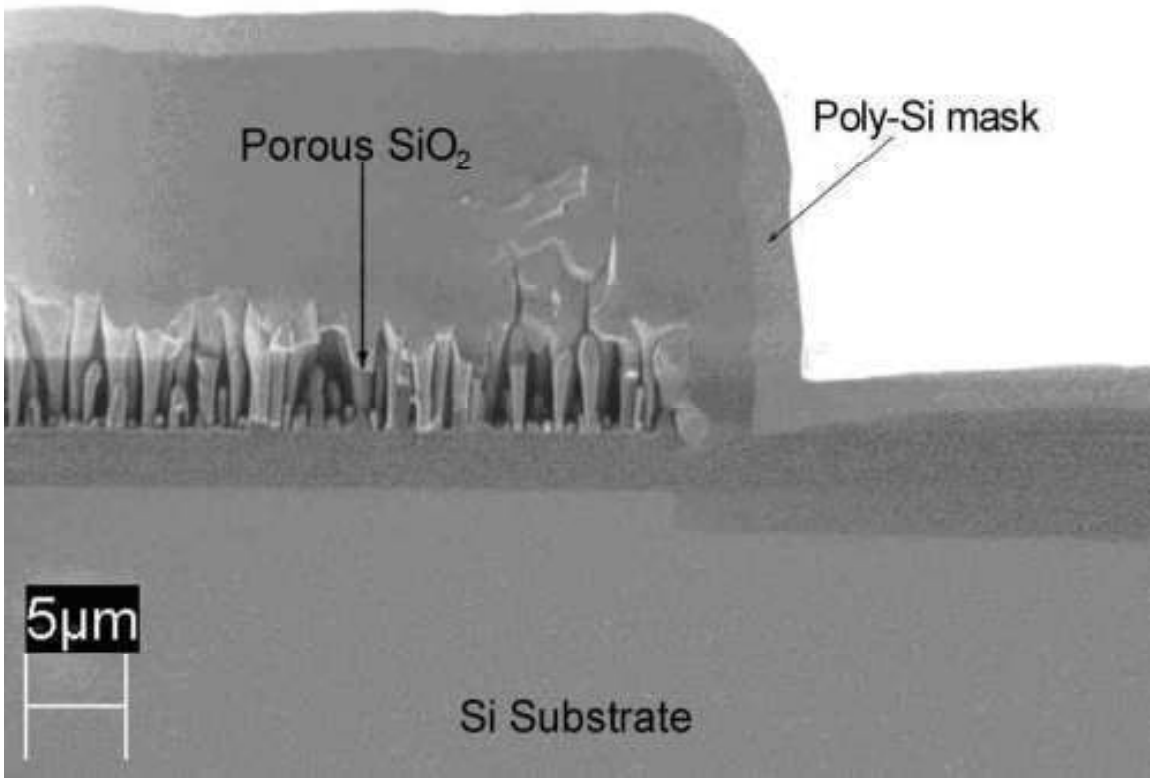

Figure 1.4 Cross-sectional scanning electron microscopy (SEM) image of an on-chip nanoporous monolith formed by coating a nanopillar array with a "roof" of PECVD silicon oxide. Reprinted with permission from reference [86].

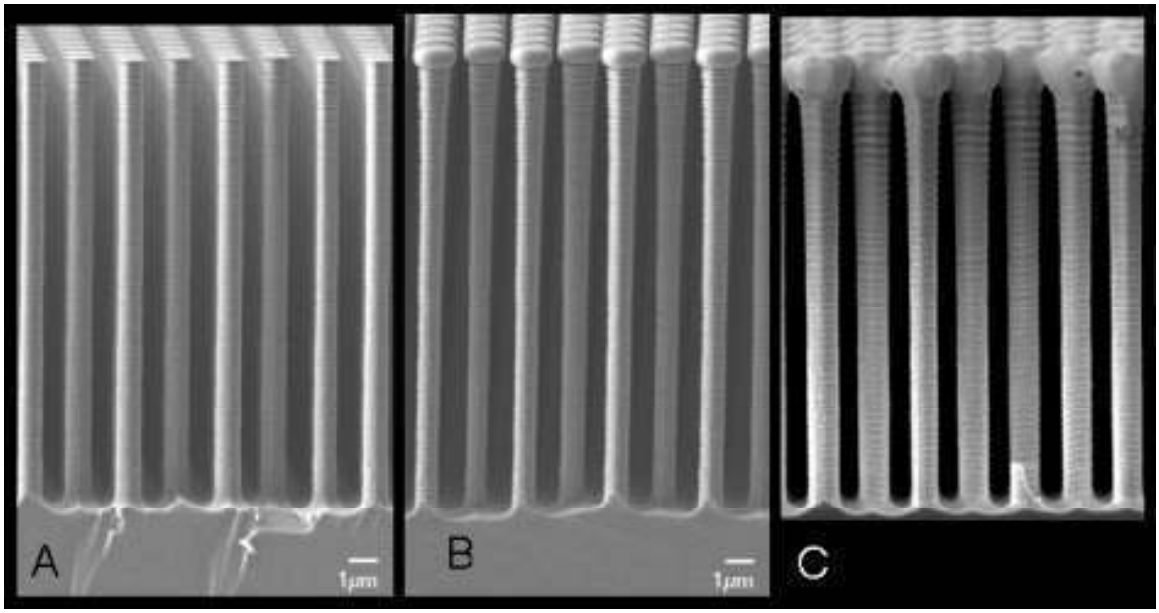

Figure 1.5 Cross-sectional SEM images illustrate geometrical modifications of high aspect ratio Si pillars with nonconformal PECVD layers of silicon oxide and formation of an enclosed 2-D network of pores with submicron widths. Cross-sectional SEM images Illustrating of different stages of capping of high aspect ratio silicon pillars with PECVD silicon oxide layer: (A) Si pillars before PECVD, (B) Si pillars partially capped with PECVD silicon oxide (C) completely sealed pillar array. Adapted from reference [54].

A unique part of a PD LC system not typically found in other types of microfluidic devices is a stationary phase support, i.e. a highly porous material that combines microscale (external) and nanoscale (internal) porosity. The two main types of stationary phase supports used in conventional HPLC columns are silica gel microspheres[33, 90, 91] and porous monoliths.[22, 24] Continued refinements of these types of materials have been a major factor in improving separation performance of HPLC columns over the last decade.[16, 92-94] Integration of a similar porous phase into a microfluidic system is one of the main challenges in successful development of on-chip HPLC devices. From the standpoint of this challenge, technologic strategies of on-chip LC separation systems can be broadly divided into the two categories: (i) adaptation of conventional monolith or packed stationary phase technologies to on-chip formats and (ii) utilization of a unique wafer level or chip level processing sequences. Examples of the former strategy include microfluidic channels packed with spherical silica particles[95, 96] and in-situ formed monoliths.[83, 97-100] Figure 1.6 shows an example of a polymeric monolith bed formed *in situ* in the chip channel and used for anion-exchange chromatography.[83] The most attractive feature of such hybrid designs is that they rely on previously developed and already well characterized stationary phases.

Furthermore, they offer greater flexibility in selecting polymeric, glass or ceramic substrate materials that are most practical as a structural platform for a high-pressure microfluidic system. A notable example of this approach that relies on a combination of several fairly mature technologies is the HPLC Chip[73] developed and commercialized by Agilent Technologies. The Agilent HPLC Chip is a miniature disposable device that integrates conventional HPLC packing material with microfluidic channels, valves, and an electrospray ionization (ESI) emitter on a disposable polyimide substrate. Standard

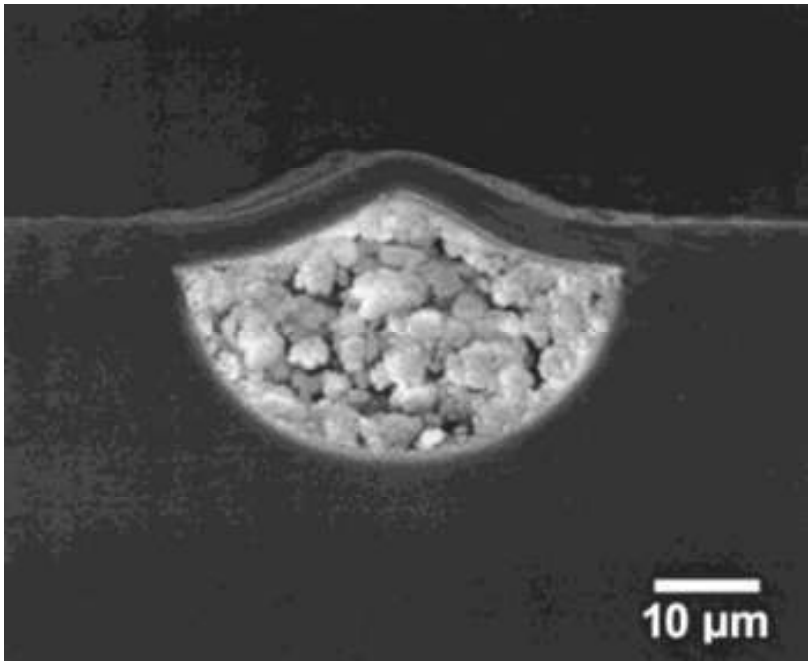

Figure 1.6 Cross-sectional SEM image of polymeric monolith bed formed *in situ* in the chip channel. The bed was used for anion-exchange chromatography. Reprinted with permission from reference [83].

commercially available versions of Agilent HPLC Chip are supplied packed with Zorbax™ silica gel phases. Alternatively, polymeric monolith phases were formed *in-situ* in channels of similar polyimide HPLC chips. [98, 99] Their performance was found to be comparable to that of the chips with packed stationary phases. The ability to form polymeric monoliths through a great variety of chemical routes in microscopically confined spaces is their distinct advantage for on–chip HPLC devices. A detailed review of monolith preparation techniques can be found in the recent literature. [101]

Despite a relatively straightforward path to practical HPLC chips based on particulate and monolith porous materials mentioned above, such separation devices would share the key fundamental limitations[39, 40] of conventional capillary and macroscopic LC columns. This points to the idea of exploring unique wafer level processes for entire device fabrication, including formation of a stationary phase support represented by an ordered network of microscale or nanoscale channels with well controlled shapes.[26, 30, 45, 51, 54, 65-67, 72, 80, 89, 102-108] "Top-down" technological strategies based on lithographic patterning and wafer level processing provide unsurpassed precision and flexibility in creating such 2-D networks of channels of any arbitrary geometry; however, "bottom up" technological strategies are necessary in order to impart nanoscale internal porosity to such a lithographically patterned stationary phase support. One such strategy utilizes electrochemical formation of porous Si.[106, 107] The porous Si shells were obtained by anodization of the solid Si pillars formed by DRIE. The available surface area increased at least two orders of magnitude when approximately 500 nm thick nanoporous Si shells were formed (Figure 1.7). Another very promising strategy that relies on formation of silica gel coating on the surface of Si pillars has been recently implemented by Detobel *et al.* [66] A

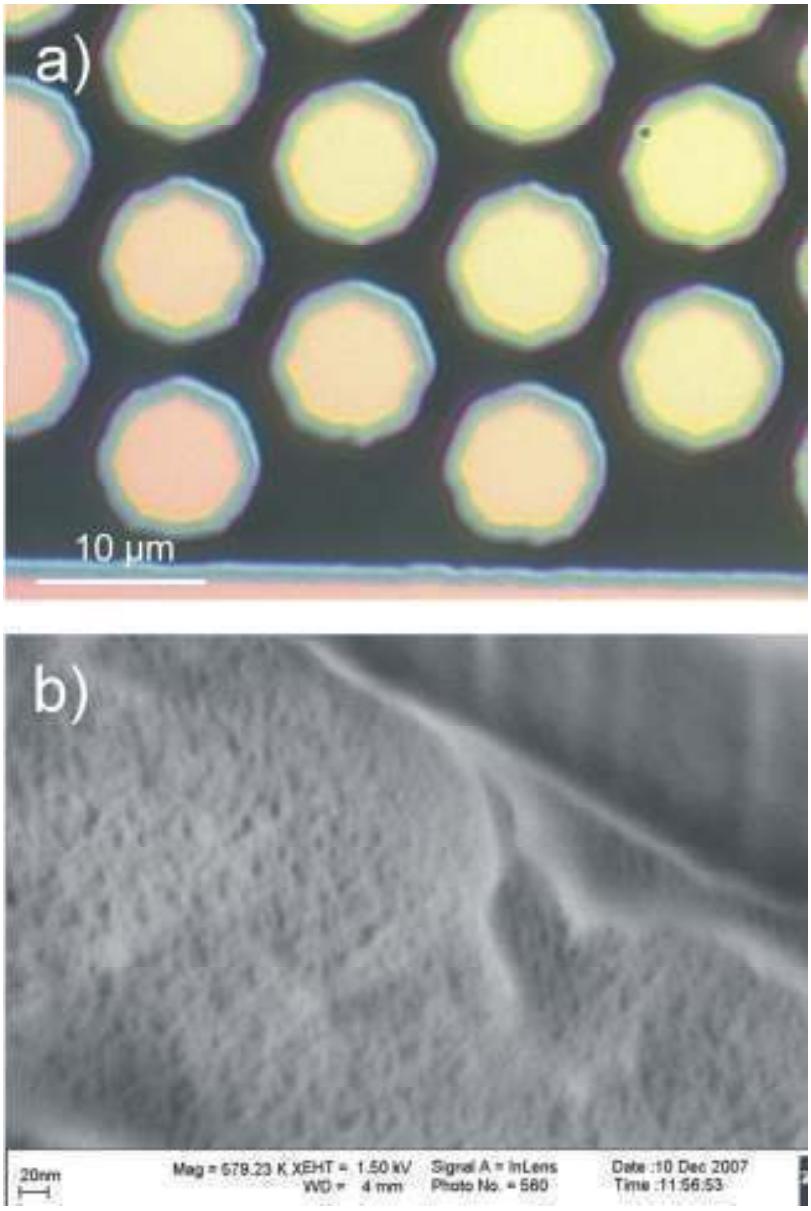

Figure 1.7 Schematic illustration of an ordered separation bed with an integrated sample injector formed by channels at the bottom of the chip. Reprinted with permission from reference [30]

0.5 μm thick porous shell of silica was thus created on the pillars that were 2.4 μm in diameter (Figure 1.8). The column was used for separations of coumarin dyes after hydrothermal treatment and chemical derivatization with octyldimethylchlorosilane.

It is worth noting that various bottom up technological approaches have been successfully used to create mesoporous pillared channels[86, 109, 110] promising for separation applications. Such nondeterministic bottom up techniques eliminate the need for high resolution lithographic patterning, enable rapid fabrication and are cost efficient. However, their applicability to highly ordered networks of channels are yet to be demonstrated.

1.3.5 On-chip integration: injection, detection and fluid control

Because of substantial technological challenges involved in development of fully integrated HPLC chips, the majority of the research and development efforts in this area have focused on hybrid LC systems that combine on-chip and off-chips components. It was not until 2006 when Lazar and co-workers reported on implementation and characterization of the first fully integrated on-chip HPLC system.[56] It is worth noting that integration of certain components of an HPLC system is expected to directly improve the analytical performance, while integration of others serves mostly to facilitate miniaturization, cost reduction, and scaled up fabrication. In particular, absence of frits and fittings between the injector and the column play a major role in improved performance of HPLC chips compared to analogous modular HPLC systems based on small diameter capillary columns.[96] Therefore, elimination of dead volumes in interconnects by integrating an appropriately designed injector with an on-chip column is the most critical step in reducing extra column variances.

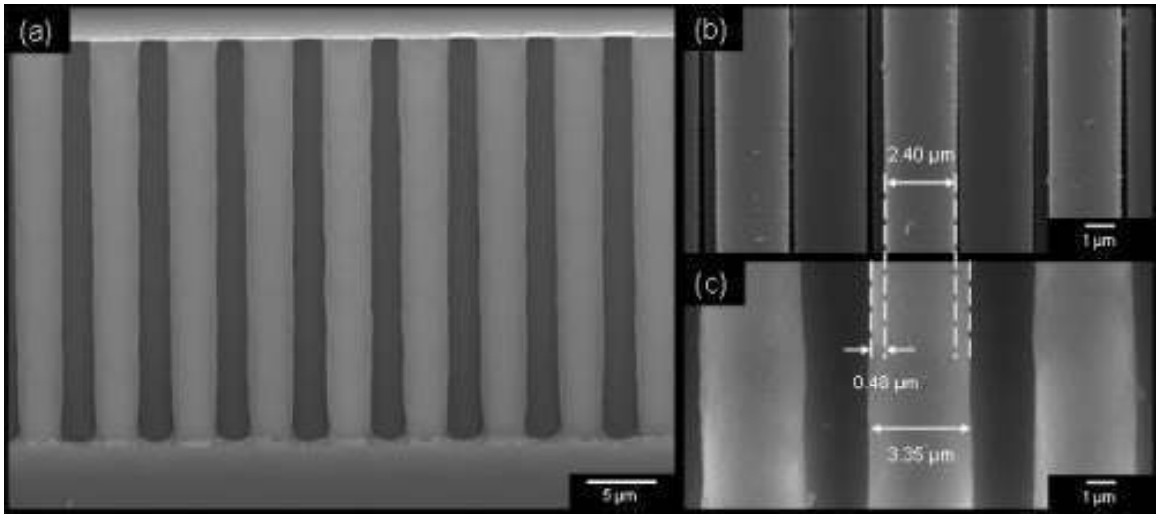

Figure 1.8 Fluorescence (left) and schematic (right) images of attoliter sample injection using a nanoscale T-injector. Different times after injection are shown: (a) 0, (b) 4, and (c) 6 s. Yellow lines indicate extended nanospace channels; green and light blue indicate sample solution and mobile phase, respectively. Reprinted with permission from reference [111]

The simplest type of on-chip injectors can be formed by a microfluidic "double-T" junction[97] or a cross-channel geometry[54, 72] at the column inlet. Such injectors do not require any on-chip valves and are able to generate sample plugs with volumes in the tens of nanoliters range upon alternating fluid pressures at the sample and mobile phase ports. The main drawbacks of such "valveless" injectors include the need for an external pressure controller for each microfluidic port and, more importantly, their tendency to exhibit sample dilution and leakage that can cause broadening and tailing of the sample plug before it enters the column. In order to minimize sample plug broadening, more sophisticated designs of on-chip valveless injectors were explored. For instance, excellent sample plug profiles were obtained by using sample injection channels formed at the bottom of the chip[30] and carefully controlling pressures at inlets and outlets of sample and mobile phase channels (Figure 1.9). More recently, Wang *et al*. have devised a "three-T" injector in order to eliminate problems with sample dilution and improve sample injection reproducibility.[112] A remarkably scaled down version of a T-injector (Figure 1.10) has been implemented by Kato *et* al. in order to enable injection of attoliter sample volumes into a nanochannel column with a femtoliter volume[111] and explore a new separation mode of charged solutes. To the best of our knowledge, however, no reliable operation of valveless injectors at pressures substantially above 100 psi has been reported. It can be concluded that that valveless injectors and injectors based on "virtual valves" [113] offer a reasonable trade-off between the performance and device complexity for PD LC systems operating at low-to-moderate pressures. In order to address the challenge of microfluidic flow control at pressures of several thousands psi, mobile polymer monoliths formed in microfluidic channels *in situ* were explored.[84, 114] In particular, Reichmuth *et al.*[84] implemented a chemically robust

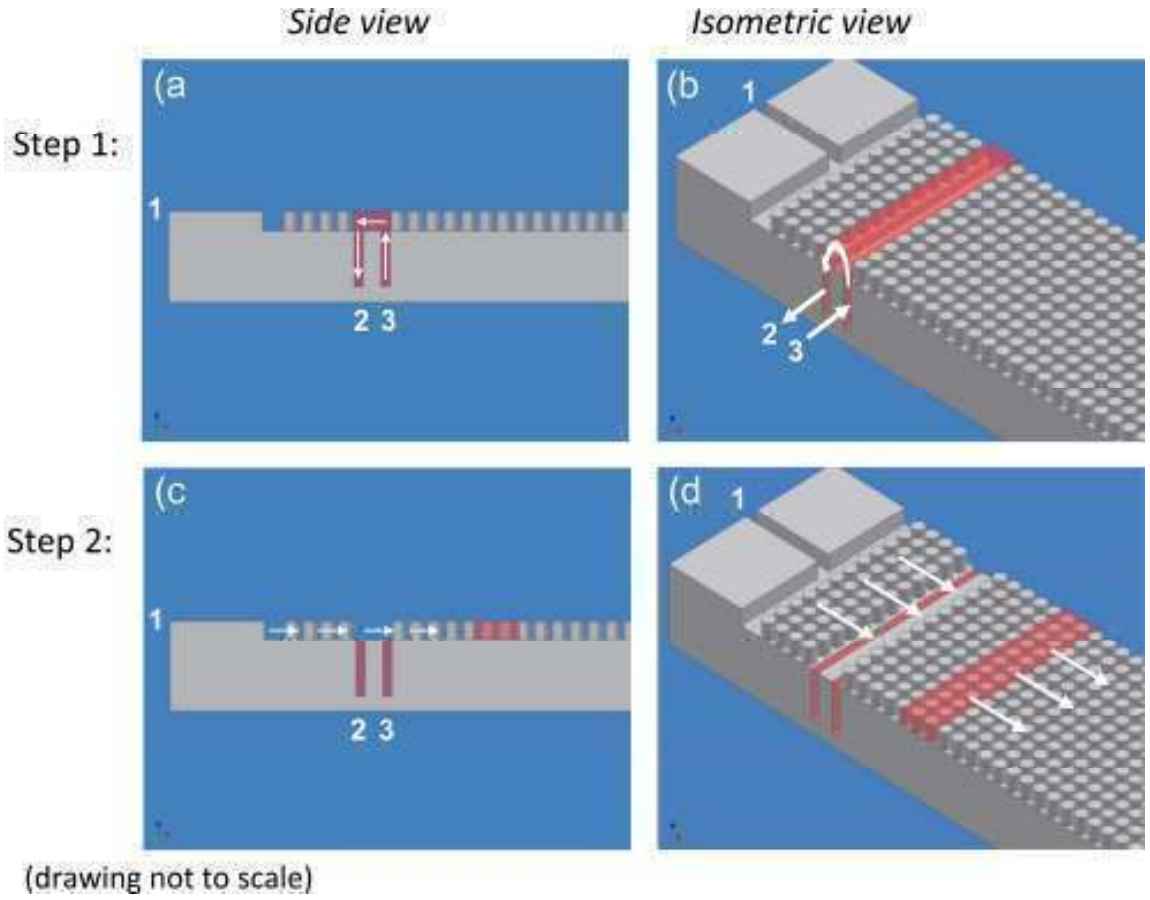

Figure 1.9 (a) Top view optical microscopy image of Si pillar array with a 1 μm thick porous Si shell layer on the side walls. The nonporous tops of the pillars served as a bonding surface for subsequent anodic bonding to a glass substrate. (b) Scanning electron microscopy image of the porous Si on the pillars. Reprinted with permission from reference [107]

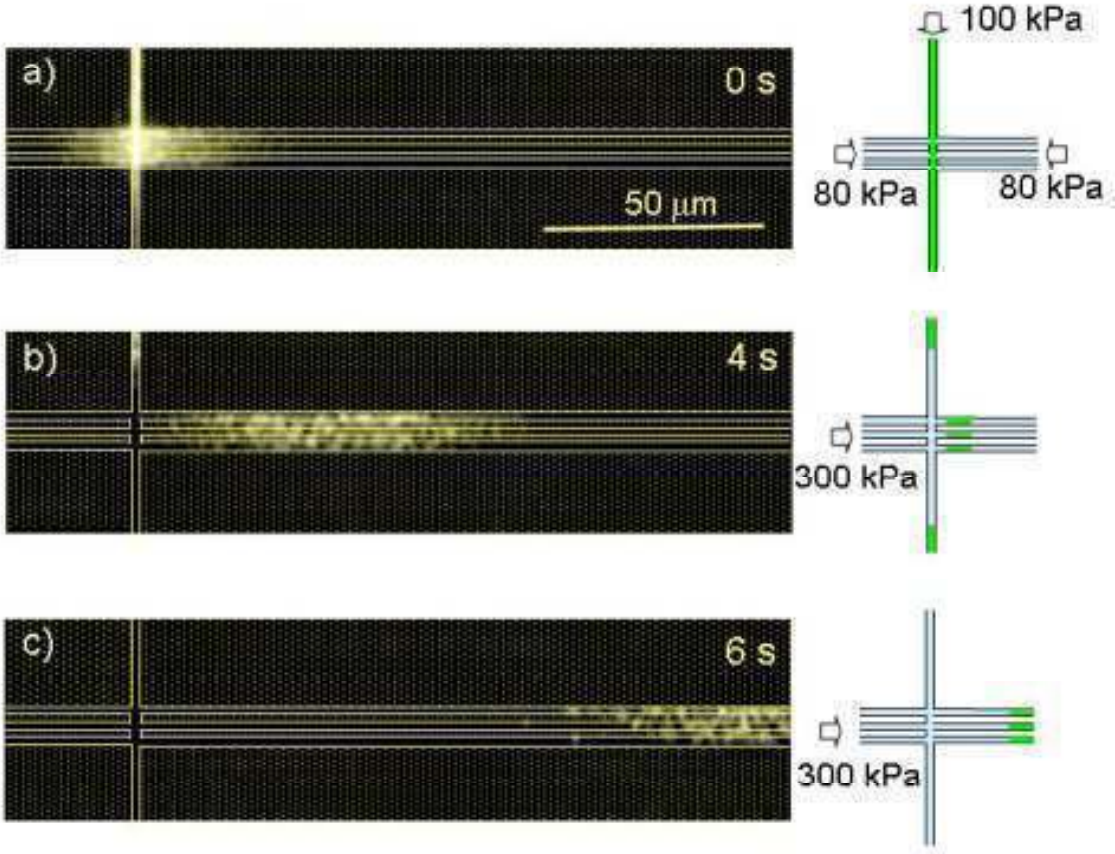

Figure 1.10 (a) Cross-sectional SEM image shows a porous-shell pillar array. Reprinted with permission from reference [66] The estimation of the porous-layer thickness was based on the difference in pillar diameter before (b) and after (c) silica-layer deposition.

high pressure on-chip injector by photopolymerizing fluorinated acrylates inside wet-etched silica microchips and demonstrated reproducible injections of volumes as small as 180 pL with less than 250 ms duration. Photo-actuated, [115] thermally actuated[116] and electrically addressable[117] valves incorporated into micro-fluidic manifolds are also promising concepts rely on *in-situ* polymerization and may ultimately be utilized in on-chip HPLC systems for sample injection.

Despite the potential of various types of in-situ polymerized microfluidic valves, more conventional technological approaches are preferable for practical devices. For instance, a very practical approach to on-chip injection of ultra small volumes at pressures in the range of up to several thousands psi consists in using a planar rotary valve integrated in a three-layer laminated polyimide chip[73, 96]. This design is used in the Agilent HPLC chip[73] and provides highly reliable and reproducible injections of volumes in the nanoliter range.

Another technologically challenging aspect of fully integrated HPLC chips is related to the need for a high pressure pump. Typical pump requirements for PD LC system include continuous fluid flow at a constant pressure in the range of hundreds to well above 1000 psi. Pumping flow rates in PD LC scale with the column cross-sectional area as dictated by optimal linear fluid velocities in the range of few mm/sec. This corresponds to typical flow rates well below 10 mL min^{-1} for conventional analytical HPLC columns while flow rates in capillary columns and on-chip PD LC systems rarely exceed a few μL/min and often just a few nL min^{-1}. In a conventional HPLC system the fluid flow is provided by a mechanical reciprocating pump with either solid pistons or flexible diaphragms. While such reciprocal pump designs can be scaled down and adapted to wafer level microfabrication,[118-120]

their applicability to on-chip PD LC chips has not been demonstrated yet. By contrast, various electroosmotic pumping systems[121-124] have been successfully demonstrated in conjunction with on chip separations.[56, 124-126] Planar architectures and absence of moving components parts are key advantages of electroosmotic[127] and similar continuous flow pumps[128] that facilitate their on-chip integration. A very promising design of an eletroosmotic pump particularly suitable for integrated PD LC systems was implemented by Lazar and coworkers.[56, 125] The pump had an open-channel configuration consisting of hundreds of parallel microchannels that were 1 to 6 μm deep, 4 to 50 mm long and occupied an overall area of a few square millimeters. While the pump operation was relied on electroosmotic pumping principles, it enabled fluid pressures of about 100 psi and stable flow rates in the low nL min^{-1} range in electrical field-free regions of the chip. The pump could be straightforwardly coupled with other microfluidic components on the same chip. For further details on various approaches to on-chip fluid pumping suitable for PD LC systems, we refer readers to several excellent reviews on this topic.[128-130]

The overall performance and extracolumn variances of an on-chip separation system critically depend on the availability of an appropriate sample detection technique. Upon column downscaling, the amount of the sample eluted from the column decreases dramatically. This translates into very challenging requirements with respect to the detector sensitivity and its spatial resolution. As a result, not all types of detectors used in conventional HPLC[131] are equally suitable for on-chip systems. Optical absorption detectors are common in conventional HPLC systems and were also used in to characterize separation efficiency of particle packed HPLC microchips.[96] However, they are become less suitable as the column volume decreases since their sensitivity scales with the optical

path available for sample detection. In order to compensate for the loss of sensitivity in the case of on-chip detection of sub nanoliter sample volumes, chip designs that utilize a multiple optical path[132] and an optical cavity[133] were devised. Sensitivity of fluorescence detection depends less dramatically on the sample volume. This explains extensive use of standard fluorescence microcopy in proof of principle studies focused on characterization of newly developed separation chips[54, 63, 67, 80, 85, 89, 102, 107, 108, 134, 135]with detection zone volumes down to the attoliter level.[111] In analogy to fluorescence detection, Raman probing is advantageous when only minute sample volumes are available. Raman spectroscopy, particularly surface enhanced, was used for sample detection in both capillary separation systems[136, 137]and on-chip applications.[138-143] Importantly, Raman spectroscopic detection provides an additional mode of selectivity and therefore is particularly suitable for differentiating analytes that are otherwise difficult to separate. This quality is further explored in Chapter 5 with the incorporation of a pillar array channel with post separation SERS detection capabilities.

Other types of detectors that tend to retain their sensitivity despite the minute sample volumes and facilitate on-chip integration a complete HPLC system include electrochemical[144] and electrical impedance detectors.[145] An important aspect of electrical interrogation techniques is that they take advantage of micropatterned planar electrodes and, by contrast to optical detectors, do not require any off-chip components. Mass sensitive micro and nanoscale resonators[146, 147] are among newly emerging types of detectors very promising for on-chip analytical devices, including PD LC chips. Within the last decade, their sensitivity improved from the femtogram level[148] to the zeptogram

level[149] and mass sensitive detectors integrated into microfluidic systems were demonstrated.[150]

In addition to the sample detection based on the approaches mentioned above, direct coupling of an ESI-MS system to an outlet of a nano-column or an LC chip is often used as it offers many advantages for analysis of biological samples. [1] The main advantages of such a hyphenated LC-ESI-MS technique are related to the ability of MS analysis to differentiate molecules and molecular fragments according to their size and charge. Furthermore, very high sensitivity of ESI-MS techniques[151, 152] make them particularly suitable for analysis of minute sample quantities contained in the bands eluted from LC chips and nano-LC columns. ESI emitters can be straightforwardly integrated with on-chip LC columns. [1] A typical on-chip ESI emitter is a fluidic channel with embedded thin film electrodes that tapers down towards the edge of the chip.[70, 73, 125] The Agilent HPLC chip [73] is a notable example of this detection approach that had a significant practical impact. [145, 153, 154]

Portions of this review article are not included in this dissertation, and can be found in the original work. These sections focus on newly emerging separation techniques and modes of separation as well as describe several selected examples of the implemented on-chip PD LC systems, providing a brief overview of the demonstrated separation performance.

1.3.6 Acknowledgement

A portion of this work at Oak Ridge National Laboratory's Center for Nanophase Materials Sciences was sponsored by the Scientific User Facilities Division, Office of Basic Energy Sciences, U.S. Department of Energy. NVL acknowledges support by the Scientific User Facilities Division, U.S. Department of Energy. This research was also supported by the US

Environmental Protection Agency STAR Program under grant EPA-83274001 with the University of Tennessee

1.4 References

[1] S. Koster, E. Verpoorte, Lab on a Chip, 7 (2007) 1394.
[2] V. Dolnik, Electrophoresis, 27 (2006) 126.
[3] L. Suntornsuk, Anal Bioanal Chem, 398 (2010) 29.
[4] D.J. Harrison, A. Manz, Z.H. Fan, H. Ludi, H.M. Widmer, Analytical Chemistry, 64 (1992) 1926.
[5] S.C. Jacobson, R. Hergenroder, L.B. Koutny, J.M. Ramsey, Analytical Chemistry, 66 (1994) 1114.
[6] V. Dolnik, S.R. Liu, Journal of Separation Science, 28 (2005) 1994.
[7] Y.W. Lin, M.F. Huang, H.T. Chang, Electrophoresis, 26 (2005) 320.
[8] M.C. Breadmore, Electrophoresis, 28 (2007) 254.
[9] K.D. Dorfman, Reviews of Modern Physics, 82 (2010) 2903.
[10] M.C. Breadmore, J.R.E. Thabano, M. Dawod, A.A. Kazarian, J.P. Quirino, R.M. Guijt, Electrophoresis, 30 (2009) 230.
[11] J.H. Knox, R. Boughtflower, Trac-Trends in Analytical Chemistry, 19 (2000) 643.
[12] J. Curling, U. Gottschalk, Biopharm International, 20 (2007) 70.
[13] J.J. Kirkland, Journal of Chromatographic Science, 10 (1972) 593.
[14] J.J. Kirkland, Journal of Chromatography, 83 (1973) 149.
[15] J.J. Kirkland, Journal of Chromatographic Science, 38 (2000) 535.
[16] R.E. Majors, Lc Gc North America, 23 (2005) 1248.
[17] M.E. Swartz, Journal of Liquid Chromatography & Related Technologies, 28 (2005) 1253.
[18] J.J. Kirkland, Chromatographia, 8 (1975) 661.
[19] T. Tsuda, M. Novotny, Analytical Chemistry, 50 (1978) 271.
[20] M. Novotny, Analytical Chemistry, 60 (1988) A500.
[21] F. Svec, J.M.J. Frechet, Analytical Chemistry, 64 (1992) 820.
[22] F. Svec, Lc Gc Europe, 23 (2010) 272.
[23] N. Ishizuka, H. Minakuchi, K. Nakanishi, N. Soga, N. Tanaka, J. Chromatogr. A, 797 (1998) 133.
[24] K. Cabrera, Journal of Separation Science, 27 (2004) 843.
[25] K. Saito, R.A. Dixon, L. Willmitzer, T. Ikegami, E. Fukusaki, N. Tanaka, Plant Metabolomics (Biotechnology in Agriculture and Forestry), Springer Berlin Heidelberg, 2006, p. 49.
[26] B. He, F. Regnier, Journal of Pharmaceutical and Biomedical Analysis, 17 (1998) 925.
[27] B. He, N. Tait, F. Regnier, Analytical Chemistry, 70 (1998) 3790.

[28] F.E. Regnier, HRC-Journal of High Resolution Chromatography, 23 (2000) 19.
[29] D.S. Tezcan, A. Verbist, W. De Malsche, J. Vangelooven, H. Eghbali, D. Clicq, G. Desmet, P. De Moor, 2007 Ieee International Electron Devices Meeting, Vols 1 and 2 (2007) 839.
[30] H. Eghbali, W. De Malsche, D. Clicq, H. Gardeniers, G. Desmet, Lc Gc Europe, 20 (2007) 208.
[31] I.D. Wilson, R. Plumb, J. Granger, H. Major, R. Williams, E.A. Lenz, Journal of Chromatography B-Analytical Technologies in the Biomedical and Life Sciences, 817 (2005) 67.
[32] R.E. Majors, Journal of Chromatographic Science, 11 (1973) 88.
[33] J.J. Kirkland, J.J. DeStefano, J. Chromatogr. A, 1126 (2006) 50.
[34] J.C. Giddings, Journal of Gas Chromatography, 2 (1964) 167.
[35] J.M. Miller, Chromatography: Concepts and Contrasts, John Wiley & Sons, Inc, New Jersey, 2005.
[36] B.L. Karger, L.R. Snyder, C. Horvath, An Introduction to Separation Science, John Wiley & Sons, Inc., Canada, 1973.
[37] G. Deininger, Chromatographia, 9 (1976) 251.
[38] J.C. Giddings, Unified Separation Science, John Wiley & Sons, Inc., United States of America, 1991.
[39] J.H. Knox, J. Chromatogr. A, 960 (2002) 7.
[40] G. Guiochon, J. Chromatogr. A, 1126 (2006) 6.
[41] J.J. DeStefano, T.J. Langlois, J.J. Kirkland, Journal of Chromatographic Science, 46 (2008) 254.
[42] J.S. Baker, J.C. Vinci, A.D. Moore, L.A. Colon, Journal of Separation Science, 33 (2010) 2547.
[43] S. Fekete, K. Ganzler, J. Fekete, Journal of Pharmaceutical and Biomedical Analysis, 54 (2010) 482.
[44] F. Gritti, I. Leonardis, J. Abia, G. Guiochon, J. Chromatogr. A, 1217 (2010) 3819.
[45] P. Gzil, N. Vervoort, G.V. Baron, G. Desmet, Analytical Chemistry, 75 (2003) 6244.
[46] J. De Smet, P. Gzil, N. Vervoort, H. Verelst, G.V. Baron, G. Desmet, Analytical Chemistry, 76 (2004) 3716.
[47] P. Gzil, N. Vervoort, G.V. Baron, G. Desmet, Journal of Separation Science, 27 (2004) 887.
[48] P. Gzil, N. Vervoort, G.V. Baron, G. Desmet, Analytical Chemistry, 76 (2004) 6707.
[49] M.R. Schure, R.S. Maier, D.M. Kroll, H.T. Davis, J. Chromatogr. A, 1031 (2004) 79.
[50] S. Sukas, G. Desmet, H.J.G.E. Gardeniers, ELECTROPHORESIS, 31 (2010) 3681.
[51] X.H. Yan, Q.W. Wang, H.H. Bau, J. Chromatogr. A, 1217 (2010) 1332.
[52] S.K. Anton Daneyko, Alexandra Holtzel, Andreas Seidel-Morgenstern, Ulrich Tallarek, J. Chromatogr. A, 1218 (2011) 8231.
[53] J.C. Giddings, Dynamics of Chromatography - Part I, , Marcel Dekker Inc., New York, 1965.
[54] N.V. Lavrik, L.C. Taylor, M.J. Sepaniak, Lab on a Chip, 10 (2010) 1086.

[55] R.D. Kamien, A.J. Liu, Physical Review Letters, 99 (2007).
[56] I.M. Lazar, P. Trisiripisal, H.A. Sarvaiya, Analytical Chemistry, 78 (2006) 5513.
[57] M.J. Madou, CRC press, Boca Raton, 2002.
[58] G.T.A. Kovacs, McGraw-Hill, 1998, p. 944.
[59] T. McCreedy, Trac-Trends in Analytical Chemistry, 19 (2000) 396.
[60] S.C. Terry, J.H. Jerman, J.B. Angell, Ieee Transactions on Electron Devices, 26 (1979) 1880.
[61] A. Manz, Y. Miyahara, J. Miura, Y. Watanabe, H. Miyagi, K. Sato, Sensors and Actuators B-Chemical, 1 (1990) 249.
[62] G. Ocvirk, E. Verpoorte, A. Manz, M. Grasserbauer, H.M. Widmer, Analytical Methods and Instrumentation, 2 (1995) 74.
[63] K. Loutherback, J. Puchalla, R.H. Austin, J.C. Sturm, Physical Review Letters, 102 (2009).
[64] R.M. Tiggelaar, V. Verdoold, H. Eghbali, G. Desmet, J.G.E. Gardeniers, Lab on a Chip, 9 (2009) 456.
[65] C. Aoyama, A. Saeki, M. Noguchi, Y. Shirasaki, S. Shoji, T. Funatsu, J. Mizuno, M. Tsunoda, Analytical Chemistry, 82 (2010) 1420.
[66] F. Detobel, S. De Bruyne, J. Vangelooven, W. De Malsche, T. Aerts, H. Terryn, H. Gardeniers, S. Eeltink, G. Desmet, Analytical Chemistry, 82 (2010) 7208.
[67] L.C. Taylor, N.V. Lavrik, M.J. Sepaniak, Analytical Chemistry, 82 (2010) 9549.
[68] J. Vangelooven, W. De Malsche, J. Op De Beeck, H. Eghbali, H. Gardeniers, G. Desmet, Lab on a Chip, 10 (2010) 349.
[69] Y.N. Xia, G.M. Whitesides, Annual Review of Materials Science, 28 (1998) 153.
[70] Y.N. Yang, C. Li, J. Kameoka, K.H. Lee, H.G. Craighead, Lab on a Chip, 5 (2005) 869.
[71] J. Kameoka, H.G. Craighead, H.W. Zhang, J. Henion, Analytical Chemistry, 73 (2001) 1935.
[72] X. Illa, W. De Malsche, J. Bomer, H. Gardeniers, J. Eijkel, J.R. Morante, A. Romano-Rodriguez, G. Desmet, Lab on a Chip, 9 (2009) 1511.
[73] H.F. Yin, K. Killeen, Journal of Separation Science, 30 (2007) 1427.
[74] J.M.K. Ng, I. Gitlin, A.D. Stroock, G.M. Whitesides, Electrophoresis, 23 (2002) 3461.
[75] J.C. McDonald, G.M. Whitesides, Accounts of Chemical Research, 35 (2002) 491.
[76] A.A.S. Bhagat, P. Jothimuthu, I. Papautsky, Lab on a Chip, 7 (2007) 1192.
[77] L.E. Khoong, Y.M. Tan, Y.C. Lam, Journal of the European Ceramic Society, 30 (2010) 1973.
[78] Y.T. Zhang, F. Bottausci, M.P. Rao, E.R. Parker, I. Mezic, N.C. MacDonald, Biomedical Microdevices, 10 (2008) 509.
[79] M.F. Aimi, M.P. Rao, N.C. Macdonald, A.S. Zuruzi, D.P. Bothman, Nature Materials, 3 (2004) 103.
[80] W. De Malsche, H. Eghbali, D. Clicq, J. Vangelooven, H. Gardeniers, G. Desmet, Analytical Chemistry, 79 (2007) 5915.
[81] R.M. Guijt, E. Baltussen, G. van der Steen, R.B.M. Schasfoort, S. Schlautmann, H.A.H. Billiet, J. Frank, G.W.K. van Dedem, A. van den Berg, Electrophoresis, 22 (2001) 235.

[82] N. Kaji, Y. Tezuka, Y. Takamura, M. Ueda, T. Nishimoto, H. Nakanishi, Y. Horiike, Y. Baba, Analytical Chemistry, 76 (2004) 15.
[83] C. Ericson, J. Holm, T. Ericson, S. Hjerten, Analytical Chemistry, 72 (2000) 81.
[84] D.S. Reichmuth, T.J. Shepodd, B.J. Kirby, Analytical Chemistry, 76 (2004) 5063.
[85] P. Mao, J. Han, Lab on a Chip, 9 (2009) 586.
[86] R. Costa, K.B. Mogensen, J.P. Kutter, Lab on a Chip, 5 (2005) 1310.
[87] K. Obata, K. Sugioka, N. Shimazawa, K. Midorikawa, Applied Physics a-Materials Science & Processing, 84 (2006) 251.
[88] X. Illa, W. De Malsche, H. Gardeniers, G. Desmet, A. Romano-Rodriguez, J. Chromatogr. A, 1217 (2010) 5817.
[89] X. Illa, W. De Malsche, H. Gardeniers, G. Desmet, A. Romano-Rodriguez, Journal of Separation Science, 33 (2010) 3313.
[90] N.D. Danielson, J.J. Kirkland, Analytical Chemistry, 59 (1987) 2501.
[91] R.E. Majors, American Laboratory, 35 (2003) 46.
[92] M. Vazquez, B. Paull, Anal Chim Acta, 668 (2010) 100.
[93] D. Guillarme, J. Ruta, S. Rudaz, J.L. Veuthey, Anal Bioanal Chem, 397 (2010) 1069.
[94] N. Ishizuka, H. Minakuchi, K. Nakanishi, N. Soga, H. Nagayama, K. Hosoya, N. Tanaka, Analytical Chemistry, 72 (2000) 1275.
[95] S. Jung, S. Ehlert, J.A. Mora, K. Kraiczek, M. Dittmann, G.P. Rozing, U. Tallarek, J. Chromatogr. A, 1216 (2009) 264.
[96] S. Ehlert, K. Kraiczek, J.A. Mora, M. Dittmann, G.P. Rozing, U. Tallarek, Analytical Chemistry, 80 (2008) 5945.
[97] A. Ishida, T. Yoshikawa, M. Natsume, T. Kamidate, J. Chromatogr. A, 1132 (2006) 90.
[98] P.A. Levkin, S. Eeltink, T.R. Stratton, R. Brennen, K. Robotti, H. Yin, K. Killeen, F. Svec, J.M.J. Frechet, J. Chromatogr. A, 1200 (2008) 55.
[99] K.M. Robotti, H.F. Yin, R. Brennen, L. Trojer, K. Killeen, Journal of Separation Science, 32 (2009) 3379.
[100] J.K. Liu, C.F. Chen, C.W. Tsao, C.C. Chang, C.C. Chu, D.L. Devoe, Analytical Chemistry, 81 (2009) 2545.
[101] F. Svec, J. Chromatogr. A, 1217 (2010) 902.
[102] H. Eghbali, V. Verdoold, L. Vankeerberghen, H. Gardeniers, G. Desmet, Analytical Chemistry, 81 (2009) 705.
[103] H. Eghbali, W. De Maische, J. De Smet, J. Billen, M. De Pra, W.T. Kok, P.J. Schoenmakers, H. Gardeniers, G. Desmet, Journal of Separation Science, 30 (2007) 2605.
[104] F. Detobel, H. Eghbali, S. De Bruyne, H. Terryn, H. Gardeniers, G. Desmet, J. Chromatogr. A, 1216 (2009) 7360.
[105] H. Eghbali, S. Matthijs, V. Verdoold, H. Gardeniers, P. Cornelis, G. Desmet, J. Chromatogr. A, 1216 (2009) 8603.
[106] W. De Malsche, D. Clicq, V. Verdoold, P. Gzil, G. Desmet, H. Gardeniers, Lab on a Chip, 7 (2007) 1705.
[107] W. De Malsche, H. Gardeniers, G. Desmet, Analytical Chemistry, 80 (2008) 5391.

[108] W. De Malsche, L. Zhang, J.O. De Beeck, J. Vangelooven, B. Majeed, G. Desmet, Journal of Separation Science, 33 (2010) 3613.
[109] M. Faustini, M. Vayer, B. Marmiroli, M. Hillmyer, H. Amenitsch, C. Sinturel, D. Grosso, Chemistry of Materials, 22 (2010) 5687.
[110] L. Sainiemi, H. Keskinen, M. Aromaa, L. Luosujarvi, K. Grigoras, T. Kotiaho, J.M. Makela, S. Franssila, Nanotechnology, 18 (2007).
[111] M. Kato, M. Inaba, T. Tsukahara, K. Mawatari, A. Hibara, T. Kitamori, Analytical Chemistry, 82 (2010) 543.
[112] Z.W. Wang, W.J. Wang, G.N. Chen, W. Wang, F.F. Fu, Journal of Separation Science, 33 (2010) 2568.
[113] T. Braschler, J. Theytaz, R. Zvitov-Marabi, H. Van Lintel, G. Loche, A. Kunze, N. Demierre, R. Tornay, M. Schlund, P. Renaud, Lab on a Chip, 7 (2007) 1111.
[114] E.F. Hasselbrink, T.J. Shepodd, J.E. Rehm, Analytical Chemistry, 74 (2002) 4913.
[115] F. Benito-Lopez, R. Byrne, A.M. Raduta, N.E. Vrana, G. McGuinness, D. Diamond, Lab on a Chip, 10 (2010) 195.
[116] Z.M. Li, Q.H. He, D. Ma, H.W. Chen, Anal Chim Acta, 665 (2010) 107.
[117] B.J. Kirby, T.J. Shepodd, E.F. Hasselbrink, J. Chromatogr. A, 979 (2002) 147.
[118] W.H. Grover, A.M. Skelley, C.N. Liu, E.T. Lagally, R.A. Mathies, Sensors and Actuators B-Chemical, 89 (2003) 315.
[119] M. Koch, N. Harris, R. Maas, A.G.R. Evans, N.M. White, A. Brunnschweiler, Measurement Science & Technology, 8 (1997) 49.
[120] V. Gass, B.H. Vanderschoot, S. Jeanneret, N.F. Derooij, Sensors and Actuators a-Physical, 43 (1994) 335.
[121] S.L. Zeng, C.H. Chen, J.C. Mikkelsen, J.G. Santiago, Sensors and Actuators B-Chemical, 79 (2001) 107.
[122] C.H. Chen, J.G. Santiago, Journal of Microelectromechanical Systems, 11 (2002) 672.
[123] T.E. McKnight, C.T. Culbertson, S.C. Jacobson, J.M. Ramsey, Analytical Chemistry, 73 (2001) 4045.
[124] A. Manz, C.S. Effenhauser, N. Burggraf, D.J. Harrison, K. Seiler, K. Fluri, J Micromech Microeng, 4 (1994) 257.
[125] I.M. Lazar, B.L. Karger, Analytical Chemistry, 74 (2002) 6259.
[126] J.F. Borowsky, B.C. Giordano, Q. Lu, A. Terray, G.E. Collins, Analytical Chemistry, 80 (2008) 8287.
[127] M.A. Lerch, S.C. Jacobson, Analytical Chemistry, 79 (2007) 7485.
[128] L. Chen, S. Lee, J. Choo, E.K. Lee, J Micromech Microeng, 18 (2008).
[129] D.J. Laser, J.G. Santiago, J Micromech Microeng, 14 (2004) R35.
[130] N.T. Nguyen, X.Y. Huang, T.K. Chuan, Journal of Fluids Engineering-Transactions of the Asme, 124 (2002) 384.
[131] M. Swartz, Journal of Liquid Chromatography & Related Technologies, 33 (2010) 1130.
[132] H. Salimi-Moosavi, Y.T. Jiang, L. Lester, G. McKinnon, D.J. Harrison, Electrophoresis, 21 (2000) 1291.
[133] K.M. van Delft, J.C.T. Eijkel, D. Mijatovic, T.S. Druzhinina, H. Rathgen, N.R. Tas, A. van den Berg, F. Mugele, Nano Letters, 7 (2007) 345.

[134] M. De Pra, W.T. Kok, J.G.E. Gardeniers, G. Desmet, S. Eeltink, J.W. van Nieuwkasteele, P.J. Schoenmakers, Analytical Chemistry, 78 (2006) 6519.
[135] W. De Malsche, J.O. De Beeck, H. Gardeniers, G. Desmet, J. Chromatogr. A, 1216 (2009) 5511.
[136] W.F. Nirode, G.L. Devault, M.J. Sepaniak, Analytical Chemistry, 72 (2000) 1866.
[137] N. Leopold, B. Lendl, Anal Bioanal Chem, 396 (2010) 2341.
[138] R.J. Dijkstra, F. Ariese, C. Gooijer, U.A.T. Brinkman, Trac-Trends in Analytical Chemistry, 24 (2005) 304.
[139] R.M. Connatser, L.A. Riddle, M.J. Sepaniak, Journal of Separation Science, 27 (2004) 1545.
[140] R.M. Connatser, M. Cochran, R.J. Harrison, M.J. Sepaniak, Electrophoresis, 29 (2008) 1441.
[141] H. Chon, C. Lim, S.M. Ha, Y. Ahn, E.K. Lee, S.I. Chang, G.H. Seong, J. Choo, Analytical Chemistry, 82 (2010) 5290.
[142] C. Lim, J. Hong, B.G. Chung, A.J. deMello, J. Choo, Analyst, 135 (2010) 837.
[143] L.X. Quang, C. Lim, G.H. Seong, J. Choo, K.J. Do, S.K. Yoo, Lab on a Chip, 8 (2008) 2214.
[144] J.A. Abia, J. Putnam, K. Mriziq, G.A. Guiochon, J. Chromatogr. A, 1217 (2010) 1695.
[145] L. Callipo, P. Foglia, R. Gubbiotti, R. Samperi, A. Lagana, Anal Bioanal Chem, 394 (2009) 811.
[146] K.L. Ekinci, X.M.H. Huang, M.L. Roukes, Applied Physics Letters, 84 (2004) 4469.
[147] N.V. Lavrik, M.J. Sepaniak, P.G. Datskos, Review of Scientific Instruments, 75 (2004) 2229.
[148] N.V. Lavrik, P.G. Datskos, Applied Physics Letters, 82 (2003) 2697.
[149] Y.T. Yang, C. Callegari, X.L. Feng, K.L. Ekinci, M.L. Roukes, Nano Letters, 6 (2006) 583.
[150] S. Son, W.H. Grover, T.P. Burg, S.R. Manalis, Analytical Chemistry, 80 (2008) 4757.
[151] M. Wilm, A. Shevchenko, T. Houthaeve, S. Breit, L. Schweigerer, T. Fotsis, M. Mann, Nature, 379 (1996) 466.
[152] G.A. Valaskovic, N.L. Kelleher, D.P. Little, D.J. Aaserud, F.W. McLafferty, Analytical Chemistry, 67 (1995) 3802.
[153] J. Hardouin, M. Duchateau, R. Joubert-Caron, M. Caron, Rapid Communications in Mass Spectrometry, 20 (2006) 3236.
[154] J. Hardouin, R. Joubert-Caron, M. Caron, Journal of Separation Science, 30 (2007) 1482.

Chapter 2

Introduction to microfabrication methods

2.2 Abstract

Microfabrication techniques, similar to those applied in the semiconductor industry, have garnered increasing interest as a promising method for creating fully integrated miniaturized systems. Most commonly applied to silicon wafer technology, these processes have the ability to tailor design parameters down to the nanometer scale while providing methods in controlling the substrates mechanical properties. As described in the previous chapter, packing size and homogeneity are very important parameters when designing any chromatographic format. Accordingly, microfabrication methods have been applied to create highly ordered miniaturized separation beds for use as microfluidic devices for conducting biological and chemical separations. A standard fabrication process involves a precise combination of various steps. These steps most often include a lithographic process to create the pattern of the design, an etching process which permanently defines said pattern by removing specific portions of the material surface, and finally modifying the substrate by a choice of deposition processes. This chapter briefly discusses the main principle of those techniques directly applied to the research discussed within this dissertation. More complete information can be found in textbooks focusing on micro and nano fabrication methods. [1-5]

2.2 Overview of Fabrication Approaches

2.2.1 Photolithography

Lithography is a complex technique used to transfer patterns, usually generated by computer software, as part of a process which creates multipurpose substrates and integrated circuits. A successful and efficient lithographic process satisfies three central objectives[6], (i) is able

to distinguish between nearby features with adequate resolution, (ii) produces patterns of high fidelity without defects, and (iii) is mindful of economical concerns, including achieving high throughput. The final consideration, although not essential for all process applications, is the reason that photolithographic techniques are the most widely used lithographic method, rather than processes including electron beam and X-ray lithography.

A typical photolithographic process[3, 5] (Figure 2.1) begins with substrate preparation to improve the adhesion of subsequent photoresist coatings. This process can include cleaning procedures, a dehydration bake, or coating with a primer or other adhesion promoter. Next, a uniform coating of photoresist is spincoated onto the substrate to a specific thickness. Photoresist is a polymeric photosensitive material that, when exposed to the light source, triggers a solubility switch in which either the material exposed to the source is soluble (positive photoresist) or the material masked from the source is soluble (negative photoresist). Resist systems also provide etch resistance and thermal stability. The substrate is subsequently soft baked to remove solvent and improve adhesion. Then the substrate is aligned to the photomask, a quartz plate patterned with the design, and is exposed for a finite period of time. There are three different modes of exposure termed according to the separation between the mask and the substrate (Figure 2.2). The simplest systems utilize contact or proximity lithography. While contact methods provide better resolution they can also cause damage to the photomask and substrate causing feature defects. Projection lithography systems are the most commonly used as they provide the best resolution by expanding, homogenizing, and then reducing the pattern, by a factor of four or five, through a dual lens optical system onto the substrate.[7]

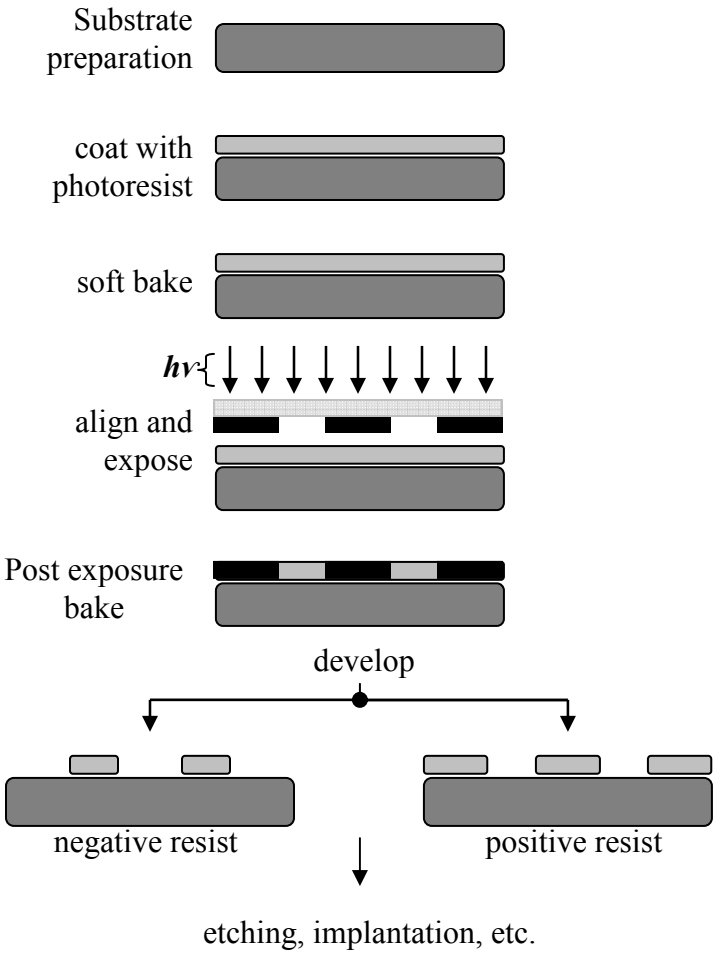

Figure 2.1 Typical sequence for lithographic process, illustrating both negative and positive photoresist methods.

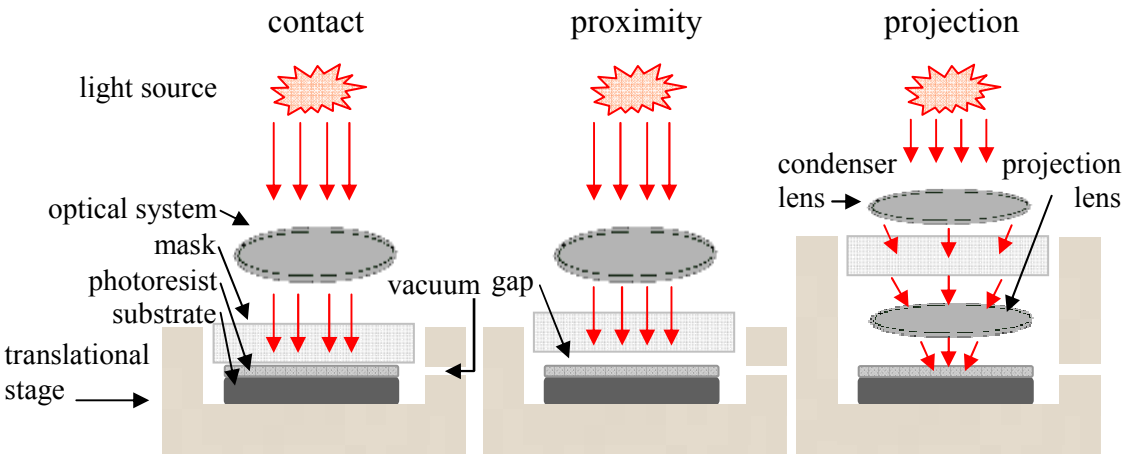

Figure 2.2 Photolithography modes of exposure.

After exposure, the substrate can be processed with a post exposure bake (PEB). This procedure is used for two purposes. For conventional photoresists it is applied to reduce the standing wave effect which is created when monochromatic light is projected onto the wafer over a range of angles. The light travels into the photoresist and is reflected off the substrate. These light waves interfere and form a wave of high and low intensity which may be replicated onto the resist and form ridges on the sidewalls of the design, detrimentally affecting the quality of the features.[3] For chemically amplified photoresists, the PEB additionally produces a chemical reaction that assists in increasing the solubility of the polymer resin. Finally, the photoresist is developed resulting in the final definition of design features ready for further processing.

One of the key metrics of photolithography, Resolution (*W)*, which defines the smallest feature that can be accurately patterned onto a substrate, is described by the Rayleigh scaling equation[4]

$$W = \frac{k_1 \lambda}{NA} \qquad (1)$$

where k_1 is a dimensionless scaling parameter, λ is the exposure wavelength, and NA is the numerical aperture of the optical system. This equation shows the significant improvement in resolution that is achieved when reducing exposure wavelength. Figure 2.3 describes this evolution of photolithography sources from the 1980's to the technology of today.[7, 8] The first UV light sources were broad band light sources, commonly mercury arc lamps, used in combination with filters specific to exposure wavelength (500 nm minimum feature size). The transition to laser light sources allows for smaller features (32 nm), however are more expensive to operate. Current research is focused on developing F_2 laser and extreme

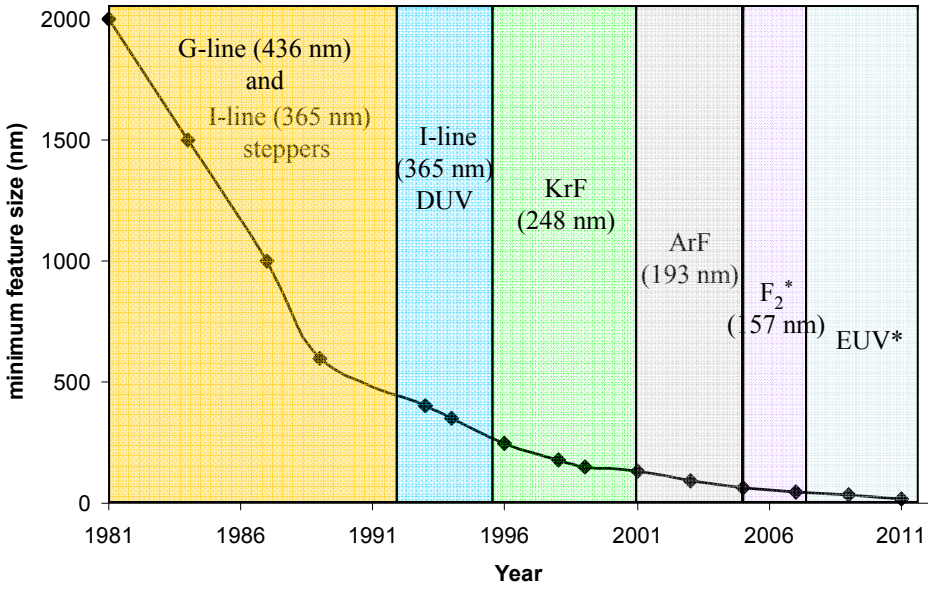

Figure 2.3 Historical timeline of optical lithographic wavelength generation with reduction in minimum feature size. G and I line sources are mainly broad band mercury lamps. Eximer lasers are used for more advanced systems. * Denotes developing technology whose progress is not well defined in literature..

ultraviolet (EUV) technology; though these advances are challenging due to the need for compatible optic and mask material and the difficulty of EUV generation, respectively. In addition to the progress in photolithography light sources, optical systems have advanced to improve resolution, often in an effort to create optics with materials that are compatible with exposure technology. Resist materials have also evolved to improve exposure sensitivity and provide high contrast resist systems.

Photolithography enhancement techniques have been developed to further decrease feature sizes without consideration of tool limitations. A few of these techniques include immersion lithography and double patterning. The later is possible due to the use of dark field alignment which allows for the application of multiple masks for multiple exposures onto the same substrate.[4] For the studies described in this dissertation, a photolithography tool equipped with a G-line (436 nm) exposure system for contact lithography was used. To improve upon the fundamental resolution limitation of the instrument we employed an additive processing technique, slightly different from the more common subtractive method (Figure 2.1), in which the lithography process creates a negative feature pattern and is then followed by deposition of a material into the unprotected areas of the design. Specifically, we utilized a sacrificial two layer lift-off resist system, described in Figure 2.4. In this technique the bottom photoresist layer is undercut during lithographic development. Afterwards, a thin metal layer is blanket deposited onto the substrate and the resist is stripped so that metal which was deposited on the sacrificial layer is removed, while any metal which was in direct contact with the substrate remains, producing a hard metal mask of high fidelity features.

2.2.2 Reactive ion etching

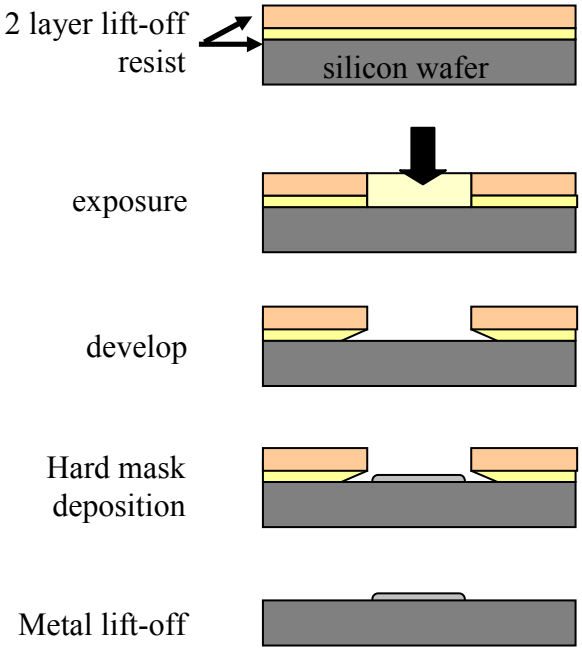

Figure 2.4 Two layer lift-off photoresist method for high resolution lithographic process

The pattern imprinted onto the substrates mask material (photoresist, metal, etc.) is transferred onto the substrate via an etching process which selectively creates structures onto the surface. This is achieved through either wet chemical of dry plasma etching. Both methods can produce either of two characteristic profiles as depicted in Figure 2.5, (i) anisotropic in which the vertical etch rate is faster than the horizontal etch rate, or (ii) isotropic in which the etch is independent of position and direction. Most fabrication processes require anisotropic etch profiles as they produce sharp controlled features, while an isotropic etch produces undercut features. Common wet chemical etching methods include the use of KOH and HF solutions.

Dry etch systems remove material by ion bombardment of the surface. For the most common method, reactive ion etching (RIE), the substrate is placed within a reactor where reactive species are generated in a plasma using an RF power source and a gaseous mixture (see Figure 2.6). Ions are accelerated toward the surface causing two distinct etch reactions termed the physical and chemical etch. The physical process is a result of high energy ions knocking atoms out of the material by transfer of kinetic energy, similar to a sputtering process. Alternatively, the chemical process occurs due to a chemical reaction and formation of gaseous material at the substrate surface. In this process a bond between the reactive ion and the silicon atom is formed, chemically removing the silicon atoms from the surface. The physical process is responsible for anisotropic etch properties, while the chemical process is predominately isotropic in nature. Multiple parameters such as gas flow rate, RF power, and temperature may be adjusted so that one process may dominate over the other. The challenge in creating an optimal etch profile using the dry etch method is often determining the proper balance between these two processes.

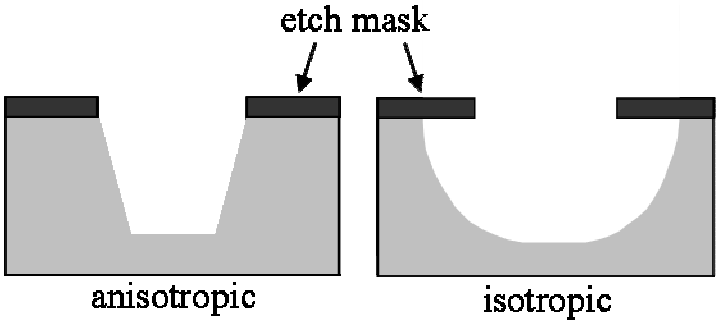

Figure 2.5 Schematic illustration of the result of anisotropic and isotropic etching.

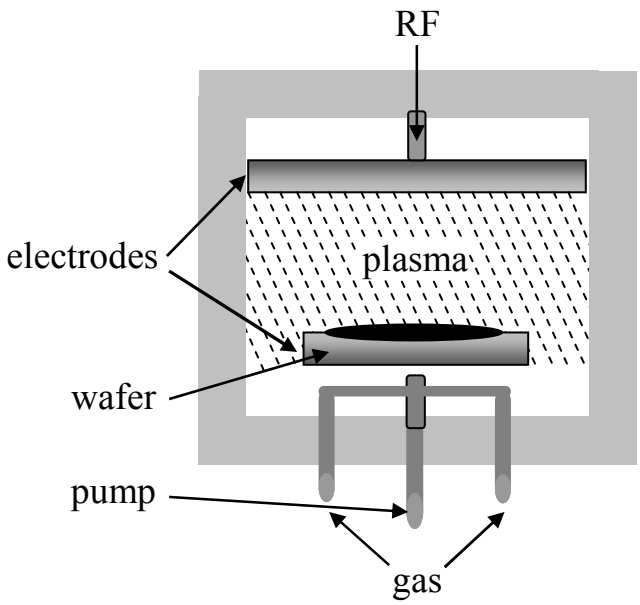

Figure 2.6 Schematic representation of a typical RIE chamber

In order to create high-aspect-ratio anisotropic features a cyclic technology, termed deep reactive ion etching (DRIE), has become popular for advanced 3-D wafer designs. One of the main DRIE techniques is the Bosch process, which can be used to create vertical sidewalls as well as etch through an entire wafer due to its high etch rate and selectivity for silicon. Figure 2.7 describes a typical Bosch process which is defined by two repetitive steps. In the first step the exposed silicon is etched by an isotropic SF_6 gas. In the second step a C_4F_8 polymer is deposited as a passivation layer onto all surfaces of the substrate, including etched side walls. When the first cycle is repeated, the polymer is immediately sputtered away by the physical part of the etching. Being that the teflon like polymer dissolves very slowly during the chemical process of the etch, it builds up and protects the sidewalls from etching. This two step cyclic process can be repeated for multiple loops, varying the time of both the etch and the deposition steps, ultimately producing vertical side walls that appear as a series of isotropic etches stacked on top of one another. This process is able generating features with aspect ratios above 20:1.

2.2.3 Thin film deposition

The thin film deposition process is an essential component of numerous fabrication schemes. Thin films are characterized as a material with a thickness between a few nanometers to approximately 100 micrometers. Most deposition processes can be classified as forming due to either a chemical or physical reaction. In the chemical process, the substrate is exposed to gases within a reactor. A chemical reaction occurs producing a solid material which further condenses on all surfaces within the chamber. In the physical process, a material is released from a source via an energetic process, and then travels onto the substrate, commonly by an evaporation or sputtering mechanism. Consequently, chemical deposition processes usually

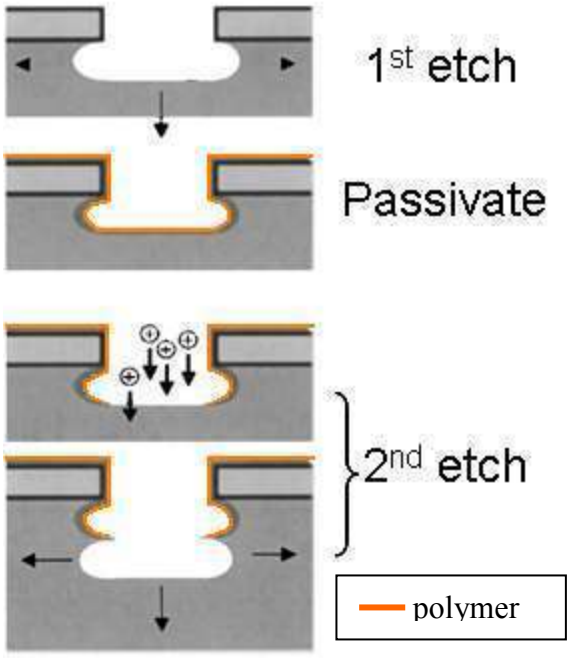

Figure 2.7 Typical two step Bosch process for DRIE

produce a more conformal multidirectional deposition, whereas physical deposition processes are most often non-conformal and directional, as described in Figure 2.8.

Some of the characteristics of a deposition technique to consider when choosing the best possible process for a specific application are the deposition rate, deposition uniformity, conformality, and temperature requirements. High quality thin films are generally deposited through thermal oxidation or thermal chemical vapor deposition, excluding those applications which experience temperature limitations. Plasma enhanced chemical vapor deposition (PECVD) is typically used to deposit thin dielectric films onto substrates which cannot be subjected to extreme temperatures. In these systems a plasma reactor is used to dissociate precursor gases into small, reactive molecules for deposition. The typical chamber temperature for a PECVD system is in the range of 200 to 300 °C, in comparison to Low pressure chemical vapor deposition (LPCVD) which uses temperatures more than double these amounts. These lower deposition temperatures can help to avoid defect formation, diffusion, and degradation of the substrates metal layers. As chemical vapor depositions are surface reaction limited, the use of the plasma discharge enhances chemical reaction rates increasing the deposition rate. However, LPCVD systems offer improvement in film quality as typical PECVD deposited films have a rougher film morphology and higher impurity content.[9]

For our research purposes we utilized both a physical deposition system (E-beam evaporator) and a PECVD. The novel aspect of our specific fabrication technique, as will be discussed in subsequent chapters, primarily relied on our ability to adjust PECVD deposition parameters in order to create high rate non-conformal depositions.

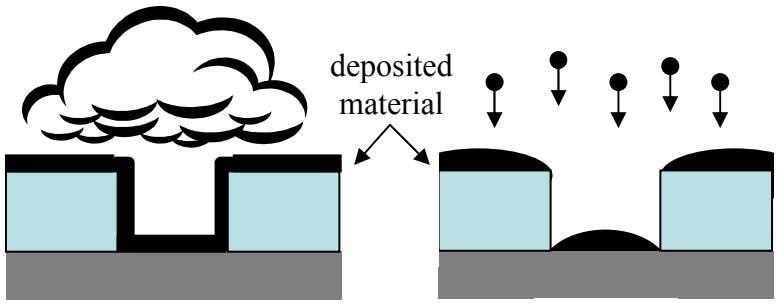

Figure 2.8 Schematic representation of a chemical vapor deposition vs. physical vapor deposition.

2.3 References

[1] G. Timp (Ed.), Nanotechnology, Springer-Verlag New York, Inc, New York, 1999.
[2] A.A. Tseng (Ed.), Nanofabrication fundamentals and applications, World Scientific Publishing Co., Toh Tuck Link, Singapore, 2008.
[3] C.A. Mack, Fundamental Principles of Optical Lithography: the science of microfabrication, Wiley, Hoboken, NJ, 2007.
[4] G.L.-T. Chiu, J.M. Shaw, IBM journal of research and development, 41 (1997).
[5] B. Bhushan, Springer Handbook of Nanotechnology, Springer-Verlag Berlin Heidelberg, Germany, 2003.
[6] T.A. Brunner, Journal of vacuum science technology B, 21 (2003) 2632.
[7] M. Rothschild, T.M. Bloomstein, T.H. Fedynyshyn, R.R. Kunz, V. Liberman, M. Switkes, N.N.E. Jr., S.T. Palmacci, J.H.C. Sedladek, D.E. Hardy, A. Grenville, Lincoln Laboratory Journal, 14 (2003) 221.
[8] P.J. Silverman, Intel Technology Journal, 6 (2002) 55.
[9] M.F. Ceiler, P.A. Kohl, S.A. Bidstrup, J Electrochem Soc, 142 (1995) 2067.

Chapter 3

Enclosed pillar arrays integrated on a fluidic platform for on-chip separations and analysis

Portions of Chapter 3 are an adaptation of a research article *Lab on a Chip* 2010, 10 (8), pg 1086-1094. This chapter discusses the unique fabrication of mechanically robust high-aspect-ratio pillar arrays as well as the integration of a compatible fluidic interface. The fluidic structures are suitable for handling picoliter sample volumes and offer prospects for substantial improvements in separation efficiency and permeability over traditional packed and monolithic columns.

3.1 Abstract

Due to the difficulty of reliably producing sealed 3-D structures, few researchers have tackled the challenges of creating pillar beds suitable for miniaturized liquid phase separation systems. Herein, we describe an original processing sequence for the fabrication of enclosed pillar arrays integrated on a fluidic chip, which we believe, will further stimulate interest in this field. Our approach yields a mechanically robust enclosed pillar system that withstands mechanical impacts commonly incurred during processing, sealing and operation, resulting in a design particularly suitable for the research environment. A combination of a wafer level fabrication sequence with chip-level elastomer bonding allows for chip reusability, an attractive and cost efficient advancement for research applications. The characteristic features in the implemented highly ordered pillar arrays are scalable to submicron dimensions. The proposed fluidic structures are suitable for handling picoliter sample volumes and offer prospects for substantial improvements in the separation efficiency and permeability over traditional packed and monolithic columns. Our experimental observations indicate plate heights as low as 0.76 μm for a 10 mm long pillar bed. Theoretical calculations confirm that ordered pillar arrays with submicron pore sizes

combine superior analysis speed, picoliter sample volumes, high permeability and reasonably large plate numbers on a small footprint. In addition, we describe a fluidic interface that provides streamlined coupling of the fabricated structures with off-chip fluidic components.

3.2 Introduction

Highly ordered arrays of high aspect ratio pillars created on a chip using lithographic techniques offer substantial fundamental advantages[1-4] over more traditional separation phases, such as packed and monolithic columns. As the sizes of the separation media shrink, the random nature and polydispersity of porosity in the latter two systems becomes a significant factor that limits the separation efficiency.[1, 2, 5, 6] Surmounting this limitation is particularly crucial for designing on-chip separation systems with lengths 1-2 orders of magnitude shorter than conventional macroscopic separation columns. Indeed, decreasing characteristic pore sizes in a separation bed allows one to proportionally decrease the column length thus making it more compatible with an on-chip format. Recent studies by Desmet and coworkers[5] provide convincing evidence that breakthrough advances in on-chip separation technology can be gained by adapting lithographic patterning and wafer level processing techniques similar to those developed for the semiconductor industry and capable of delivering fabrication accuracy of tens of nanometers. However, identifying specific technological approaches that can lead to successful implementations of efficient on-chip separation beds is far from being trivial. This can largely explain the fact that, despite the fundamental advantages of lithographically patterned ordered separation beds first proposed and implemented by Regnier *et al.*[3, 7] more than a decade ago, few researchers have chosen to further explore this idea.

The first applications of ordered pillar arrays as related to pressure driven separations have been reported only recently.[1, 5, 8, 9] Notably, some of these studies explored pillar arrays as a platform for a newly emerging particle separation technique based on deterministic lateral displacement [8, 9] rather than conventional liquid chromatography. While groundbreaking studies by Desmet and coworkers have convincingly demonstrated the potential of on-chip separation columns based on ordered pillar arrays, they also identified important experimental, technological and methodological challenges of such systems. One clear indication of the high level of these challenges is that only a few researchers have tackled them successfully. To our best knowledge, no successful implementation of lithographically patterned pillar arrays for pressure driven liquid phase separations analogous to those conducted using conventional packed or monolithic columns have been reported by researchers outside Desmet's team and their collaborators.

The key challenges involved in fabrication and operation of lithographically patterned separation columns can be broadly divided into the four categories: (i) decreasing the pillar sizes while increasing their aspect ratios without compromising mechanical robustness of the system, (ii) sealing of the pillar bed and coupling of the on-chip separation bed with macroscopic off-chip fluidic components, (iii) creating retentive properties of the arrays, and (iv) sample injection and detection compatible with very small plate heights. The main goal of our present work is to addresses the first two challenges. By combining and refining technological approaches similar to those described previously in several independent studies,[2, 7, 10-13]we established an innovative fabrication sequence that yields high-aspect-ratio pillar arrays embedded into channels on a reusable fluidic chip that facilitates experiments and further optimization. Our fabrication sequence relies on standard cleanroom

processing techniques, in particular, photolithographic patterning, anisotropic reactive ion etching (RIE) of silicon and plasma enhanced chemical vapor deposition of (PECVD) of silicon oxides. As compared to pillar arrays for on-chip separations implemented by De Malsche *et al.,*[5] He *et al*.,[7] and Kaji *et al.,*[13] the key advantage of the technological strategy presented here is the formation of a robust network of pores scalable down to submicron characteristic sizes and enclosed into a silicon oxide scaffold. Moreover, the enclosed array of pores is seamlessly integrated into a system fluidic channels that can be sealed using either soft (elastomer based) or hard (such as frit) bonding techniques. At this stage, we focus on a chip level sealing technique using elastomer bonding since this approach streamlines chip assembly and is compatible with various surface modification techniques that can be applied prior to the final chip assembly. The proposed approaches yield re-sealable fluidic chips that are especially suitable for extensive studies of separation and transport phenomena in a laboratory setting. While being beyond the scope of the present study, the scaled up fabrication of analytical separation systems based on the proposed strategy may ultimately benefit from wafer level anodic or frit bonding. At the same time, it is the absence of complicated and irreversible anodic bonding in our processing sequence that, we believe, will stimulate more extensive exploration of the ordered pillar arrays in conjunction with various liquid phase separation techniques.

3.3 Experimental

3.3.1 Chip design and fabrication of enclosed pillar arrays

As a starting material, we used p-type Czochralski grown 100 mm, (100) orientation single side polished silicon wafers with nominal thickness in the range of 300 to 500 μm and

resistivity in the range 0.01 to 20 Ohm cm. Our designs accommodated 9 chips on a 100 mm wafer. Each chip in our design was 22 mm x 22 mm and contained one main straight channel with approximately 10 mm of its length populated with a pillar array. Using the CAD software, pillars in the arrays were defined as hexagons placed in the corners of equilateral triangles (Figure 3.1) in analogy to ordered pillar arrays first proposed and evaluated by Gzil *et al.*[2] Among several possible ways to terminate a pillar array at a channel side wall, we choose the "embedded pillar" design [14] with 50% of the pillar embedded into the side boundary of the array (Figure 3.1). In addition to several pillar array parameters (Table 3.1) varied to elucidate technologically viable design space, we explored alternative channel geometries that provided sample injection upstream from the pillar array as well as the addition of a detection reagent downstream from the pillar array. Our fabrication sequence involved two photolithographic patterning steps applied to, respectively, the front and back side of the wafer. Photolithography was performed using a contact aligner (Quintel, Inc). The front side pattern included an array of hexagons placed on the equilateral grid and boundaries of fluidic channels and reservoirs. The back side pattern for each chip consisted of 10 through-wafer access ports arranged in an equally spaced pattern centered on an 18 mm diameter circle matching our fluidic interface. In the first step, wafers were spin-coated with a double-layer resist system (lift-off resist LOR-3A overcoated by positive tone photoresist 955CM-2.1, MicroChem Corp) capable of submicron resolution and optimized for the subsequent lift-off patterning of a 15 nm thick Cr masking layer. Physical vapor deposition of the 15 nm thick Cr layer was performed using an e-gun evaporator. Once a patterned Cr layer was formed on the front side, anisotropic deep reactive ion etching (DRIE) of silicon was performed using a Bosch process (System 100 Plasma etcher, Oxford Instruments) until

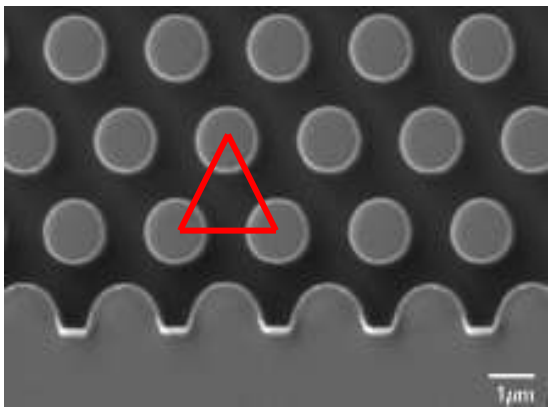

Figure 3.1 Geometrical placement of pillar structures positioned in an equilateral triangle pattern and terminated at the sidewall.

Table 1. Geometrical design parameters of fabricated pillar arrays				
Design iteration	Channel width (μm)	Pillar diameter (μm)	Pillar pitch (μm)	Etch depth (μm)
A1	1800	0.8	1.8	10-12
A2	2100	0.8	1.8	12-15
B1	250	1.4-1.6	2.4	18-25
C1	100	1.4-1.6	2.4	18-22

Table 3.1 Geometrical design parameters of fabricated pillar arrays.

targeted channel depths and pillar heights were achieved. The etched profiles and patterns were inspected using a contact profilometer (Dektak, Veeco Inc.) and scanning electron microscopy (JSM-7400F SEM, Jeol, Inc.). The front side processing was concluded by deposition of a nonconformal capping layer of silicon oxide with a nominal thickness in the range of 2.5 to 6 μm using PECVD (System 100 plasma deposition tool, Oxford Instruments). This step was followed by deposition of a 2 to 2.5 μm thick masking PECVD silicon oxide layer on the back side. Spincoating and photolithographic patterning of a positive tone photoresist (SPR 220-4.5, MicroChem Corp) on the back side created a mask for RIE to etch through the masking silicon oxide layer and to expose the Si substrate in the areas corresponding to the through-wafer ports. In the final processing step, Si in the exposed areas was etched entirely through the wafer using DRIE Bosch process. The processed wafers were scribed and cleaved and silicon oxide membranes remaining on the front side of the through wafer ports were removed manually using sharp pointed tweezers.

3.3.2 Sealing procedure

Adhesive cover windows were prepared by spincoating a photopatternable silicone compound (Dow Corning WL5150) to a film thickness of approximately 10 μm onto a 2 mm thick glass slides. The silicone coated glass slides were then cured using a modification of the procedures described previously. More specifically, the coated slides were placed onto hotplates using in the following sequence: 2.5 min at 90 °C, 2.5 min at 115 °C, and 5 min at 130 °C. Further curing of the silicone compound was initiated by a flood exposure on a contact aligner for 55 sec followed by heating on a hotplate for 15 min at 115 °C. Finally, the prepared glass cover window and the processed silicon microfluidic chip were placed into

contact, creating a sealed device, which was further cured for an additional 20 min at 90 °C under pressure of approximately 20 psi.

3.3.3 Fluidic interface

Our experimental setup included a fluidic interface designed to facilitate coupling of the fabricated chips and an external fluidic system that provided controlled eluent flow and sample injection. Fig. 3.2 depicts the main components of our experimental setup. The overall design of this system is analogous to those previously used in conjunction with medium pressure separation chips.[5, 15] A pressure regulator on the nitrogen tank provided nitrogen flow at pressures of up to 120 psi that was split into three channels. Each of the channels contained a precision regulator (Airtrol Components Inc.) that enabled further attenuation of pressure in the range of 0-120 psi with an accuracy of ± 0.1 psi. A 10-port valve (Valco Instruments Co. Inc.) provided switching between the two regimes: (i) injection of the sample plug into the main channel and (ii) sweeping the plug with the eluent. Fluorescein sodium salt (Sigma Aldrich) and Rhodamin B (Lambda Physik) in a form of methanol (Sigma Aldrich) or methanol-water solutions were used as model analytes in our sample injection experiments.

Table 3.2 shows the valve connections which provided the functionality required for sample plug injection and separation experiments. In addition to the sample and eluent channels, a third channel was included in our setup in order to explore prospective new modes of post-column detection, for instance, based on generation of fluorescence or Raman scattering signals [16, 17] upon addition of an appropriate reagent. This channel was controlled with a separate in-line shut-off valve (Idex Health and Science) inserted between the chip and a pressurized vessel.

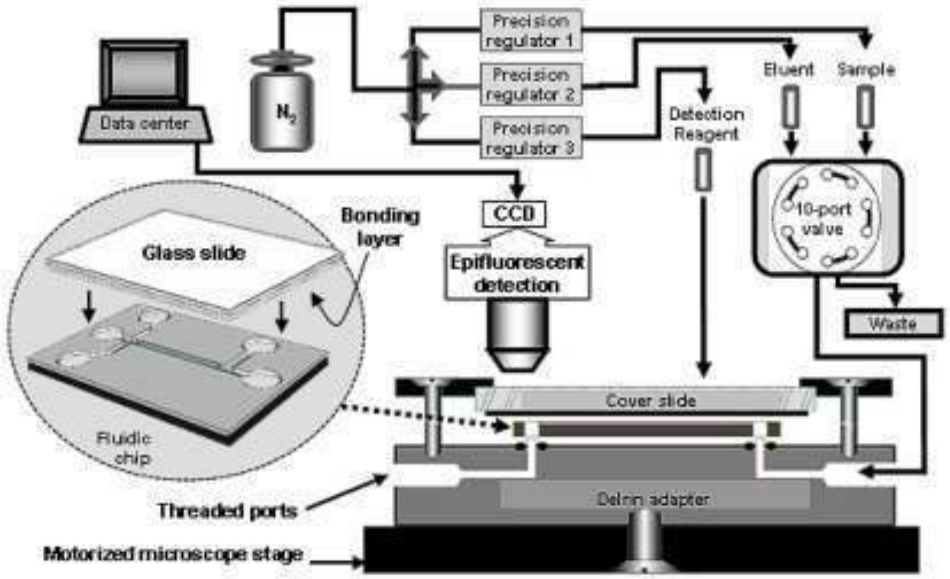

Figure 3.2 Schematic illustration of the experimental system with a fluidic interface for fluorescence imaging and functional characterization of the chips with pillar arrays.

Table 2. 10-port valve for injecting sample plugs into the column: port connections in the system shown in Fig. 1			
Eluent flow		Sample Injection	
(1) ⟷ (2)		(1) ⟷ (10)	
Eluent	Column inlet	Eluent	Blocked
(3) ⟷ (4)		(2) ⟷ (3)	
Blocked	Sample injection	Column inlet	Blocked
(5) ⟷ (6)		(4) ⟷ (5)	
Sample	Blocked	Sample injection	Blocked
(7) ⟷ (8)		(6) ⟷ (7)	
Column outlet	Waste	Blocked	Column outlet
(9) ⟷ (10)		(8) ⟷ (9)	
Sample Waste	Blocked	Waste	Sample waste

Table 3.2 10-port valve for injecting sample plugs into the column: port connections in the system shown in Fig. 1

In order to provide a quick, reliable and reversible connection of the chip to several fluidic inlets, we have designed and implemented a chip holder that also serves as a chemically inert fluidic manifold. The overall idea of this interface is analogous to that recently described by Burg *et al.*,[18] except that no electrical connections are needed for our experiments. The chip holder is comprised of a delrin disc with 10-32 threaded ports that can be readily attached to 1/16" OD tubing via standard HPLC type fittings (Upchurch Scientific Inc.). A series of 1/16" diameter holes drilled in the delrin disc form a fluidic manifold; top portions of the holes are machined to accommodate standard size O-rings (size 0, SIMRIZ perfluoroelastomer, Small Parts Inc.). An aluminum ring placed on top of the chip and secured by six screws provided the pressure necessary to hold the chip and seal it against the top surface of the manifold while allowing for microscope objective access, *i.e.* a clear view of 75 % of the area of the chip. The dimensions of the components in this assembly mounted onto a motorized microscope stage of a Nikon Eclipse 100 microscope were chosen to accommodate 5x to 20x microscope objectives with working distances as small as 3 mm. The microscope was equipped with a high pressure Hg light source, a multicolorfilter cube, and a Digital sight CCD camera (DS-2M, Nikon, Inc) controlled by NIS-Elements software. The joystick controlled motorized stage was used to match the field of view to the part of the channel with a sample plug. In particular, the motorized stage enabled convenient tracking of sample plugs along the fluidic channel during time series image acquisition at rates of up to 12 frames per second. The CCD camera acquisition timers were in the range of 80 to 120 ms.

3.4 Results and Discussion

3.4.1 Optimization of pillar shapes and the capping layer

Fabrication of enclosed pillar arrays with high aspect ratios and approaching perfectly cylindrical shapes required several iterations of fabrication sequence and down selection among alternative processes. This primarily involved optimization of the Bosch etch of silicon and non-conformal PECVD of silicon oxides. It is worthy to note that non-conformal deposition of PECVD layers is frequently used as a technological strategy for sealing or capping high-aspect-ratio structures for on-chip fluidic applications. Examples include a method for sealing high-aspect-ratio channels[10] and producing porous SiO_2 microfluidic channels for electrokinetic separations.[19] In the majority of such studies evolution of pore shapes as a result of the PECVD capping was not critical and, therefore, no particular attention was paid to maximizing non-conformality. By contrast, the predicted performance of highly ordered pillar arrays for pressure driven separations depends critically on the constant pore size along the channel depth.[20] Hence, our key task was to optimize a sequence of the Bosch etch and the PECVD process so that near perfect vertical sidewalls could be formed in the resulting structures.

Fine tuning of the Bosch etch involved varying durations of the etch and deposition steps (see Table 3.3 for recipe). Pillar arrays with nominal diameters of 0.8 to 1.6 μm, aspect ratios (height-to-diameter) as high as 25:1, and sidewall angles with deviations of less than 1 degree from vertical were obtained. These qualities were confirmed with the use of high resolution SEM. Reliance on a Cr film as a hard masking layer for Bosch etch rather than on a silicon oxide or photoresist appeared to be quite critical to reliably achieve high-aspect-ratio pillar shapes and to eliminate possible photolithographic artifacts. In addition to the

	T	Time	Pressure	RF power	ICP Power	C_4F_8 flow rate	SF_6 flow rate
	° C	s	mTorr	W	W	sccm	sccm
Deposition cycle	15	4	20	10	1750	140	1
Etch cycle	15	5	20	30	1750	1	120

Table 3.3 Bosch etch parameters optimized for etching of high-aspect-ratio pillars with diameters in the range of 0.7 to 1.6 μm and diameter-to-height ratios of up to 1:25.

excellent masking capacity of 15 nm thick Cr layers for the Bosch silicon etch, we also found that a slight overhang of a Cr mask formed on the top of each pillar were favorable for subsequent sealing with PECVD silicon oxide. In order to identify parameters of the Bosch etch that corresponded to optimal pillar geometries, SEM images of the pillar arrays were taken and analyzed at different stages during the nonconformal PECVD deposition of silicon oxide. As can be seen in Fig. 3.3 (a-c), in addition to capping pillar arrays with PECVD silicon oxide, this step tends to widen the pillars slightly, preferentially in their top portion. Therefore, pillars with slightly negatively slopped sidewalls (*i.e* with base narrower than top) resulted in almost perfectly cylindrical pillars after PECVD sealing was completed.

In order to achieve maximum degree of non-conformality and minimize "keyholing" effects, several parameters of the PECVD process were adjusted. In particular, relatively high pressures in the range of 1.4 to 1.8 Torr were used. Other parameters of the optimized PECVD process included RF power of 60 W and flow rates of silane (5% SiH_4 in Ar) and nitrous oxide ratio was selected to obtain nearly stoichiometric silicon oxide verified by a refractive intex of 1.46 to 1.47 at 633 nm. We found that deposition of silicon oxide on the sidewalls in the upper part of the pillars became much more pronounced at pressure below 1.4 Torr while pressures above 1.8 Torr did not cause further improvement in the capping layer. The PECVD parameter space used in this work is included in Table 3.4.

Fig. 3.3 (d-e) shows bird's eye views of the array before and after silicon oxide deposition. Figure 3.3e depict the inlet and outlet geometry that was introduced to inhibit the deposition process from overcoating the side walls of the pillars at the edges of the array. Without the use of this geometry Based on the obtained SEM images, it was evident that PECVD silicon oxide layer of varying thickness covers the whole surface of the pillars. This

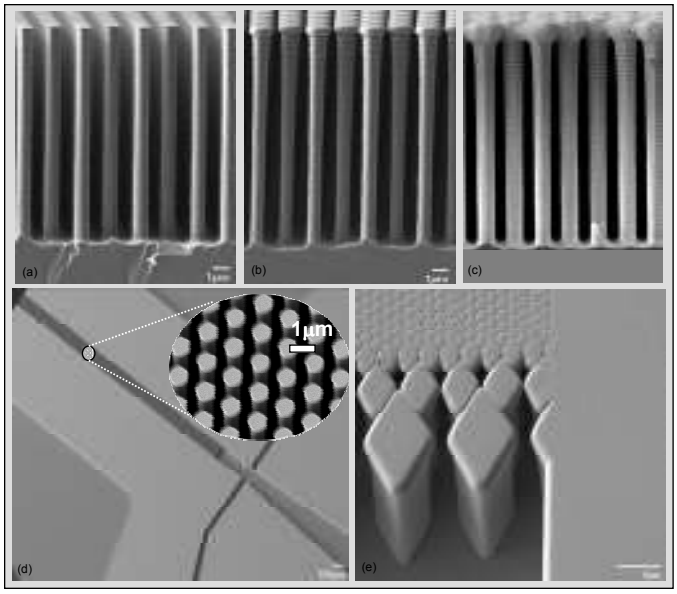

Figure 3.3 Top: Cross-sectional SEM images illustrating different stages of capping of high aspect ratio silicon pillars with PECVD silicon oxide layer: (a) before capping, (b) partially capped pillars and (c) completely sealed pillar array. Bottom: fragments of the chip viewed in the SEM at a 30 degrees tilt: (d) before and (e) after capping with PECVD silicon oxide.

Temperature	Pressure	High frequency RF power	SiH_4 (5%) / Ar flow rate	N_2O flow rate	Deposition rate
° C	mTorr	W	sccm	sccm	nm/min
250-350	1600-1800	50	170	710	100

Table 3.4 PECVD parameters optimized for high non-conformal deposition of SiO_2 on high-aspect-ratio pillars.

observation justified a streamlined fabrication sequence without any cleaning of the residual fluoropolymer inevitably formed on the pillar sidewalls as a result of the Bosch etch. The surface of the pillars was thus coated with a non-porous, rather hydrophilic PECVD silicon oxide layer. Although no retentive coating was created on the pillar surface for the purpose of the present study, surface silanol groups of the PECVD silicon oxide provide a straightforward pathway for functionalizing the pillars with a reverse phase coating via silane chemistry. Characterization of the loading capacity and retentive properties is a subject of our ongoing work.

In the case of pillars with nominal diameters of 1.4 μm centered on a hexagonal grid with 2.4 μm spacing, PECVD of a film with effective thickness (i.e. thickness on a planar part of the structure) of approximately 4 μm resulted in a pillar array completely sealed under silicon oxide capping layer. It appeared, however, that the capping layer also tends to seal the pillar array at its boundaries with an open channel, *i.e.* at the pillar array entrance and exit. This challenge was successfully addressed by introducing additional rows of larger, diamond-shaped features at the entrance and exit of the pillar array shown in Fig. 3.3 (e). We found that pillar arrays with two to three rows of such features always retained their permeability after PECVD sealing was completed.

3.4.2 Chip assembly

We explored a soft bonding approach based on a photopatternable silicone compound and established a procedure that provided a good yield and eliminated the need for more technologically involved anodic bonding used previously in fabricating analogous structures. It is generally accepted that, compared to anodic bonding, soft bonding is more forgiving with respect to minor defects and imperfections on the surfaces to be bonded. Among many

candidates, we identified WL5150 silicone as a compound well suited to form a 10 to 20 μm thick film by spincoating. Although we did not take advantage of the photo patterning capability of this compound, a combination of UV exposure and thermal baking provided gradual and well controllable curing. We identified the curing conditions, which yielded films with significant tackiness, in turn creating a reliable and reproducible seal upon contact with applied pressure without clogging channels.

Since WL5150 silicone forms a bonding film similar to other crosslinked silicones, its solvent compatibility was expected to be similar to that of the Sylgard PDMS extensively used in microfluidic devices and examined by the Whitesides group.[21] Silicone-solvent compatibility must be considered not only when performing separations, but also when functionalizing the pillars as solvents are commonly used when creating stationary phases for reverse phase chromatography. We examined the solvent effects of several organic solvents typically used as mobile phase components for chemical separations. Solutions of toluene, acetonitrile, ethanol, methanol, and isopropyl alcohol were flowed through the main pillar channel while observing device behavior using bright field microscopy. Using this method solvent flow and bubbles were easily visualized. All solvents tested, except methanol, produced leakage. Our assumption is that these solvents cause the PDMS to swell to a significant extent, eventually attacking the bonded device. During the constant flow of pure methanol through the device at 30 psi slight leakage was sometimes observed after 12 hours. However, when decreasing the mobile phase concentration to 70% methanol and 30% water, the structures showed no leakage during several weeks of continuous experiments. Pure water and aqueous solutions are also compatible with the bonding film. To test the pressure threshold of our device we tested our devices by flowing 50:50 methanol:water solution at

pressures of 0 to 150 psi. Leakage was observed at pressures above 100 psi. As will be justified in a later discussion, these pressures are adequate for many separation applications. Although the question of solvent compatibility is of high importance to chemical analysis, it should also be recognized that methanol-water solutions are routinely used solvents for many chromatographic applications. Another important similarity of this silicon elastomer and PDMS is the adsorption of small hydrophobic molecules in its surface. In analogy to other microfluidic structures with exposed PDMS surface, certain surface treatments may be used to eliminate or minimize these effects.[22]

Due to the swelling of the bonding silicone film in certain solvents, the cover windows can be removed from the assembled chips. This allowed us to reuse them after cleaning. We found that cover windows could be removed by soaking them in isopropyl alcohol or toluene. The residual bonding material could be removed from the chip and cover slide with common oxidizers, for instance, concentrated sulfuric acid.

3.4.3 Theoretical implications

A series of recent studies by Desmet's group provided extensive theoretical and computational analysis of various aspects of chromatographic beds based on ordered pillar arrays.[2, 23, 24] They provide compelling evidence that the potential of such perfectly ordered chromatographic beds is high. Consistent with the goals of our present work, we would like to reiterate and highlight specific implications of the pillar arrays with higher densities and characteristic sizes on a lower end of the previously explored range. Generally, the performance measure of a chromatographic separation system is given by:

$$H_T = H_c + H_{ec} \tag{1}$$

That is, total plate height, H_T, is a sum of the column, H_c, and the extra-column, H_{ec}, contributions given that band variances, σ^2, are additive. Extra-column variances are attributed to band dispersion due to injectors, connectors, and spatial and temporal contributions from detection. These are factors dependent on system design; they can be improved upon but seldom altogether eliminated. As can be seen from the relationship $H=\sigma^2/L$, the task of minimizing extra-column variances becomes progressively more critical and challenging as the length of the column, L, decreases, as extra-column variances inevitably become a larger contributing factor to the overall plate height for on-chip applications.

According to recent fluid dynamics studies [2, 23, 24] plate heights smaller than a particle (or pillar) diameter are possible in uniformly packed systems. A simplified semi-quantitative approach to evaluating the separation performance of ordered pillar arrays and predicting important scaling trends can be based on the well established empirical relationship described by van Deemter:

$$H_C = A + \frac{B}{u} + (Cs + Cm)u \tag{2}$$

wherein plate height, H_C, is dependent on eddy diffusion, A, longitudinal diffusion, B, and resistance to mass transfer in both the stationary and mobile phases, C_s and C_m, respectively. The A, B, and C terms in Equation 2 further expand to describe kinetics in a packed column as:[25]

$$H_C = 2\lambda dp + \frac{2\gamma D_M}{u} + \frac{qk' d_f^2 u}{(1+k')^2 D_S} + \frac{\omega dp^2 u}{D_M} \tag{3}$$

where d_p is particle diameter, k' is the partition coefficient, d_f is the average film thickness of the stationary phase, D_S and D_M are the diffusion coefficients in the stationary and mobile

phase, and q, λ, γ, and ω are independent factors conditional to the packing or ordering of the column.

As can be seen from Equations (2) and (3), dominating contributions from different terms may lead to plate heights that are either directly or inversely proportional to linear velocity, u. As a result of this relationship, there is an optimum velocity at which the terms combine to yield a minimum plate height. Differentiation of equations (1) and (2), *i.e.* $\delta H/\delta u = 0$, yields the equations for optimum mobile phase velocity, u_{opt}, and minimum plate height, H_{min}:

$$u_{opt} = \sqrt{\frac{B}{C}} \tag{4}$$

$$H_{\min} = 2\sqrt{BC} + A \tag{5}$$

For the purpose of our analysis, we will consider our ordered arrays of high aspect ratio pillars as performing similarly to a conventional packed column under close to ideal conditions. Although there is a strong dependence of plate height on packing factors (λ, γ, and ω), previously reached conclusions about advantages of perfectly ordered packed beds justify this approach to make conservative estimates. Ideally, all paths in the pillar bed are equivalent and there is no stagnant pools of mobile phase, Therefore, it is reasonable to assume that the packing factor λ approaching zero, and thus A-term contribution to plate height was not considered here.[4] Experimentally, the factor γ has yielded a value as low as 0.5 for the B-term,[26] which results in $B = D_m$. All solutes are assumed to be unretained, *i.e.* having a capacity factor of $k' = 0$, making $Cs = 0$. Finally, for homogeneous packing, the best case packing factor found in literature is $\omega = 0.02$,[27] so that $C_m = 0.02dp^2/D_M$. Central to our analysis is the strong dependence upon d_p, which is typically referred to as equivalent

of the particle diameter. It is worthy to note, however, that there is contention concerning this parameter. Alternatively to d_p, researchers use the term "domain size", d_{dom} , that combines the packing particle diameter and pore size, [6, 24, 28, 29] others describe d_p as dependent upon external porosity and pillar diameter.[30] While delineating the differences that stem from these alternative treatments is beyond the scope of our current study, we focus on the overall scaling trends, in particular, when characteristic sizes (whether it is d_p *or* d_{dom}) approach and extend into a submicron range.

By taking into account the assumptions above, we calculated H_{min} and u_{opt} for an unretained species and plotted results of these calculations as function of d_p (Fig. 3.4). As expected, the values of H_{min} decrease linearly with d_p. This relationship shown in Fig. 3.4 is consistent with more rigorous theoretical studies by Gzil *et al.* [2] that predict plate heights of 0.3 to 2 μm for uniform 2-D pillar arrays with sizes of 1-3 μm (dependent upon *k'* values), and also with experimental plate height values of H=0.9 which were obtained for a uniform pillar array column with a pillar diameter of 4.45 μm.[1] As previously discussed, this is a significant improvement compared with both traditional packed and monolithic silica columns.[31]

While decreasing d_p increases the separation efficiency, it is important to ensure that reduced pore sizes do not translate into pressure requirements beyond what would be practically feasible. Thus, along with estimated plate heights, Fig. 3.4 shows optimum velocities calculated as a function of d_p for analytes with various diffusion coefficients, D_M. We used two values of D_M that are representative for typical analyte samples with molecular masses of roughly 100 and 100,000 amu. [32]

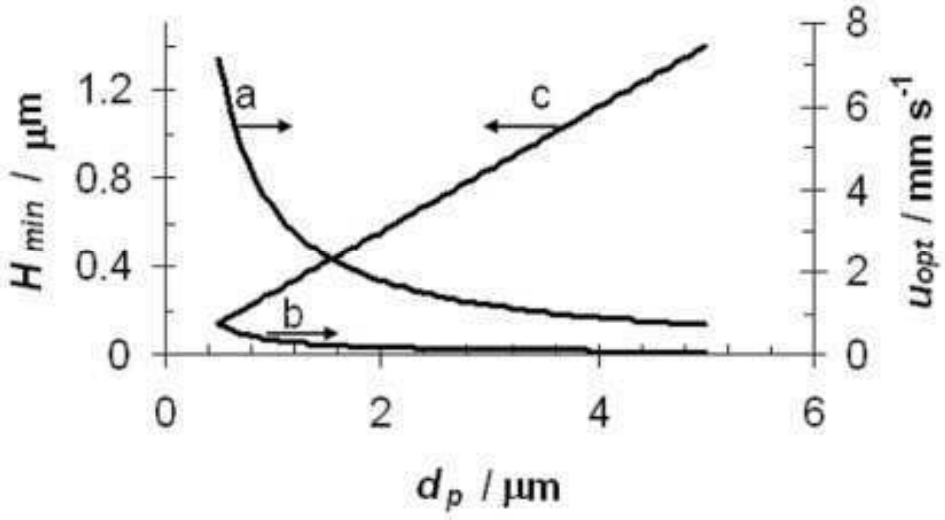

Figure 3.4 Theoretically predicted dependencies of u_{opt} (a and b) and H_{min} (c) and on pillar size, d_p. Dependencies of u_{opt} are calculated for $D_M = 5\text{x}10^{-6}$ cm ^{2} s $^{-1}$ (curve a) and $D_M = 5\text{x}10^{-7}$ cm ^{2} s $^{-1}$ (curve b), diffusivities representative of typical samples with molecular masses of 100 and 100,000 amu, respectively.

Considering that $N=L/H$, where N is plate number, well ordered on-chip arrays with submicron *dp* have the potential to achieve column performances similar to monolithic and packed columns of conventional lengths. A standard 6" or 8" wafer can accommodate designs with straight channels up to approximately 10 cm long. For a pillar diameter of 1.9 μm, a 10 cm long array was calculated to yield N=130,000.[6] It is, however, difficult to fit more than one chip with 10 cm long columns on a single wafer. Although serpentine channels can be designed to decrease the chip size, column curvature is known to have an adverse effect on band dispersion and, as a rule, should be avoided. Therefore, pillar arrays scaled down to submicron characteristic sizes is a prerequisite of high performance separation beds with a footprint comparable to that of integrated circuits.

Our implemented design accommodates 9 chips per 100 mm wafer, each with a 10 mm long pillar array integrated into a system of fluidic channels. If theoretically estimated H_{min} is achieved, this design would yield N=25,000, a sufficient plate number for many applications. Importantly, such a short column length should also translate into decreased analysis times.

Apart from technologically nontrivial aspects of dense pillar arrays with submicron effective pore sizes, their operation may involve challenges of a more fundamental nature, in particular due to the squared dependence of pressure on d_p. Described by Darcy's law and modified for microscopic flow through a packed bed this dependency can be written as: [33]

$$\Delta P = \frac{u_o \eta L \phi}{dp^2} \tag{7}$$

where η is viscosity and ϕ is the flow resistance parameter. Of importance to chip applications is the relationship of column length to pressure. Since pressure is directly related

to column length it is easy to surmise that decreasing the length of the column may help to alleviate the possible pressure issues that could arise from decreasing pillar/gap dimensions.

To assess permeability of the implemented pillar arrays, flow rate data were collected under varying input pressures. We found that the pressures required to meet the u_{opt} plotted in Fig. 3.4 are readily accessible for our pillar arrays, even with the employed soft bonding technique. For our C1 design (see Table 3.1), the pressures in the range of 5-25 psi were sufficient to achieve mobile phase velocities in the range of 0.1 to 0.5 mm s^{-1} (Figure 3.5) The experimentally measured pressure-flow rates dependency for C1 design showed excellent correlation (R^2= 0.989) with a linear function u_o= 0.026 ΔP , where units of velocity and pressure are mm s^{-1} and psi, respectively. A notable trend in the plot shown in Fig. 3.4 is that u_{opt} increases as d_p decreases. This trend means that, as the pillars are scaled down, it may become more challenging to achieve optimal velocities unless the chip retains its functionality under progressively higher pressures. Yet as already mentioned above, shorter columns are proportionally more permeable and recent study of pillar arrays predict permeability also increases with ordered channel packing. [24]

3.4.4 Functional tests

In order to evaluate the overall performance of the designed system and identify areas most critical for its further improvement, we conducted a series of basic functionality tests that included: (i) pressurizing the channels and checking for leaks; (ii) injecting a model fluorescent analyte and analyzing the analyte bands using fluorescence microscopy; and (iii) characterizing permeability (separation impedance) of the pillar array by measuring fluid velocity as function of pressure. The protocols for these tests were selected to be analogous

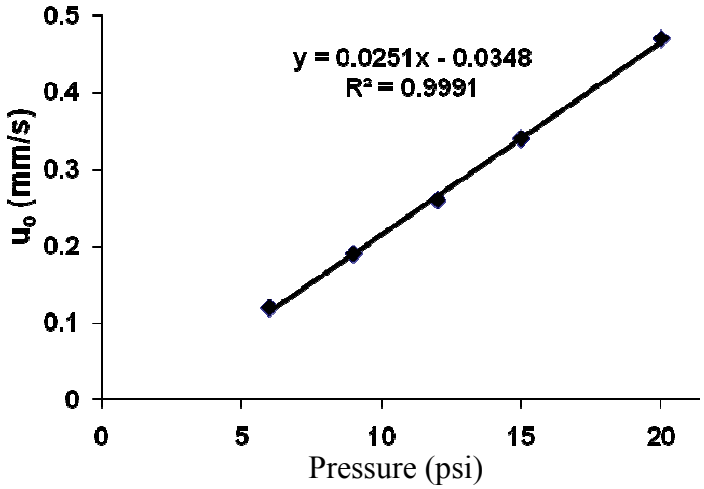

Figure 3.5 Flow rate study of rhodamine B in pure methanol. The linear velocity of the band was determined by collecting time gated fluorescent images as the sample eluted from the pillar channel.

to those utilized previously[1] in characterizing similar pillar arrays with larger pillar diameter so that the results of our test could be analyzed comparatively.

The obtained analyte plug and flow images are shown in Fig. 3.6. In order to create discrete sample plugs for injection into the pillar bed, our design incorporated crossed channels geometry upstream from the array as shown in Fig. 3.6(a). Using the manual 10-port valve described in the previous section we performed a two-step injection procedure. In the first step, the sample channel crossing the main channel was loaded by flowing the sample from the sample inlet to the sample waste while the column inlet and outlet were closed. In the second step, the sample plug seen in Fig. 3.6(a) was swept into the column by closing the sample inlet and waste ports, and opening the column inlet and outlet. Despite timing uncertainties of manual valve switching, this injection procedure could produce sample plugs with volume below 30 pL.

Fig. 3.6(b) and Fig. 3.6(c) show the sample plug behavior as it enters the pillar bed and 6 mm down the pillar array, respectively. The artifacts seen in the images of the pillar beds in the assembled chips resulted from the air cavities formed frequently upon bonding of the chip and the cover. We found that, upon curing, the silicone elastomer tends to produce a film with slightly undulated (wrinkled) surface, which, in turn, makes it difficult to form a defect free bond. Remarkably, such sealing defects had no adverse effect on the flow behavior and column functionality since the array area of the channel was additionally sealed by the capping silicon oxide layer. This highlights an important advantage of our technological approach that relies on soft bonding combined with pillar capping with a PECVD silicon oxide layer: the silicon oxide layer forms a robust scaffold, protects the pillars from damage and simultaneously seals the pillar bed. On the other hand, in our

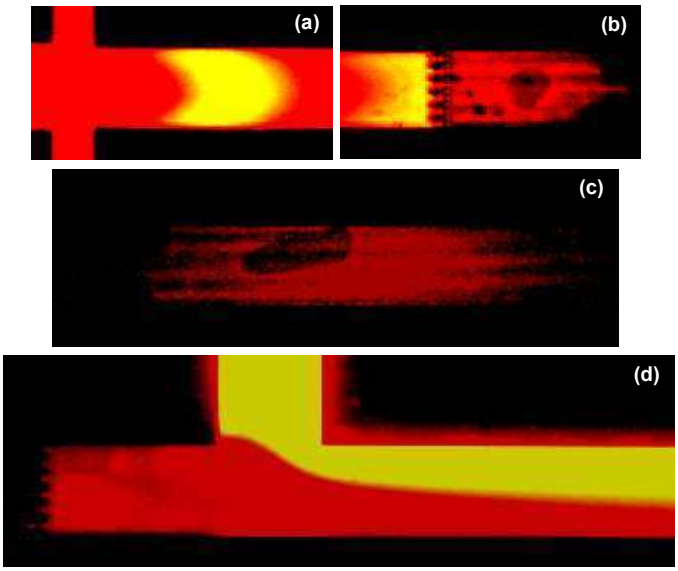

Figure 3.6 Fluorescence micrographs of sample plugs injected into the 100 μm wide fluidic channel with an enclosed pillar array: (a) prior to entering the pillar bed, (b) entering the pillar bed and (c) 6 mm downstream inside the pillar bed. The broadening interdiffusion zone at the interface of laminar flows exiting the pillar array and the reagent channel is also shown (panel d). Fluid flow is from left to right. Images obtained using $1x10^{-4}$ M fluorescein sodium salt in MeOH. Contrast and brightness of the images were adjusted to improve their visual clarity.

preliminary fabrication runs, there were instances when the silicon oxide capping layer did not seal the pillar array completely. In these cases, permeation of fluorescent sample through the capping layer and its adsorption on the silicone layer could be visualized; nonetheless, the chips maintained its functionality.

Fig. 3.6 (d) shows the flow of a fluorescein solution injected through the auxiliary reagent port into a channel merging with the post-column flow. As expected, the exact flow patterns in this area were found to depend strongly on the pressure difference between the column inlet and the reagent ports. The observed fluorescence images of the sample/reagent interdiffusion zone provide encouraging evidence that, although the flow remains laminar, noticeable flow mixing occurs within 5 mm from the column exit. Therefore, the additional post-column reagent port can be used as a viable means for on-chip modification of the sample exiting the column without any significant band disturbance. We believe this indicates a promising direction in addressing the need to derivatize samples so that they are detectable with a wider range of detection schemes, for instance, based on fluorescent tagging or mixing of a silver colloid to induce surface enhanced Raman signals.[16, 17, 34] Implementation and evaluation of these approaches is a subject of our future work.

When both the column outlet and the auxiliary reagent port were closed during the sample injection phase, sample plug shapes indicative of a parabolic flow profile were observed (Fig. 3.6). In the subsequent experiments, we achieved substantial improvement of the plug shapes be leaving the auxiliary reagent port open during the loading phase. Although we could not establish the exact reason for such an improvement, we believe it was related to more abrupt changes in pressure and flow velocity in the system with the column outlet was completely blocked during sample injection. Previous studies indicate that

profiles of the pressure driven flow in beds of ordered pillar arrays are not always parabolic and, more importantly, negligible local disturbances of the flow at the side walls are possible.[14] In particular, the flat side wall design was shown to create the side wall effect opposite to a commonly observed parabolic flow profile while side walls with 66% of the pillar diameter protruding from the wall caused negligible disturbances of the flow in the wall vicinity.[14]

Using the design (see Table 3.1 for details), analysis of band dispersion inside the pillar array was performed by collecting time series images as the sample band migrated along the pillar bed and plotting the intensity profiles, as depicted in Fig. 3.6. As stated in previous sections, no additional stationary phase coating was employed. As can be concluded from our fabrication sequence and SEM images of the pillar arrays (see for instance Fig 3.3(a-c)) the pillar surface is presented by PECVD silicon oxide, and therefore, the resulting pillar arrays have little to no retentive properties. In particular, the single component sample of 1×10^{-4} M Rhodamine B in pure methanol was expected to exhibit no retention.

It should be noted that the presence of densely spaced high-aspect-ratio pillars significantly decreases efficiency of the optical excitation of the dye and collection of the light emitted within the pillared area. This optical effect is common for high aspect ratio silicon structures, in which light (either incident or generated within) undergoes numerous partial reflections so that very small fraction of the light escapes the structure. In other words, gaps between the pillars act in analogy to blackbody cavities. We found that, in the case of submicron inter-pillar gaps with height-to-width ratios in excess of 20:1, this effect becomes strong enough to attenuate measured fluorescence intensity by approximately an order of

magnitude in comparison with channel areas without pillars. Due to this factor, the acquired fluorescence images of the sample within pillared areas are characterized by rather low signal-to-noise ratios (see Figure 3.7), which, in turn, make analysis of the band dispersion inside the pillar array more challenging. On the other hand, the efficiency of post-column fluorescence band detection is not affected by the blackbody cavity effect of the pillar array.

Since acquisition time of up to 120 ms were used in our experiments, it is reasonable to assume that imaging of fluorescence sample bands moving at linear velocities of approximately 1.7 mm s^{-1} involved a significant degree of "motion blur". We found, however, that a contribution of the motion blur effect to apparent widening of a sample band dispersion, σ, is much less that a product of exposure time, Δt, and linear flow velocity,u. The exposure time effect is particularly small in the case of imaging sample bands with a wide gaussian profile. We quantified apparent band widening due to a non-zero exposure time by analyzing computer generated gaussian profiles (see Figure 3.8 a-c) and found that for a liner flow velocity of 1.7 mm s^{-1} and band dispersion, σ, in the range of 50 to 200 μm, 90 ms exposure time corresponds to, respectively, a 24 to 6 μm increase in apparent dispersion. Hence, the exposure time effect is stronger for shorter sample bands, and therefore, it tends to decrease apparent band dispersion. We found that for a sample plugs with σ >120 μm, the camera blur effect adds less than 10% error when deducing the on-column plate height $H= \Delta\sigma_x^2/\Delta x$ from our experimental data. Therefore, sample plugs with σ >120 μm were selected and used in our plate height analysis.

Recognizing somewhat limited sensitivity of our fluorescent measurements, we assumed that a part of the sample band far from its center corresponded to the fluorescence intensity level below the noise floor. We further assumed that there is no change in the

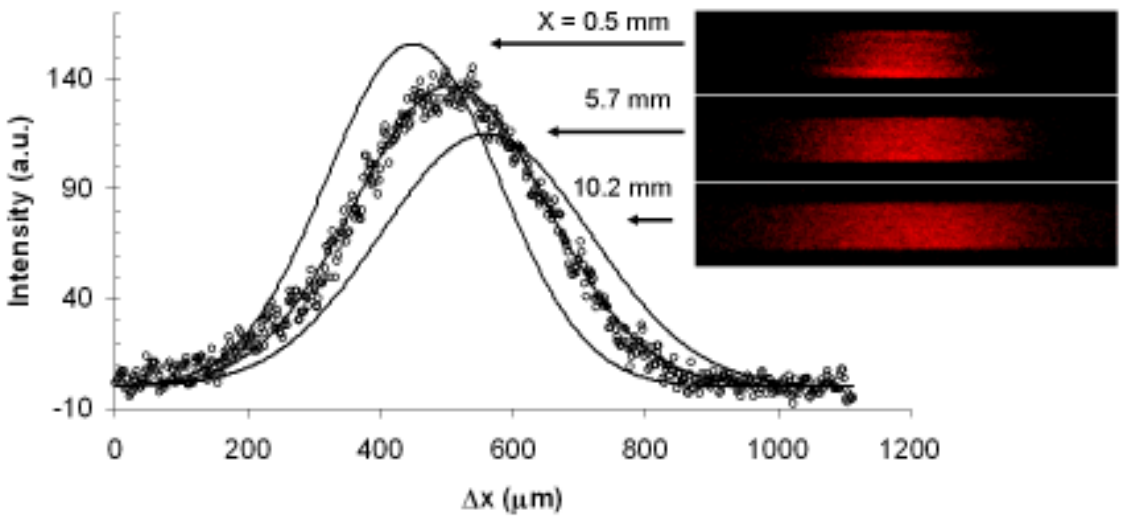

Figure 3.7 Intensity profiles and corresponding fluorescence images of a dye plug (injected as 10^{-4} M Rhodamine B solution in MeOH) migrating down the pillar bed of design C1 (see Table 1) at a velocity of 1.7 mm s^{-1}. The experimental intensity profile (open circles in the plot) extracted from the image of the plug centered at x=5.7 mm is shown together with the Gaussian fit (solid lines) of intensity profiles for each image (see details of the fitting procedure in the text). Intensity profiles were measured using unprocessed images prior to any adjustments in brightness and contrast. Contrast and brightness were subsequently adjusted to improve visual clarity of the images shown on the right.

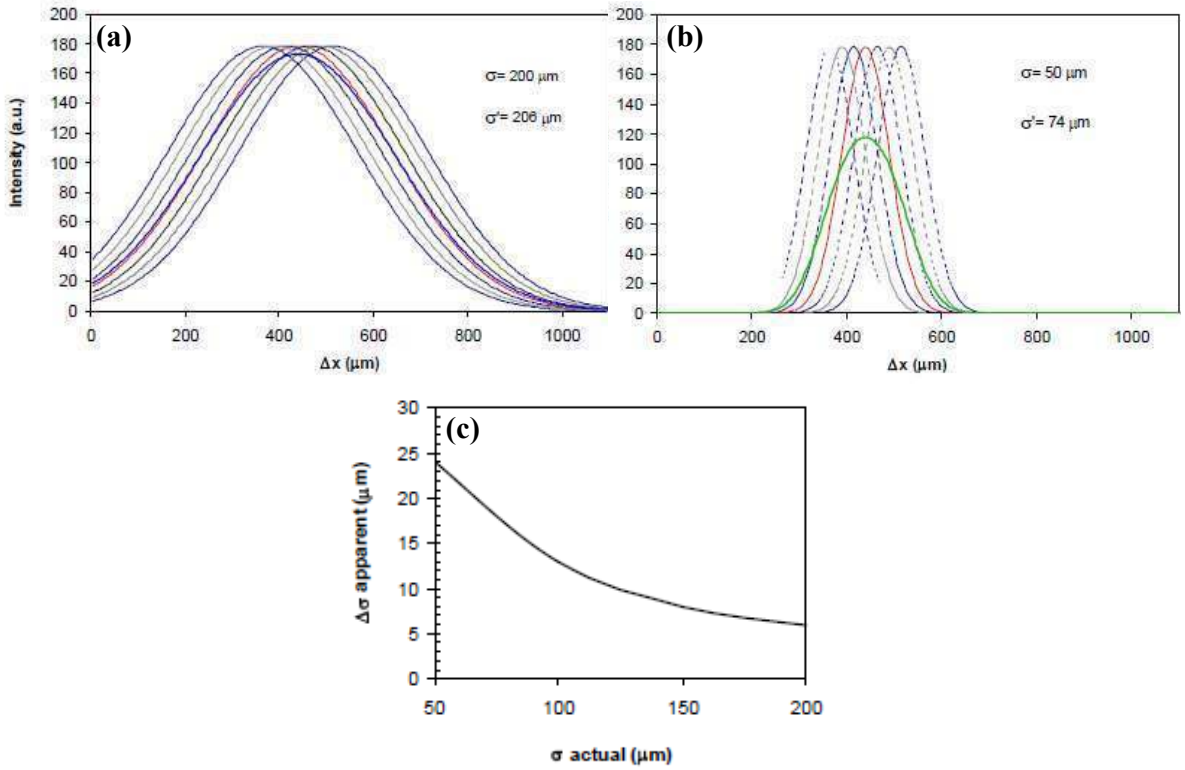

Figure 3.8 (a) A series of Gaussian profiles with σ= 200 μm (gray and red lines) and maximum shift along x axis by Δx=150 μm. Analysis of their normalized superposition (blue line) yields σ'=206 μm. (b) The same shift of a series of Gaussian profiles with σ= 50 μm (dashed lines) yields anormalized superposition characterized by σ'=74 μm (solid green line) (c) Dependency of apparent band broadening on the actual band dispersion, σ. The sample plug travel distance during the camera exposure time, Δx=150 μm.

optical response factor or loss of sample material within the column, and, therefore, the area under intensity profiles can be expected to remain constant. Next, the peak height and the dispersion, σ^2, were determined by fitting the experimental data (symbols in Fig. 3.7) to a Gaussian distribution (solid lines in Fig.3.7) using the non-linear fit function in Origin 8. As can be seen in Fig. 3.7, the experimental data fit reasonably well to the Gaussian distribution when the noise floor is taken into account.

The on-column plate height ($H=\Delta\sigma_x^2/\Delta x$) experimentally determined by analyzing intensity profiles centered at x= 0.5 mm, x=0.57mm, and and x=10.2 mm (Fig. 3.7) was found to be H=0.76 μm. This indicates that experimentally observed band dispersion is noticeably higher than the theoretically predicted value of H_{min} =0.28 μm. Taking into account previously reported data on the band dispersion in ordered pillar arrays with larger domain sizes[14], a conclusion can be made that disturbances near the channel side walls as well as bottom and top walls are largely responsible for the difference between the theoretically predicted and experimental values. Indeed, side wall effects are always present and inevitably contribute to on-column band dispersion. As the pillar diameter and channel width decrease, the local flow at the side walls becomes more sensitive to the imperfections and inaccuracies in the pillar array design. In addition to the channel side wall effects, the following factors could contribute to the deviations of the experimentally determined plate heights from theoretical predictions: (i) the system was operated at flow velocities below the theoretically predicted optimal u_{opt} = 3.2 mm s^{-1}, (ii) as discussed previously, a finite A-term in the van Deemter equation may exist even in a perfect pillar array, and (iii) the B and C terms of the van Deemter equation were treated under the assumption of an ideal packed bed with perfectly uniform sizes (iv) a more rigorous model may more accurately describe the

behavior of pillar array separation beds. Nonetheless, the value of H=0.76 μm, corresponding to remarkably low on-column dispersion, shows improvement upon previous reports and validates the motivation for additional studies of submicron pillar arrays with applications for on-chip separations and analysis.

It is important to emphasize that the theoretically evaluated plate height, H_C, is entirely a result of variances (*i.e.* band dispersion) intrinsic to the column, as described by equation (1). The total plate height of the system incorporates additional contributions determined by other factors, in particular, the finite length of the injected sample plug. While our current chip designs meet the goal of a streamlined fabrication sequence and characterization of on-column band dispersion, we recognize that improvements in the sample injection will involve significantly more complex chip designs. The task of precise high-pressure injection of substantially shorter than 100 μm sample plugs with volumes below 10 pL is not trivial. Analysis of the literature data as well as our own observations indicate that controllable injection of such sample plugs will require on-chip sample manipulation, for instance by using on-chip valves. Several types of previously developed on-chip microfluidic valves can be integrated with ordered separation pillar arrays described in the present study. Identifying and implementing the best strategy to injection of very short sample plugs is a subject of our ongoing effort. Our preliminary analysis of several different approaches, in particular bottom slit injection, [5] virtual valve approach, [37] on-chip mobile monolith, [38] and elastomer membrane valves, [39] indicate that the latter is most promising and compatible with the enclosed pillar arrays described herein.

3.5 Conclusions

Compared to traditional separation columns, fundamental advantages of ordered pillar arrays were unambiguously demonstrated in recent theoretical and experimental studies. Technological and experimental challenges of such systems, however, have been an impeding factor for the wide spread adaptation of this novel concept. Theoretical estimates indicate that very dense pillar arrays scaled down to submicron characteristic sizes is a prerequisite of separation beds suitable for high performance separation with a footprint comparable to that of integrated circuits. Therefore, a viable technological path toward submicron pillar arrays with submicron theoretical plate heights is a critically significant milestone in this area. By refining well established fabrication processes and implementing novel technological sequences, we demonstrated ordered uniform beds of pillar arrays that are integrated into a system of on-chip fluidic channels and are scalable well into the submicron range. The implemented structures satisfy fundamental criteria of high performance separation in the on-chip format while also providing reasonably high fabrication throughput. We anticipate that the demonstrated system will facilitate further experimental studies of ordered pillar arrays with applications in pressure driven liquid chromatography as well as newly emerging separation techniques.[8,18,40]

3.6 Acknowledgements

A portion of this research at Oak Ridge National Laboratory's Center for Nanophase Materials Sciences was sponsored by the Scientific User Facilities Division, Office of Basic Energy Sciences, U.S. Department of Energy. This research was also supported by the US Environmental Protection Agency STAR Program under grant EPA-83274001 with the University of Tennessee.

3.7 References

[1] H. Eghbali, W. De Malsche, D. Clicq, H. Gardeniers, G. Desmet, Lc Gc Europe, 20 (2007) 208.
[2] P. Gzil, N. Vervoort, G.V. Baron, G. Desmet, Analytical Chemistry, 75 (2003) 6244.
[3] F.E. Regnier, Hrc-Journal of High Resolution Chromatography, 23 (2000) 19.
[4] M.R. Schure, R.S. Maier, D.M. Kroll, H.T. Davis, Journal of Chromatography A, 1031 (2004) 79.
[5] W. De Malsche, H. Eghbali, D. Clicq, J. Vangelooven, H. Gardeniers, G. Desmet, Analytical Chemistry, 79 (2007) 5915.
[6] M. De Pra, W. De Malsche, G. Desmet, P.J. Schoenmakers, W.T. Kok, Journal of Separation Science, 30 (2007) 1453.
[7] B. He, F. Regnier, Journal of Pharmaceutical and Biomedical Analysis, 17 (1998) 925.
[8] L.R. Huang, E.C. Cox, R.H. Austin, J.C. Sturm, Science, 304 (2004) 987.
[9] D.W. Inglis, J.A. Davis, R.H. Austin, J.C. Sturm, Lab on a Chip, 6 (2006) 655.
[10] P. Mao, J. Han, Lab on a Chip, 9 (2009) 586.
[11] D.S. Tezcan, A. Verbist, W. De Malsche, J. Vangelooven, H. Eghbali, D. Clicq, G. Desmet, P. De Moor, 2007 Ieee International Electron Devices Meeting, Vols 1 and 2 (2007) 839.
[12] L. Sainiemi, H. Keskinen, M. Aromaa, L. Luosujarvi, K. Grigoras, T. Kotiaho, J.M. Makela, S. Franssila, Nanotechnology, 18 (2007).
[13] N. Kaji, Y. Tezuka, Y. Takamura, M. Ueda, T. Nishimoto, H. Nakanishi, Y. Horiike, Y. Baba, Analytical Chemistry, 76 (2004) 15.
[14] M. De Pra, W.T. Kok, J.G.E. Gardeniers, G. Desmet, S. Eeltink, J.W. van Nieuwkasteele, P.J. Schoenmakers, Analytical Chemistry, 78 (2006) 6519.
[15] E. Chmela, R. Tijssen, M. Blom, H. Gardeniers, A. van den Berg, Analytical Chemistry, 74 (2002) 3470.
[16] W.F. Nirode, G.L. Devault, M.J. Sepaniak, Analytical Chemistry, 72 (2000) 1866.
[17] R.J. Dijkstra, F. Ariese, C. Gooijer, U.A.T. Brinkman, Trac-Trends in Analytical Chemistry, 24 (2005) 304.
[18] T.P. Burg, A.R. Mirza, N. Milovic, C.H. Tsau, G.A. Popescu, J.S. Foster, S.R. Manalis, Journal of Microelectromechanical Systems, 15 (2006) 1466.
[19] R. Costa, K.B. Mogensen, J.P. Kutter, Lab on a Chip, 5 (2005) 1310.
[20] J. De Smet, P. Gzil, G.V. Baron, G. Desmet, Journal of Chromatography A, 1154 (2007) 189.
[21] J.N. Lee, C. Park, G.M. Whitesides, Analytical Chemistry, 75 (2003) 6544.
[22] M.W. Toepke, D.J. Beebe, Lab on a Chip, 6 (2006) 1484.
[23] J. De Smet, P. Gzil, N. Vervoort, H. Verelst, G.V. Baron, G. Desmet, Analytical Chemistry, 76 (2004) 3716.
[24] P. Gzil, N. Vervoort, G.V. Baron, G. Desmet, Journal of Separation Science, 27 (2004) 887.

[25] J.M. Miller, Chromatography: Concepts and Contrasts, John Wiley & Sons, Inc, New Jersey, 2005.
[26] G. Deininger, Chromatographia, 9 (1976) 251.
[27] C.F. Poole, Elsevier, Amsterdam, 2003, p. 32.
[28] H. Minakuchi, N. Ishizuka, K. Nakanishi, N. Soga, N. Tanaka, Journal of Chromatography A, 828 (1998) 83.
[29] P. Gzil, N. Vervoort, G.V. Baron, G. Desmet, Analytical Chemistry, 76 (2004) 6707.
[30] G. Desmet, D. Cabooter, P. Gzil, H. Verelst, D. Mangelings, Y. Vander Heyden, D. Clicq, Journal of Chromatography A, 1130 (2006) 158.
[31] G. Desmet, D. Clicq, P. Gzil, Analytical Chemistry, 77 (2005) 4058.
[32] B.L. Karger, L.R. Snyder, C. Horvath, An Introduction to Separation Science, John Wiley & Sons, Inc., Canada, 1973.
[33] J.C. Giddings, Unified Separation Science, John Wiley & Sons, Inc., United States of America, 1991.
[34] M.J. Sepaniak, W.F. Nirode, G. Devault, N.V. Lavrik, Abstracts of Papers of the American Chemical Society, 223 (2002) 015.

Chapter 4

High-aspect-ratio, silicon oxide-enclosed pillar structures for microfluidic liquid chromatography

Portions of Chapter 4 are an adaptation of a research article *Analytical Chemistry* 2010, 82 (22), pg 9549-9556. This article further characterizes the surface of silicon oxide pillar arrays, and discusses their ability to separate chemical species. Separations were carried out under pressure-driven flow conditions using an elastomeric bonding technique which resulted in silicone contamination of the device, producing separation behavior similar to reverse phase chromatography. After publication, additional chromatographic studies were performed using dynamically modified and gas phase modified pillar array channels (see sections 4.3.2 and 4.4.4).

4.1 Abstract

The present paper discusses the ability to separate chemical species using high-aspect-ratio silicon oxide enclosed pillar arrays. These miniaturized chromatographic systems require smaller sample volumes, experience less flow resistance, and generate superior separation efficiency over traditional packed bed liquid chromatographic columns; improvements controlled by the increased order and decreased pore size of the systems. In our distinctive fabrication sequence, plasma enhanced chemical vapor deposition (PECVD) of silicon oxide is used to alter the surface and structural properties of the pillars for facile surface modification while improving the pillar mechanical stability and increasing surface area. The separation behavior of model compounds within our pillar systems indicated an unexpected hydrophobic-like separation mechanism. The effects of organic modifier, ionic concentration, and pressure-driven flow rate were studied. A decrease in the organic content of the mobile phase increased peak resolution while detrimentally effecting peak shape. Resolution of 4.7 (RSD=3.7%) was obtained for nearly perfect Gaussian shaped peaks,

exhibiting plate heights as low as 1.1 μm and 1.8 μm for fluorescein and sulforhodamine B, respectively. Contact angle measurements and DART mass spectrometry analysis indicate that our employed elastomeric soft bonding technique modifies pillar properties creating a fortuitous stationary phase. This discovery provides evidence supporting the ability to easily functionalize PECVD oxide surfaces by gas phase reactions.

4.2 Introduction

Recent research has indicated that advances in on-chip separation technology can be gained by adapting fabrication practices similar to those developed for the semiconductor industry. Current processing techniques have the ability to decrease defined geometries to nanoscale dimensions with nanometer accuracy, thereby becoming well suited for lab-on-chip platforms. In addition to the open channel geometries prevalent in nano chromatography applications,[1-5] recent research has focused on creating chromatographic supports integrated within fluidic channels.[6-9] This alternative approach to packed bed chromatography, first proposed by Regnier et al.,[10, 11] introduced the concept of creating pillar arrays within channels with the capability of tailoring pillar position, size, shape, and pitch in a highly controllable and ordered manner. Extensive theoretical studies[12-14] and experimental studies[15] have shown that this increased order imparts fundamental advantages over the traditional packed and monolithic columns. These improvements include eliminating the polydispersity of packing particle size and heterogeneity of the packing porosity which limits separation efficiency. Additional advantages identified by recent studies show that nearly perfect ordered pillar arrays are highly permeable with less flow

resistance than comparable traditional packed and monolithic columns.[6, 12, 16, 17] This characteristic lends itself to the application of pressure-driven liquid chromatography.

Reports in the recent literature suggest that as characteristic dimensions of separation channels decrease, nanoscale modes of separation may arise under pressure-driven conditions. These include electrostatic-derived hydrodynamic separations[18-20] and streaming potential generated electrokinetic separations.[21-25] Additional novel separation mechanisms, like the use of deterministic lateral displacement[26] discovered for particle separation, have been performed by manipulating pillar positions to impart separation by altering the path taken by varying particles. In traditional packed bed liquid chromatography, a stationary phase is distributed onto solid supports for a mobile phase – stationary phase partitioning based separation, governed by a solutes retentive behavior within the system.

Among the few applications of pressure-driven separations previously explored for pillar array systems, modification of the pillar supports by a hydrophobic reverse phase stationary component is the most common. Desmet and coworkers have conducted impressive chromatographic separations using C8 and C18 liquid phase modifications of both porous[27] and non-porous[16, 28, 29] pillar arrays. While these experiments have clearly demonstrated the feasibility of applying this emerging technology to real world samples, they have also identified fundamental and practical challenges which must be addressed for these chip level devices to be able to progress towards competing with traditional packed bed HPLC columns.

Firstly, to achieve the same mass loadability as conventional HPLC columns, lab-on-chip devices will require geometries or treatments which would increase the surface area available for chromatographic exchange. Theory provides convincing evidence of the

advantages gained with the use of high surface area porous pillar arrays.[13, 14] Recent innovations by Malsche et al.[30] and Tiggelaar et al.,[31] which introduced the use of electrochemical anodisation to create porous silicon shell pillars, were highly successful in increasing the surface area of pillar arrays. However, they also sacrificed the mechanical stability of high-aspect-ratio pillars fabricated in this manner. Secondly, liquid phase functionalization of pillar surfaces is not trivial, as it is an intensive and timely procedure that has a poor success rate for usable devices due to the frequency of occlusion.[28] We report, herein, efforts to meet these challenges.

In our previous work[6] we introduced a fabrication sequence which implemented ordered high-aspect-ratio pillar arrays as a robust, uniquely sealed network of pores integrated into a system of fluidic channels. These enclosed systems increased the mechanical stability of the pillars. This allows for pillar diameters to be scaled down to 1 μm or less, having aspect ratios of approximately 20:1, while maintaining the ability to withstand damages potentially incurred during processing, handling, and sealing of the devices. The pillar arrays were tested for chromatographic efficiency and produced plate heights (H) as low as 0.7 μm.

In this study we build upon our earlier work and further analyze the effect of this enclosure procedure on the separation characteristics of the pillar system. Examination into the pillar side walls produced during this fabrication sequence shows that this streamlined fabrication process produces beneficial surface characteristics for improving mass loadability as well as stationary phase functionalization. This includes generating roughened side walls absent of deep pores, thereby increasing surface area without creating deep non-swept voids which can detrimentally contribute to band variances caused by resistance to mass transfer in

the stationary phase. In this aspect the pillars also act similar to core-shell type materials in which the packing structure decreases the average path length of retained solute particles during the diffusion process.[32, 33] In addition, the nature of the PECVD silicon oxide is known to increase surface silanol concentrations for facile stationary phase functionalization. As an alternative to liquid phase functionalization, Mery et al. demonstrated a vapor phase silane procedure which made the chip coatings process more efficient and eliminated the clogging issues. [34] Herein we analyze a serendipitous gas phase modification accomplished by the elastomeric cover window components. The retentive behavior of two model fluorescent compounds is studied.

4.3 Experimental

4.3.1 Channel fabrication

Fabrication of the fluidic chips with integrated injection system and enclosed silicon oxide layer was performed using the method described in our previous work.[6] The fabrication sequence involved photolithographic processing of both the front side (fluidic channels including 3 inlet ports orientated in a cross junction with a single straight channel, approximately 10 mm long x 50 μm wide, leading to a single outlet port) and backside (through-wafer access ports) of a standard silicon wafer. In the first step, the front side pattern were defined using a double-layer resist system (LOR 1A followed by 955CM-2.1, MicroChem Corp) and standard contact UV photolithography (Quintel, Inc). A 15 nm Cr masking layer (Electron beam dual gun evaporation chamber, Thermonics Laboratory) followed by subsequent lift-off procedures yielded a final hard masked design for etching.

Anisotropic deep reactive ion etching (DRIE) of the channel and pillar design was performed using a Bosch-process (System 100 Plasma etcher, Oxford Instruments).

To create the capping layer, the front side processing was completed by deposition of a non-conformal layer of silicon oxide with a nominal thickness of 2 to 3 μm using plasma enhanced chemical vapor deposition (PECVD, Oxford Instruments). For backside processing a 2 μm PECVD silicon oxide hard mask plus photoresist (SPR 220-4.5 MicroChem Corp) was photolithographically patterned with through-wafer ports. DRIE of first the silicon oxide, then the silicon (using a modified Bosch process) in the exposed area created access ports etched entirely through the wafer for liquid introduction during experimentation.

4.3.2 Stationary Phase preparation

Pillar and channel surfaces were purposefully modified by two methods. For traditional reverse phase chromatography, unsealed microfluidic chips were placed into a desiccator at ambient temperature and pressure next to a solution of butyl(chloro)dimethylsilane (Sigma Aldrich) for 20 hours. A more traditional approach involving dynamic modification of pillar and channel surfaces was conducted by including 2 or 4 mM hexadecyltrimethyl ammonium bromide (CTAB) (Fisher Scientific) into the mobile phase solution in order to create a pseudo stationary phase.

4.3.3 Experimental set-up and separation procedure

The fluidic interface which coupled the fabricated chips with off chip components is analogous to the design described in our earlier work.[6] Modifications to the previous design were aimed at constructing a more compact system to become more compatible with the overall goal of system miniaturization. Figure 4.1a depicts the main components of our

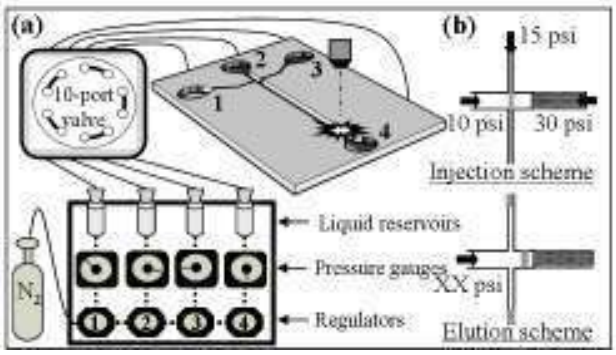

Figure 4.1 (a) Simplified schematic illustration of experimental setup (b) Sample injection and elution scheme for manipulating pressurized flow generation.

experimental setup. In short, we designed a homemade pressurized system which was operated by connecting a nitrogen gas cylinder to precision regulators (Airtrol Components Inc.) which attenuated the pressure fed to four liquid reservoirs. The flow generation at each reservoir was additionally controlled by a 10-port valve (Valco Instruments Co. Inc.) which provided switching between sample injection and elution flow regimes, as described by the protocol in Figure 4.1b. The assembled fluidic chip was mounted onto an adapter directly attached to the microscope stage for epifluorescent detection.

Prior to performing separations and functional tests on the system, the chips were bonded to elastomeric cover windows to create sealed fluidic devices. For this procedure, glass cover slides of the same dimension of the chips were first spincoated with approximately 25 μm of polyethylene glycol modified GE RTV 615 (10:1 parts A:B ratio with 0.4% polyethylene glycol methyl ether methacrylate (PEG-MEM)) and cured at 100 C° for 1 hour. Afterward, the cover window and fluidic chip were placed into contact and heated on a hotplate at 90 C° for 5 minutes. The resulting device was thus reversibly sealed, so that once attached to the adapter the fluidic system could withstand pressures up to 100 psi, and once released from the adapter the cover window could be manually removed and the chip easily washed and reused.

To visualize sample injection and characterize chromatographic separations, a Nikon Eclipse 100 microscope equipped with a high pressure Hg light source, a multicolor filter cube, and a Digital sight CCD camera (DS-2M, Nikon, Inc) controlled by NIS-Elements software was used. Separations were conducted using fluorescein sodium salt (Sigma Aldrich) and sulforhodamine B (Acros Organics) laser dye with various compositions of solvent mixtures containing methanol and phosphate buffer at a pH of 8.

4.3.4 Surface and phase characterization

The properties of the pillar array created during the fabrication process were inspected by collecting images using an FEI Dual Beam SEM/FIB (xT Nova Nanolab 200). HPLC experiments were completed using a HP series 1100 HPLC. Capillary electrophoresis experiments were conducted on a Hewlett Packard 3D CE using a 75 μm id capillary. Contact angles were measured using a Rame-Hart NRL Contact Angle Goniometer (Model 100). Stationary phase characterization was conducted using an Ion Sense DART 100 Mass Spectrometer coupled to a Joel AccuTOF JMS-T100LC.

4.4 Results and discussion

4.4.1 Channel fabrication

The optimization of our fabrication method was explored in our previous publication.[6] The established processing sequence, continued in this study, generates fluidic chips with a 10 mm x 50 μm channel of robust 1 μm diameter pillars with a pitch of 2 μm in a 20 μm deep channel, intrinsically establishing greater surface area per pillar than previously reported nonporous pillars due to the extreme high-aspect-ratio dimensions. The major advantage of this employed system is the introduction of an oxide deposition which functions to both improve mechanical stability and impart unique surface characteristics which are studied in this work. The SEM images depicted in Figure 4.2 show the pillar array before and after the PECVD silicon oxide capping layer. The PECVD process produces a slightly non stoichiometric silicon oxide with a compositional formula close to SiO_2 with relatively high silanol content in the bulk. Deposition parameters including substrate temperature, RF power level, reactor pressure, and reactant gas flow rates affect the composition and structure of the

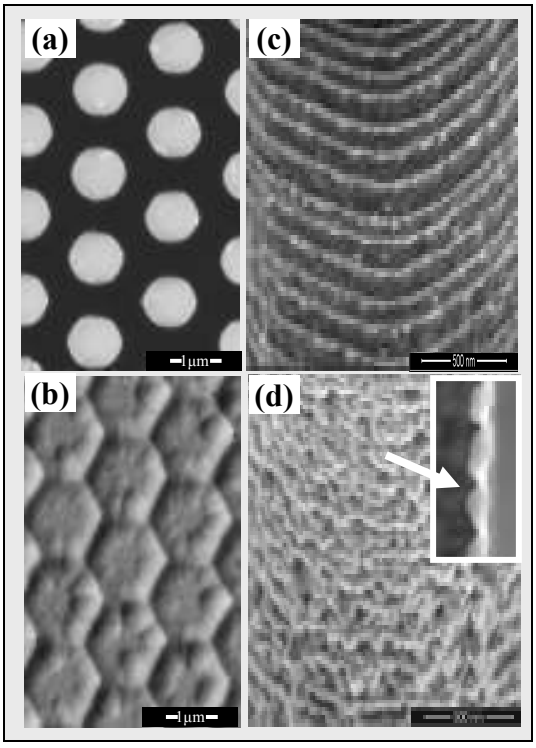

Figure 4.2 SEM images illustrating the pillar array before and after the PECVD silicon oxide capping layer: (a) and (b) top view of pillars before and after deposition, and (c) and (d) view of pillar side walls before and after deposition, respectively. Inset (d): cross sectional view of pillar side wall with oxide deposition (denoted by arrow).

growing film by altering the deposition process. We made adjustments to these parameters, most significantly by increasing deposition pressure, to create a non-conformal deposition which preferentially deposits oxide on the tops of the pillars.

Figure 4.2a and b are top view images of the pillar array before and after the deposition of silicon oxide. As the gaps between the pillars decrease, the oxide creates a mushroom capped array of pillars which eventually becomes completely sealed, creating a robust scaffold which prevents delicate pillars from damage. The enhanced mechanical stability was evident in our ability to handle, wash, seal, reseal, and even sonicate the fluidic chips without damaging the integrity of the pillars. This improved strength also allows for the ability to scale the pillars to nanoscale dimensions and very high-aspect-ratios without sacrificing the mechanical stability of the system. As pillar dimensions decrease, the effective surface area of the system increases within given channel geometries, i.e. imparting a greater surface area to volume ratio. The protective oxide enclosure also allows for facile chip sealing. A major advantage of lab-on-chip technology is the ability to use and discard these relatively inexpensive devices. However, as these pillar arrayed fluidic channels are a relatively new field, further experimentation and optimization must be conducted before adaptation as economical competitive real world systems. Our technological approach benefits from a quick and easy bonding technique which allows for chip reusability and is more forgiving of non-uniform surface topography so that sealing our devices have a near perfect success rate.

Figure 4.2c and 4.2d depicts images of the pillar side walls before and after silicon oxide deposition, respectively. As seen in figure 4.2c the anisotropic Bosch etching method creates ridges due to the unique two step cycling protocol. The Bosch process consists of

alternating etch and deposition cycles, in which the deposition step coats the feature with a fluoropolymeric layer preventing lateral etching by radicals, and the etchant step removes the polymer for the bottom of the feature, etching the underlying silicon.[35] Typically, the polymeric layers remaining on the features side walls are removed with heat and acid washing procedures.[16, 28] With our process we are able to neglect this cleaning step and instead coat this unwanted layer with silicon oxide. The deposition-to-etch ratio effects the overall etch rate and resultant feature characteristics such as established thickness of the polymer layer and the ability to maintain straight side walls without the undercutting of features. Our pillar system is created with a 5 sec deposition-to-4 sec etch ratio, which is optimized for small diameter pillars and gives a high density of ridge features.

The ridges alone do not impart a large increase in surface area per pillar, however when combined with the nanoscale dimensions of the pillar system and the nature of the silicon oxide deposition, these characteristics create an arrangement of high-aspect-ratio roughened pillars with increased surface area, as seen in Figure 4.2d. Figure 4.2d (inset) depicts the typical pillar cross-section highlighting the additive effect of the Bosch produced ridges with the non-conformal silicon oxide deposition (approximately 70 nm thick, denoted by arrow) on the pillar side wall. Without consideration of surface roughness, our current configuration (50 μm by 1 cm array) has approximately the same surface area to volume ratio as a 3 μm id open capillary while providing more than two orders of magnitude higher volumetric flow and concomitant related relaxed injection and detection volume demands. Our preliminary BET studies and analysis by SEM imaging suggest that the surface area of these pillars is likely to be increased by a roughness factor of up to 10 due to the presence of PECVD silicon oxide. Previous studies have shown that PECVD silicon oxides are more

porous, less uniform, and more silanol rich in comparison to dense stoichiometric silicon oxide films prepared by thermal oxidation of single crystal silicon. The silanol concentration of such films are between 1-6 weight percent, with values changing according to deposition temperature, pressure, and RF power level.[36] In conventional electronic applications these attributes are detrimental to the quality of the resultant film; however in our application these key features enhance pillar surface properties. Specifically, after PECVD of silicon oxide the pillar sidewalls have a granular morphology with increased surface area and as increased content of silanol groups.

4.4.2 Functional and chromatographic testing of unmodified microfluidic chips

Recognizing that our injection system is manually operated we aimed to validate the reproducibility of our experimental setup. Figure 4.3a shows progressive microscope images of the fluorescent solutes injected into the fluidic channel using the pressure scheme previously described. A major problem associated with on-chip injection valves is that diffusion and poorly controlled flow often results in cross contamination between inlets and downstream flow.[37] This was evident in our studies, as samples injected after an appreciable length of eluent flow produced immediate sample plugs of differing fluorescent intensity. We therefore used simultaneous variation of the pressure applied to different inlets, as depicted in Figure 4.1b, to be able to load the sample plug into the cross section for up to 20 minutes. This maintained the integrity of the sample composition and concentration, reliably producing low picoliter sample plug volumes. Figure 4.3b shows the reproducibility of the chromatographic separations using this injection system. Sample plugs were injected into the separation channel by varying the sample loading time (approximately 1-10 minutes) and the time between injections (approximately 2-12 minutes) with a

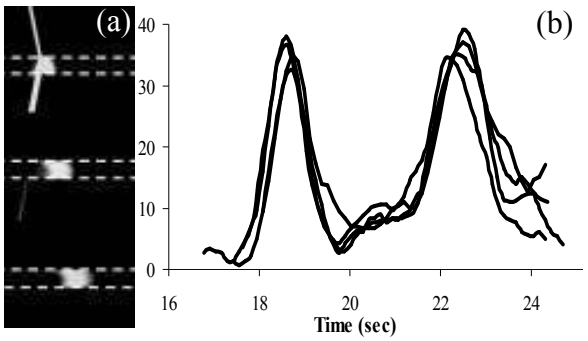

Figure 4.3 (a) Fluorescent micrographs of sample injection (b) Reproducibility of chromatograms (four repeated analyses) manually injected at 30 psi. Other conditions: mobile phase composition 20:80 methanol: 50 μM phosphate buffer (pH 8), sample composition 10:90 methanol: 50 μM phosphate buffer (pH 8) of $1x10^{-3}$ M fluorescein (peak 1) and $5x10^{-4}$ M sulforhodamine B (peak 2).

continuous mobile phase pressure of 30 psi. The relative standard deviation of the detected peak areas was approximately 2% and 7% for fluorescein and sulforhodamine B, respectively, while peak resolution had a relative standard deviation of less than 7%. These results indicate that the experimental setup used for our studies is suitable for future analyses.

To evaluate the separation performance of our fluidic devices we examined the behavior of two large organic compounds compatible with our detection system, fluorescein (FW 376.3) and sulforhodamine B (FW 558.67). The elution order of the separated compounds using our pillar array system was fluorescein then sulforhodamine B. This trend is consistent with results collected in both our HPLC C18 reverse phase chromatographic separations and our CE experiments. The CE results revealed that in our solvent systems (i.e. pH 8) the model compounds have electrophoretic mobilities of approximately $-2x10^{-3}$ and $-1x10^{-3}$ $cm^2/Vsec$ for fluorescein sodium salt and sulforhodamine B, respectively, indicating that both compounds are negatively charged anions yet exhibit adequate organic character for reversed phase HPLC retention.

Figure 4.4 shows the chromatograms obtained in our pillar system with variation of the composition of the mobile phase by adjusting the concentration of the organic modifier. As depicted, the chromatographic resolution between the two peaks greatly decreases with the increase of methanol fraction. This trend indicates that some type of hydrophobic mode of retention governs chromatographic behavior in our system. Possible separation mechanisms which act in this manner are the partition based hydrophilic interaction liquid chromatography (HILIC), a variant of normal phase chromatography, and the more common reverse phase chromatography (RPC). If operating in the HILIC mode, a thin layer of absorbed water would be formed on the pillar surface and charged polar analytes, such as the

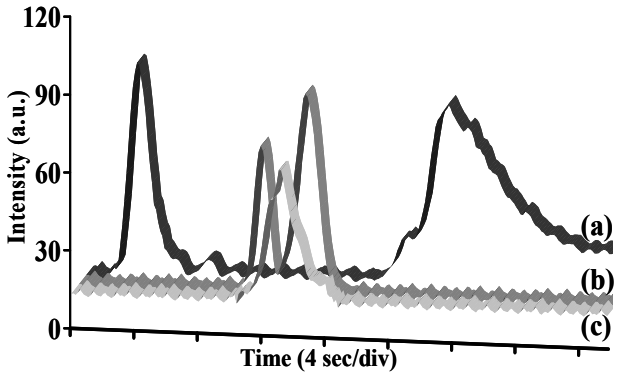

Figure 4.4. Chromatograms of fluorescein and sulforhodamine B using a mobile phase composition of (a) 90:10 methanol: buffer (b) 20:80 methanol: buffer and (c) 40:60 methanol: buffer systems. Other conditions: 50 μM phosphate buffer (pH 8), Sample composed of 30:70 methanol: buffer $5x10^{-4}$ M sulforhodamine B and $1x10^{-3}$ M fluorescein, eluent pressure of 30 psi.

dye used in these experiments, would partition into and out of the absorbed water layer as well as undergo cation exchange with charged silanol groups.[38] For this mechanism to dictate the separation the mobile phase must be highly organic.[38, 39] In contrast our separations utilize highly aqueous mobile phases, a regime which would not produce HILIC separations. We therefore determined that RPC, which would create a trend consistent with that depicted in Figure 4.4, is the more likely mode of separation. This is further supported by the tailing depicted in Figure 4.4a by the sulforhodamine B peak. In RPC, tailing may occur due to phase overload or due to interaction with exposed, free surface silanol groups. Another possible source of tailing at lower mobile phase organic content may be due to injecting the sample in a solvent stronger than the mobile phase.

The separation behavior exhibited by our system was unexpected and the exact mechanism of retention still unknown, so next we examined the effect of the ionic strength of the mobile phase, and therefore the Debye length, on the separation performance. It has been reported that an electric streaming potential can be created in nanoscale channels which ultimately imparts new separation mechanisms.[21, 40-43] Studies have also shown that localization of solutes into the center of the parabolic profile may produce electrostatically-derived hydrodynamic effects, wherein analytes may separate due to their differential access to the full parabolic flow profile, referred to by Liu et al. as nanocapillary chromatography.[18-20] Both of these aforementioned separation modes should result in similar separation trends with changes in ionic strength. Previous studies examining these separation mechanisms have only been applied to open channel geometries. We aimed to reproduce these experiments in our pillar packed channels to verify or eliminate the significance of these modes of separation in our systems. The plots depicted in Figure 4.5

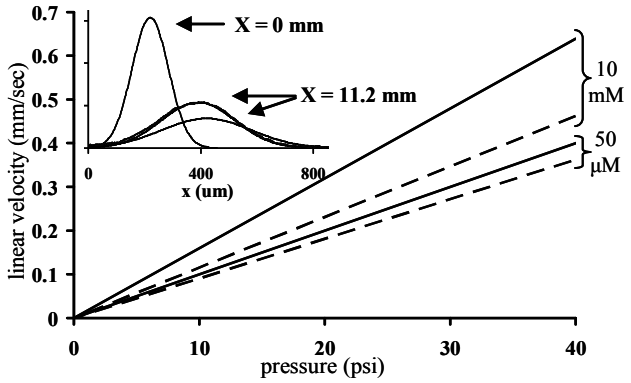

Figure 4.5 Relationship of solute velocity and pressure for fluorescein (solid lines) and sulforhodamine B (dashed lines) in different ionic strength buffers. Inset: Intensity profile of injected sample pre and post pillars using 10 mM buffer strength at 22 psi. Conditions: Mobile phase composition 20:80 methanol: phosphate buffer (pH8). Sample composed of 30:70 methanol: buffer $5x10^{-4}$ M sulforhodamine B and $1x10^{-3}$ M fluorescein. Peaks fit to a gaussian, middle peak modeled with experimental and fit curves.

show the relationship between solute velocity and pressure for given mobile phase compositions. The calculated Debye length under our conditions was approximately 3 and 40 nm for the ionic concentrations of 10 mM and 50 μM, respectively.[44, 45] If there was an appreciable streaming potential the lower ionic strength and Debye length should produce greater potential and better electrophoretic separation. The same trend should be observed with the hydrodynamic separation mechanism wherein we would expect greater localization toward channel center and increased velocities and separation of the negatively charged analytes.[5, 19] The absence of these trends (see the figure) indicates that even if present, the electric gradient and electrostatic-derived hydrodynamic effects are not the dominant mechanisms governing separation behavior.

Figure 4.5, inset, illustrates the representative intensity profiles of the sample plug at injection (x=0 mm) and detection (x=11.2 mm) positions. Plate heights were 1.1 and 1.8 μm for fluorescein and sulforhodamine B at 22 psi, respectively. Although the slopes of the plots in Figure 4.5 diverge to a great extent as pressure increases, especially in the case of the 10 mM ionic concentration, this trend should not be misconstrued as increased resolution. In fact, the resolution is nearly the same for all pressures within each individual solvent system (Res = 4.7 ± 0.2, RSD = 3.7% for the 10 mM ionic strength mobile phase). Determination of the retention factor (k) from the figure yields the values described in Table 4.1. Specifically, fluorescein is nearly unretained at both ionic strengths, while sulforhodamine B exhibits modest retention under the described conditions.

To determine if these relationships are consistent with what would occur with traditional RPC we conducted experiments similar to those described using a traditional HPLC system. The two model compounds were injected into a Varian Microsorb MV 100

C18 column (5 μm particles, 150 x 4.6 mm) at 1.5 mL/min with a 50:50 methanol: phosphate buffer mobile phase of both the 50 μM and10 mM ionic strength. To achieve the target flow rate for the 50 μM ionic strength experiments required an approximate 145 psi increase in pressure in comparison to the 10 mM ionic strength experiments, a trend consistent with the on-chip results (Figure 4.5). The retention factor (k) for both solutes are listed in Table 4.1. The retention factor of the fluorescein was approximately equal at both ionic strengths while it varied to a larger extent for sulforhodamine B, again consistent with the pillar system. For both systems increasing the ionic strength of the buffer more than doubled the retention of sulforhodamine B. These results further indicate that our pillar array system operates similar to RPC, however with less capacity than the traditional C18 HPLC column.

4.4.3 Characterization of stationary phase contaminant

Clearly our native pillar system alone should not perform in a RPC mode without functionalization, thus we sought to determine the source of this modification. We utilize an elastomeric cover window to seal our closed chip systems, resulting in an extremely confined small volume channel. This elastomeric soft bonding technique was the most obvious cause for this retentive behavior. Once in contact with a silicone substance a substrate may assume the characteristics of the elastomer, often referred to as silicone contamination.[46-48]

Commercial PDMS networks have an excess of the silane functional crosslinking agent which plays a major role in possible chemical adhesion processes. Studies suggest that silanes (Si–H) can either bond to a surface through the hydroxyl group and cross-polymerize to form a layer, or can hydrolyze to form silanol groups (Si-OH) which can form hydrogen bonds or condense with other silanol groups forming Si-O-Si bonds. [49] In our system the pillar structured channel where the separation occurs is capped with a protective oxide layer,

Separation system	MP ionic strength	k_{fluor}	$k_{10mM\ sulforhodB}$
Pillar array	50 μM	0	0.10
	10 mM	0	0.34
C18 HPLC	50 μM	0.59	1.18
	10 mM	0.65	2.52

Table 4.1 Effect of ionic concentration on the retention factor (k) of fluorescein and sulforhodamine B for separations performed in our pillar structured fluidic channels and in a traditional HPLC C18 column.

therefore it was unclear if the bonding technique affected the open channel in the same manner as the enclosed pillar array. More specifically we wanted to ascertain if silicone contamination is due to surface contact or an effect of volatile compounds. Studies suggest that 5-20% of the elastomeric material do not undergo crosslinking reactions and only 0.1% of the total mass of the elastomer is volatile at ambient temperature and pressure.[46] We tested for gas phase contamination by volatile components by measuring the contact angle (Table 4.2) of both a silicon oxide thin film as well as an array of our silicon oxide coated pillars before and after a series of exposures to the treated elastomeric coated cover window with and without the PEG additive, the individual elastomer components (GE RTV 615 part A PDMS and part B crosslinking agent), and the individual PEG-MEM additive. Exposure to the aforementioned cover window components was conducted by storing the chips next to the described components in the same desiccator at room temperature for approximately 48 hours. Contact angle measurements were collected using the sessile drop method with a 10 μL droplet, listing the results as an average of 5 measurements per sample. Measurements of the thin film prior to exposure revealed a contact angle of approximately 35°, whereas we were unable to even maintain a water droplet on the pillar surface due to the hydrophilic nature of PECVD silicon oxide. This result also confirms that the pillars are coated with silicon oxide rather that the fluoropolymer produced by the Bosch process, which would be extremely hydrophobic.

After exposure to key PDMS components the contact angle increased to an extremely hydrophobic angle (see Table 4.2). Measurement within the array exhibited markedly higher contact angles, which is expected when measuring textured surfaces which can trap air within

treatment	contact angle	
Native (untreated)	Thin film Pillar array	35.3 -
Part A PDMS	Pillar array	117.6
Part B PDMS	Pillar array	111.8
PEG-MEM	Pillar array	-
PDMS window cured 1 hr, 100 C°	Thin film Pillar array	77.2 119.8
PDMS-PEG window cured 1 hr, 100 C° * array soaked in Hexane 4 hours ** array baked at 230 C° 4 hrs	Thin film Pillar array	95.2 123.5 *120.8 **121.4
PDMS-PEG window cured 10 hr @ 100 C°	Thin film Pillar array	69.6 -
PDMS-PEG window cured 1hr, 100 C° + 25 C° > 30 days	Thin film Pillar array	61.6 -

Table 4.2 Contact angle measurement of silicon oxide thin film and silicon oxide enclosed pillars prior to and post exposure to employed cover windows and elastomeric components.

the structure.[50] PEG alone did not impart contact angle change, and, in turn, did not hinder the ability of the PDMS-PEG window in making the surfaces hydrophobic. We therefore hypothesize that vapor phase elastomeric components could modify the surfaces of both the open channel as well as the pillar array enclosed by the PECVD silicon oxide capping layer.

To understand if the surface modification is a result of chemical adsorption or chemical bonding we exposed the PDMS-PEG modified pillar array to extreme heat (by baking on a 200 °C hot plate for 2 hours) and solvent conditions. These treatments did not significantly alter the hydrophobic properties of the array. We assume that any adsorbed species would be baked or washed off by these procedures, thus we concluded that the phase is most likely chemically bound to the silicon oxide surface. It should be noted that the cover windows were exposed to the array and thin film within two weeks of forming and curing them in the same manner used for bonding. We later tried the same experiments using months old cover windows as well as windows cured for an additional 8 hours. These chips yielded no appreciable change in contact angle, especially within the pillar array. This result implies that over time the cover windows will totally degas and any volatile or non crosslinked component will either disseminate or migrate away from the surface and into the bulk of the silicone.

Further characterization of the modified silicon oxide film was performed using mass spectrometry. As with the contact angle experiments, we collected positive ion mass spectra of each individual neat elastomeric component (part A, part B, and PEG-MEM) and of the silicon oxide film exposed to our typical cover window. Figure 4.6a depicts the mass spectrum of the neat component part A, while Figure 4.6b represents the mass spectrum of the silicon oxide film before (inset) and after exposure to a cover window we use for

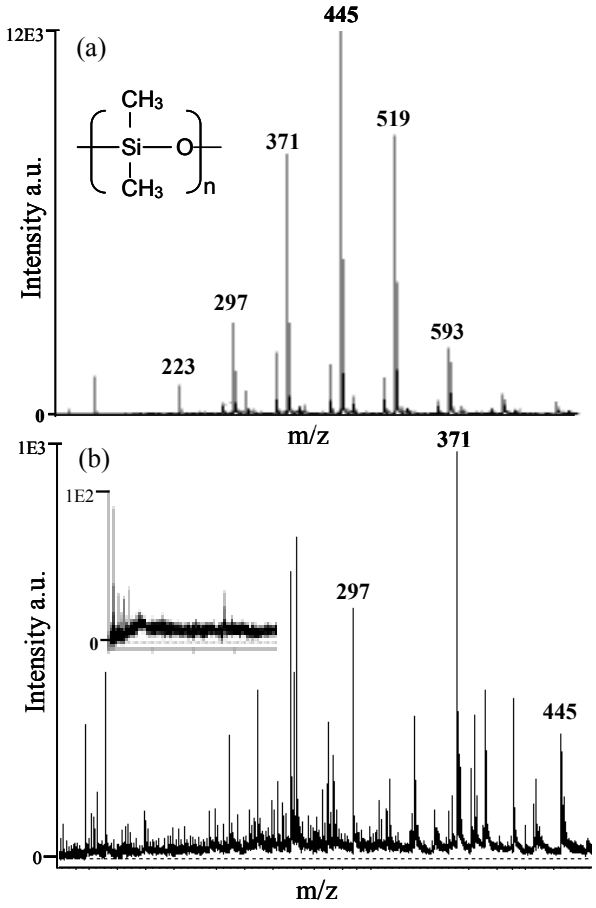

Figure 4.6 Positive ion mass spectrum of (a) neat part A PDMS and (b) a PDMS-PEG modified and unmodified (inset) silicon oxide film.

conducting separations. The labeled peaks differ by the repeating unit of the PDMS chain (inset of Figure 4.6a). Figure 4.6a and 4.6b share these characteristic fragmentations; however the other spectra collected provided no obvious direct similarities to that of the spectrum collected for Figure 4.6b. This provides some evidence that the part A component contributes to the observed surface altering effects. It should be noted that we are unable to eliminate the possibility that part B may also contribute to the phase, as many peaks collected in the spectrum were not identified. Efforts to collect a spectrum of the native film prior to surface modification with the PDMS components yielded no ionizable species (see Figure 4.6b inset). These results confirm a definite surface change for our silicon oxide coated and enclosed system, where our employed elastomeric bonding method inherently creates a phase which ultimately imparts hydrophobic-like separation characteristics. It should be noted that while we believe gas phase silicone contamination dominates the stationary phase modification, liquid phase contamination of the mobile phase during experimental use may also occur.

To determine the homogeneousness of the PDMS coating within the pillar array we measured the velocity of the most retained component (sulforhodamine B) at 3 different locations along the pillar bed. The band velocity had a RSD value of 12.56%. This indicated that the stationary phase coating within the pillar bed was sufficiently homogeneous. We would expect any long range heterogeneity of the PDMS coating to manifest as decreased band and separation efficiency. However, as previously stated, plate heights (H) of less than 2 μm and reproducible chromatograms (Figure 4.3) were obtained.

4.4.4 Separation performance of gas phase and dynamically modified microfluidic chips

The silicone contamination by this bonding method produced a reverse phase chromatographic separation with an apparent small phase ratio. This outcome suggested that there may be simpler methods for modifying these systems as alternatives to the more complicated liquid phase reactions commonly used. Consequently, we focused on two straightforward methods for creating retentive behavior for partition based chromatography. First, we tested various silylating agents with high vapor pressures to create deliberate stationary phases for chromatographic separations. Our aim was to take advantage of the high surface silanol content of the pillar walls by creating a functionalized surface without requiring stringent solvent, temperature, or pressure protocols.

Silylating reagents containing chains of two to five carbons were initially tested to determine the ability to chemically bond to representative PECVD silicon oxide surfaces at ambient temperature and pressure. The silicon oxide substrates were first cleaned in piranha, then solutions of each reagent were placed next to the test surfaces in a closed container for 20 hours. Each surface was subsequently tested to determine wettability by measuring contact angle before and after exposure to the silylating reagent. Butyl(chloro)dimethylsilane was identified as offering the most hydrophobic stationary phase under these conditions. The same reaction was then carried out, using this C4 reagent, to modify the microfluidic chips. Preliminary chromatographic tests using the C4 modified chips are depicted in Figure 4.7. Test fluorescent analytes were chosen to be compatible with our readily available instrumentation using a 633 nm laser excitation. The solvent solutions were buffered at a pH of 8.3 to discourage protonation of the analytes. Chromatograms were collected while varying the organic content of the mobile phase. While the sample matrix contained three test analytes, initial testing was unable to resolve the two most retained

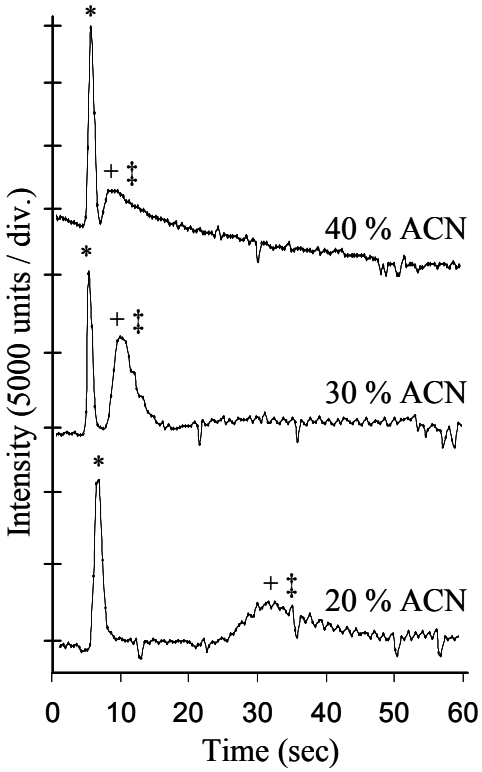

Figure 4.7 Effect of the organic content of the mobile phase on the retentive behavior of hydrophobic dyes in gas phase functionalized separations. * indicates 5E-6 M oxazine 725, + indicates 5E-6 M oxazine 750, and ‡ indicates 5E-6 M nile blue.

compounds. Nonetheless, the exhibited mobile phase - stationary phase interaction is analogous to typical reverse phase chromatographic behavior. Additionally, the clogging and channel occlusions which have materialized when using conventional liquid phase modification of pillar array systems was not evident using this process.

The second approach for a simple partition based chromatographic pillar array system was to create dynamically modified surfaces by including a hydrophobic surfactant (CTAB) in the mobile phase solution[51]. The advantage of dynamic modification is it requires no actual reaction steps and is a reversible surface modification process. The dynamic interaction of the cationic surfactant forming an ion pair with the exposed silanols of the pillar surfaces creates a pseudo-stationary phase, imparting retentive behavior. Figure 4.8 shows the chromatograms collected while varying both CTAB concentration (2mM and 4mM) and the organic content of the mobile phase. As the organic content of the mobile phase increases, the amount of CTAB not interacting with the silanol population, rather flowing in the bulk solution, also increases. This trend decreases retention at the side walls and therefore decreases the resolution of the analytes. Initial studies using these systems were not always able to attain 3 resolved bands. While these studies are incomplete, preliminary tests show that the resolution of all three bands is more readily achieved at lower CTAB concentrations (0.9mM, 2mM, and 3mM, not 4mM).

4.5 Conclusion

Lab-on-chip chromatographic systems offer fundamental advantages over traditional separation media as they require minute volumes, decreasing sample and reagent waste, they attain extremely fast analysis times achieving improved efficiency with a small footprint, and they can be produced at a fraction of the cost. However, to realize the full potential of pillar

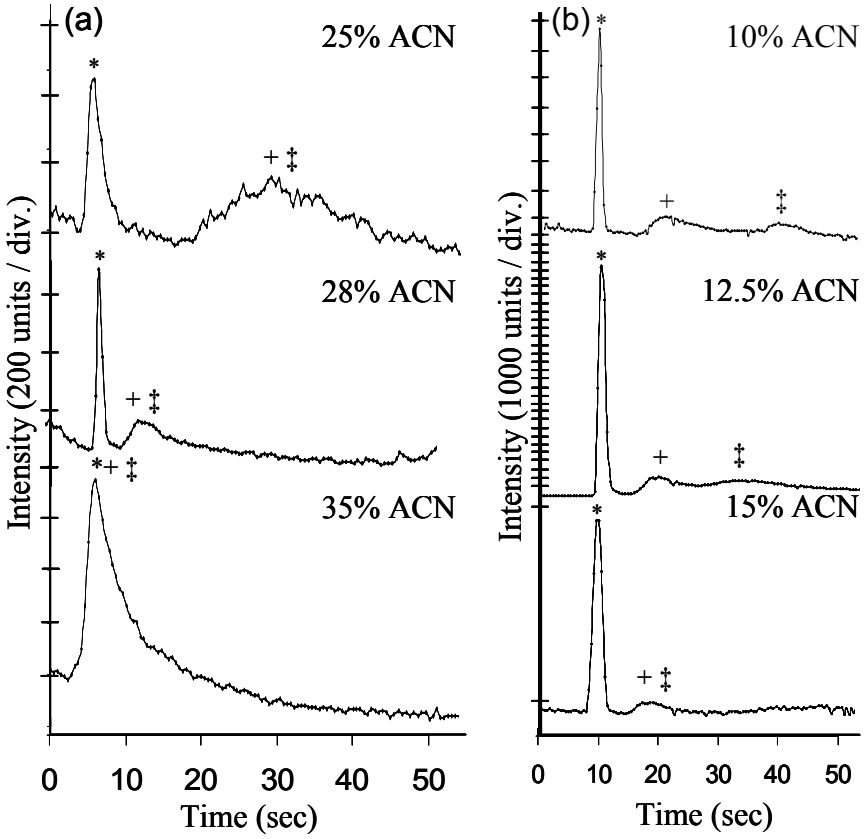

Figure 4.8 Effect of the organic content of the mobile phase on the retentive behavior of hydrophobic dyes in dynamically modified separations. (a) 4mM CTAB concentration and (b) 2mM CTAB concentration, pH 8.3. * indicates oxazine 725, + indicates oxazine 750, and ‡ indicates nile blue.

arrays as competitive chip-base separation systems improvements are needed to increase the mechanical stability, surface area and operational characteristics of the devices. We have developed a unique fabrication sequence for creating robust high-aspect-ratio pillar array separation channels which improves pillar integrity and increases pillar surface area.

Separations were carried out under pressure-driven flow conditions using an elastomeric bonding technique which allows for facile sealing, and chip reusability. Silicone contamination by this bonding method produced a reverse phase chromatographic separation with an apparent small phase ratio. This outcome suggested that a much simpler method for modifying these systems could be gas phase reactions rather than the more complicated liquid phase reactions commonly used. Accordingly, we described two simple methods for stationary phase modification. Although these methods provide a more straightforward means of accomplishing stationary phase-mobile phase partition based separations, further testing must be conducted to determine if these alternatives could ultimately produce the large phase ratio separation behavior necessary for discerning complex mixtures. Moreover, the question of suitable detection sensitivity and capacity within these pillar array systems must be analyzed to determine potential analytical utility.

4.6 Acknowledgements

A portion of this research at Oak Ridge National Laboratory's Center for Nanophase Materials Sciences was sponsored by the Scientific User Facilities Division, Office of Basic Energy Sciences, U.S. Department of Energy. This research was also supported by the US Environmental Protection Agency STAR Program under grant EPA-83274001 with the

University of Tennessee. A special thanks to Stephen Gibson and the UTK Center for Mass Sepctrometry and Dr. Bin Zhao for assistance with sample analysis.

4.7 References

[1] V.N. Phan, C. Yang, N.T. Nguyen, Microfluidics and Nanofluidics, 7 (2009) 519.
[2] F. Detobel, V. Fekete, W. De Malsche, S. De Bruyne, H. Gardeniers, G. Desmet, Analytical and Bioanalytical Chemistry, 394 (2009) 399.
[3] D. Clicq, S. Vankrunkelsven, W. Ranson, C. De Tandt, G.V. Barn, G. Desmet, Anal. Chim. Acta, 507 (2004) 79.
[4] V. Fekete, D. Clicq, W. De Malsche, H. Gardeniers, G. Desmet, Journal of Chromatography A, 1189 (2008) 2.
[5] M. Kato, M. Inaba, T. Tsukahara, K. Mawatari, A. Hibara, T. Kitamori, Analytical Chemistry, 82 (2010) 543.
[6] N.V. Lavrik, L.C. Taylor, M.J. Sepaniak, Lab on a Chip, 10 (2010) 1086.
[7] J. De Smet, P. Gzil, N. Vervoort, H. Verelst, G.V. Baron, G. Desmet, Journal of Chromatography A, 1073 (2005) 43.
[8] N. Kaji, Y. Tezuka, Y. Takamura, M. Ueda, T. Nishimoto, H. Nakanishi, Y. Horiike, Y. Baba, Analytical Chemistry, 76 (2004) 15.
[9] L. Sainiemi, H. Keskinen, M. Aromaa, L. Luosujarvi, K. Grigoras, T. Kotiaho, J.M. Makela, S. Franssila, Nanotechnology, 18 (2007).
[10] B. He, F. Regnier, J. Pharm. Biomed. Anal., 17 (1998) 925.
[11] F.E. Regnier, HRC-J. High Resolut. Chromatogr., 23 (2000) 19.
[12] M.R. Schure, R.S. Maier, D.M. Kroll, H.T. Davis, Journal of Chromatography A, 1031 (2004) 79.
[13] P. Gzil, N. Vervoort, G.V. Baron, G. Desmet, Analytical Chemistry, 75 (2003) 6244.
[14] J. De Smet, P. Gzil, N. Vervoort, H. Verelst, G.V. Baron, G. Desmet, Analytical Chemistry, 76 (2004) 3716.
[15] H. Eghbali, V. Verdoold, L. Vankeerberghen, H. Gardeniers, G. Desmet, Analytical Chemistry, 81 (2009) 705.
[16] W. De Malsche, H. Eghbali, D. Clicq, J. Vangelooven, H. Gardeniers, G. Desmet, Analytical Chemistry, 79 (2007) 5915.
[17] M. De Pra, W. De Malsche, G. Desmet, P.J. Schoenmakers, W.T. Kok, J. Sep. Sci., 30 (2007) 1453.
[18] X.Y. Wang, J.Z. Kang, S.L. Wang, J.J. Lu, S.R. Liu, Journal of Chromatography A, 1200 (2008) 108.
[19] X.Y. Wang, S.L. Wang, V. Veerappan, C.K. Byun, H. Nguyen, B. Gendhar, R.D. Allen, S.R. Liu, Analytical Chemistry, 80 (2008) 5583.
[20] X.Y. Wang, C. Cheng, S.L. Wang, M.P. Zhao, P.K. Dasgupta, S.R. Liu, Analytical Chemistry, 81 (2009) 7428.

[21] S. Pennathur, J.G. Santiago, Analytical Chemistry, 77 (2005) 6772.
[22] A. Mansouri, C. Scheuerman, S. Bhattacharjee, D.Y. Kwok, L.W. Kostiuk, Journal of Colloid and Interface Science, 292 (2005) 567.
[23] K. Morikawa, K. Mawatari, M. Kato, T. Tsukahara, T. Kitamori, Lab on a Chip, 10 (2010) 871.
[24] X.C. Xuan, Analytical Chemistry, 79 (2007) 7928.
[25] X.C. Xuan, D. Sinton, Microfluidics and Nanofluidics, 3 (2007) 723.
[26] L.R. Huang, E.C. Cox, R.H. Austin, J.C. Sturm, Science, 304 (2004) 987.
[27] W. De Malsche, H. Gardeniers, G. Desmet, Analytical Chemistry, 80 (2008) 5391.
[28] H. Eghbali, W. De Malsche, D. Clicq, H. Gardeniers, G. Desmet, Lc Gc Europe, 20 (2007) 208.
[29] H. Eghbali, S. Matthijs, V. Verdoold, H. Gardeniers, P. Cornelis, G. Desmet, Journal of Chromatography A, 1216 (2009) 8603.
[30] W. De Malsche, D. Clicq, V. Verdoold, P. Gzil, G. Desmet, H. Gardeniers, Lab on a Chip, 7 (2007) 1705.
[31] R.M. Tiggelaar, V. Verdoold, H. Eghbali, G. Desmet, J.G.E. Gardeniers, Lab on a Chip, 9 (2009) 456.
[32] F. Gritti, I. Leonardis, J. Abia, G. Guiochon, Journal of Chromatography A, 1217 (2010) 3819.
[33] A. Cavazzini, F. Gritti, K. Kaczmarski, N. Marchetti, G. Guiochon, Analytical Chemistry, 79 (2007) 5972.
[34] E. Mery, F. Ricoul, N. Sarrut, O. Constantin, G. Delapierre, J. Garin, F. Vinet, Sensors and Actuators B-Chemical, 134 (2008) 438.
[35] C.J.D. Craigie, T. Sheehan, V.N. Johnson, S.L. Burkett, A.J. Moll, W.B. Knowlton, Journal of Vacuum Science & Technology B, 20 (2002) 2229.
[36] M.F. Ceiler, P.A. Kohl, S.A. Bidstrup, Journal of the Electrochemical Society, 142 (1995) 2067.
[37] T. Braschler, J. Theytaz, R. Zvitov-Marabi, H. Van Lintel, G. Loche, A. Kunze, N. Demierre, R. Tornay, M. Schlund, P. Renaud, Lab on a Chip, 7 (2007) 1111.
[38] Z.G. Hao, B.M. Xiao, N.D. Weng, J. Sep. Sci., 31 (2008) 1449.
[39] F. Gritti, A.D. Pereira, P. Sandra, G. Guiochon, Journal of Chromatography A, 1216 (2009) 8496.
[40] S. Pennathur, J.G. Santiago, Analytical Chemistry, 77 (2005) 6782.
[41] X.C. Xuan, Journal of Chromatography A, 1187 (2008) 289.
[42] X.C. Xuan, D.Q. Li, Electrophoresis, 28 (2007) 627.
[43] S.K. Griffiths, R.H. Nilson, Analytical Chemistry, 78 (2006) 8134.
[44] R. Qiao, N.R. Aluru, Journal of Micromechanics and Microengineering, 12 (2002) 625.
[45] V. Tandon, S.K. Bhagavatula, W.C. Nelson, B.J. Kirby, Electrophoresis, 29 (2008) 1092.
[46] L.H.U. Andersson, T. Hjertberg, Journal of Applied Polymer Science, 88 (2003) 2073.
[47] L.H.U. Andersson, P. Johander, T. Hjertberg, Journal of Applied Polymer Science, 90 (2003) 3780.

[48] P.S. Hale, P. Kappen, W. Prissanaroon, N. Brack, P.J. Pigram, J. Liesegang, Applied Surface Science, 253 (2007) 3746.
[49] S. Perutz, E.J. Kramer, J. Baney, C.Y. Hui, Macromolecules, 30 (1997) 7964.
[50] M. Callies, Y. Chen, F. Marty, A. Pepin, D. Quere, Microelectronic Engineering, 78-79 (2005) 100.
[51] M.J.C. A. T. Balchunas, M.P. Maskarinec, and M.J. Sepaniak, Journal of Chromatographic Science, 23 (1985) 381.

Chapter 5

Surface enhanced Raman spectroscopy for microfluidic pillar arrayed separation chips

Portions of Chapter 5 are an adaptation of a research article currently submitted for publication and under peer review. This article addresses the need for information rich and compatible detection methods for pillar array separation chips. Laminar diffusive mixing of colloidal substrates into the eluent stream is applied to promote surface enhanced Raman spectroscopy (SERS) of test analytes. We perform Computational Fluidic Dynamic (CFD) modeling and experimental studies to analyze device performance and applicability.

5.1 Abstract

Numerous studies have addressed the challenges of implementing miniaturized microfluidic platforms for chemical and biological separation applications. However, the integration of real time detection schemes capable of providing valuable sample information under continuous, ultra low volume flow regimes has not fully been addressed. In this report we present a chip-based chromatography system comprising of a pillar array separation column followed by a reagent channel for passive mixing of sample analytes with a silver colloidal solution as surface enhanced Raman spectroscopy (SERS) substrate. With this approach we demonstrate the ability to collect distinctive SERS spectra with or without complete resolution of chromatographic bands. Computational fluidic dynamic simulations are used to model the diffusive mixing behavior and velocity profile of the two confluent streams. We evaluate the band intensity and efficiency of model analytes with respect to kinetic factors as well as signal acquisition rates. Additionally, we discuss the use of a pluronic modified colloidal solution as a means of eliminating contamination generally caused by nanoparticle adhesion to channel surfaces.

5.2 Introduction

The fundamental motivations for transforming existing technological platforms into lab on chip formats are significant to many scientific disciplines. These motivations include producing faster analysis and run times ultimately increasing throughput and decreasing power consumption, creating systems with a smaller footprint that are more compact and produce less waste, and advancing remote capabilities for in-field applications. Recent studies have focused on the advancement of analytical methods, such as liquid chromatographic separation columns, which can benefit from these numerous advantages. Research has focused on the miniaturization of separation columns, the refinement of porous separation media, and the development of hyphenated techniques.

Pillar arrayed fluidic channels, first proposed by Reigner et al., as monolith support structures,[1, 2] have garnered a good deal of attention as miniaturized separation beds which could mimic traditional packed bed chromatographic columns. Numerous theoretical[3-5] and experimental [6-10] studies have shown that pillar arrayed separation channels offer substantial promise as suitable chip based chromatographic platforms. The standard clean room procedures used to create these systems offer the ability to create highly uniform architectures with micrometer to nanometer features. These characteristics greatly improve the efficiency of the separation channel thereby allowing for system miniaturization. However, as the size of separation systems have transitioned to compact chip level devices, fundamental and technological challenges have emerged. Considerable research has been aimed at surmounting many of these challenges; include improving design integrity and overall stability of the systems, [8] improving on-chip sample injections to be capable of injecting small volume samples,[9, 11, 12] and increasing the capacity and overall surface

area available for sample phase interaction while creating retentive properties that govern analyte separation.[13-16]

Although several challenges hindering this technology from becoming comparable to or competitive with traditional HPLC columns have been addressed, few studies have focused on addressing the need for compatible detection methods. One of the main disadvantages of any miniaturized systems is that as the volume of the channel decreases the size of the spatial and temporal detection window is reduced. As a result, the signal to noise ratio often decreases, leading to the necessity for a highly sensitive detection method. This limitation is especially true for most absorbance detectors, the most common detection method for tradition HPLC columns, as the signal intensity is directly dependent upon the optical path length. As a proposed solution, the first pillar arrayed microfluidic chip to incorporate detection capabilities interfaced waveguides within the design for optical UV absorbance detection,[17] however this design has not been optimized for chromatographic efficiency. Laser induced fluorescence (LIF), a highly sensitive optical detection method that is often utilized for application with biological species, has become the most common chip-based detection method. Unfortunately, many relevant analytes do not naturally fluoresce requiring lengthy labeling protocols which can result in the creation of complex sample derivatives. Moreover, overlapping spectral peaks caused by broad fluorescence emission profiles can also detrimentally effect sample detection.[18, 19]

The direct coupling of Mass Spectrometry (MS) detectors to microfluidic devices has shown promise toward fully integrated chip based formats. This analytical tool additionally provides valuable information about sample composition based upon mass to charge ratio. Most established mass spectrometry detection methods used in conjunction with liquid

chromatography are performed off-line due to the difficulty of transferring liquid eluents within a high vacuum system.[20] Recent advances in ionization sources, such as electron spray ionization (ESI), have overcome this technical challenge. Although research in this area has improved formats which interface ESI-MS with microfluidic devices,[21-27] many of these integrated devices require complex fabrication processes and include dead volume connections which can contribute to peak broadening and reduce chromatographic resolution and efficiency.

Surface enhanced Raman spectroscopy (SERS) has become a promising analytical method which can provide for sensitivities comparable to fluorescent detection while providing information about molecular composition similar to MS. SERS provides information about the vibrational transitions of molecules, which are enhanced by proximity to certain metal substrates. Some of the first microfluidic SERS devices were created by vapor deposition of silver onto a polymeric film, and were performed off-line for use in electrophoretic separations.[28] More recent studies have embedded silver nanoclusters onto polymer monoliths to create sensitive biological sensors.[29] However, the most common substrate for integrated real time sensing has been performed using metal colloidal substrates for SERS detection. These sensors often integrate passive or active regions for mixing by diffusion,[30, 31] or chaotic advection[32-35] respectively. Microfluidic devices using SERS detection have found applications in chemical and biological sensing,[36-38] studying reaction optimization,[39] and sample immobilization and screening. [40, 41]

While SERS detection has found utility in capillary,[42, 43] and chip based[44] electrophoresis separations systems, to the best of our knowledge there has been no research focusing on integrated chip based microfluidic devices combining pressure driven

separations with real time SERS detection. Herein, we present a simple microfluidic separation device which combines a pillar array channel capable of high performance analyte separations followed by a diffusive mixing region for SERS detection of analytes during continuous monitoring. Our integrated design is unique in that it addresses the need for efficient chromatographic separations as well as provides valuable information about sample composition by collecting signature SERS spectra. The high-aspect-ratio pillar array has been shown to produces efficient separations with plate heights below 1 μm.[8] The colloidal detection reagent is introduced after the separation channel for continuous passive mixing of the sample and reagent stream without interfering with the retention characteristics of the analyte. Furthermore, we present studies which demonstrate that the use of a silver colloidal solution modified with a non-ionic polymeric surfactant can decrease the adsorption of nanoparticles onto small volume detection windows, reducing channel contamination. We discuss the effect of analyte diffusion along the mixing region and highlight the ability to deconvolute unresolved chromatographic peaks for analyte spectral identification.

5.3 Experimental

5.3.1 Channel fabrication

The fabrication sequence used to create the pillar arrayed fluidic channels is described in detail in our previous work.[8] The specific design used in this research, as depicted in Figure 5.1a, includes an on-chip injection scheme with a standard cross architecture, devoid of pillars, positioned approximately 60 μm upstream of the pillar array. For detection purposes, a 20 μm wide reagent channel for post-separation derivatization is positioned 80

μm after the pillar array separation channel (Figure 5.1b). The pillar array portion of the microfluidic chip consists of a 10 mm long and 50 μm wide channel of 1 μm diameter pillars (2 μm pitch) positioned as uniformly ordered hexagons on an equilateral triangle template. The pillars were etched to a depth of approximately 20 μm, and then coated with plasma enhanced chemical vapor deposited silicon oxide for facile surface modification and stability.[8, 9] This deposition process is highlighted in Figure 5.1b which depicts portions of the pillar array with and without silicon oxide.

The microfluidic chips were treated by gas phase reaction at ambient temperature and pressure with butly(chloro)dimethylsilane (Sigma Aldrich) for 20 hours. Devices were then sealed for subsequent fluidic testing using a nonpermanent soft bonded PDMS coated glass cover window. Flow generation was controlled using a homemade pressurized setup (Figure 5.1e) and actuated multiport valve connected to a homemade chip adapter (Figure 5.1d). The system assembly, including the components of our experimental setup and the injection protocol, were discussed in our previous reports.[8, 9]

5.3.2 Reagent preparation and data acquisition

For SERS measurements, conventional silver colloid was prepared using the chemical reduction procedure according to the description by Lee and Meisel.[45] In short, 85 mg of AgNO3 (99þ% Sigma) was dissolved in 500 mL deionized water and heated to a boil. Next, 10 mL of 1% w/v trisodium citrate (Fisher) was added drop by drop with vigorous stirring, and further boiled for one hour. This conventional colloid was next concentrated to create greater nanoparticle density by centrifuging a volume of 14 mL for 30 minutes and decanting the aqueous liquid from the top of the nanoparticles. The remaining colloidal solution (approximately 60 mgAg/mL assuming complete reduction of silver nitrate) was then diluted

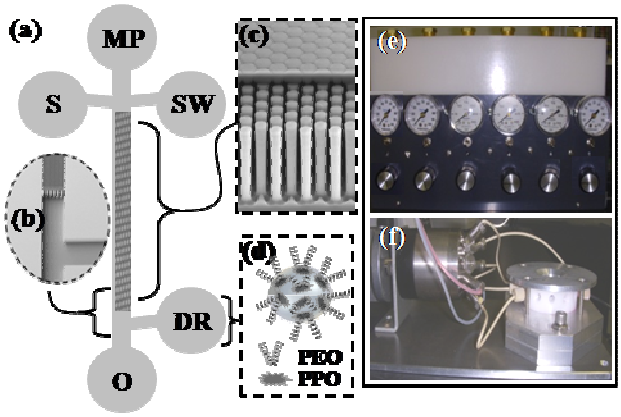

Figure 5.1 (a) Illustration of chip design with inlet ports labeled as MP (mobile phase), S (sample), SW (sample waste), O (outlet), and DR (detection reagent). Corresponding SEM images of (b) the silicon oxide enclosed pillar array and (c) the region for laminar diffusive mixing for post-pillar sample derivatization. (d) Schematic representation of pluronic modified AgNP detection reagent, as described in text. (e and f) Images of the apparatus for pressure control and the multiport injection valve with chip adapter, respectively.

with a PBS buffer system to create bead concentrations that are 2 to 6 times more concentrated per volume than the initially prepared solution. Colloidal solutions were further modified with pluronic F127 [Sigma Aldrich], by adding to solution and storing for one hour. Optical spectra of the unmodified and pluronic modified AgNPs showed no significant shift in the intensity or location of the absorbance peak centered around 420 nm.

Experiments were conducted using Rhodamine 6G (Lambda Physik) and benzene thiol (Acros Organics) with solutions composed of methanol and 100 μM phosphate buffer at a pH of 8.2. Pure methanol was used as the mobile phase solvent. All SERS spectra and chromatograms were collected using a JY-Horiba LabRam spectrograph equipped with a 50 x (0.45 NA, ∞) microscope objective and a thermoelectrically cooled HeNe laser at 633 nm, and typically delivering 2.7 mW. The data was collected with a back scattering geometry and processed using LabSpec 4.12 software. Bead density and kinetic experiments conducted to characterize the silver colloid additionally used a Stanford SR-540 frequency modulator which provided translation (via spinning) at a rate of 3000 RPM to minimize heat effects and substrate heterogeneity.{De Jesus, 2003 #283} Flow simulations were performed with COMSOL MultiphysicsTM 4.1.

5.4 Results and Discussion

5.4.1 Characterization of silver colloids

The plasmonic properties of silver nanoparticles (AgNPs) make them well-suited as a substrate for SERS detection. However, the aggregate size of the nanoparticles and signal enhancement observed by the analyte are often dependent upon factors such as the presence

of salts[46] and the binding kinetics.{Moskovits, 2009 #275} Aggregates of colloidal particles are also known to adhere to surfaces, which for chip based devices can detrimentally contaminate small volume detection windows. Recent research suggests using multiphase flows that isolate microdroplets from the channel walls for the elimination of colloidal adhesion,[47, 48] however this approach is not readily compatible with the chromatographic format. As an alternative, our studies focused on the use of amphiphilic triblock copolymers (pluronics) to stabilize interactions with both hydrophobic and hydrophilic compounds. In the case of AgNP pluronic complexes, researchers suggest that this modification results in the pluronic polypropylene oxide (PPO) block to absorb by hydrophobic reaction to the particle, leaving the hydrophilic polyethylene oxide (PEO) blocks exposed to solution,[49] as depicted in Figure 5.1d. For our studies, we modified conventional AgNPs with Pluronics F127 to control colloidal aggregation as well as to inhibit the sticking of the AgNPs onto our channel surfaces.

For our first experiment we evaluated the effects of pluronic modification of the silver colloid on the kinetic binding of our analyte to the AgNPs. Figure 5.2 shows a kinetic plot of the intensity of a representative rhodamine 6G peak (1495 cm-1) over time while varying the pluronics concentration in the colloidal solution. As our chip design only allows for a short period of time for sample/reagent mixing (up to 5 seconds) it is important that almost immediate signal is achieved. This indeed occurred in both the conventional and pluronic modified colloidal solutions, however the signal intensity was affected by the degree of modification. The smaller concentrations of pluronics modified AgNPs (3, 50, and 100 μg/mL) yielded intensities greater than that of unmodified AgNPs, in agreement with previous reports.[49] However, as the pluronic concentration increased significantly (500

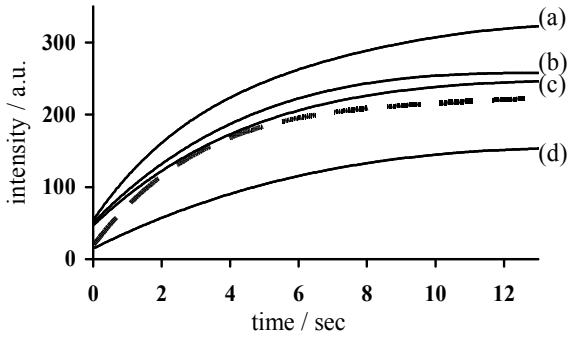

Figure 5.2 Kinetic test showing increase of the 1E-4 M rhodamine 6G SERS signal (peak 1495 cm-1) over time while mixed with AgNP pluronic complex concentrations of (a) 3 μg/mL, (b) 50 μg/mL, (c) 100 μg/mL, and (d) 500 μg/mL. Dashed line indicates the signal of non modified AgNP's.

μg/mL) peak intensity was decreased. This may be explained by the inhibition of AgNP surface analyte interactions due to extensive binding of the pluronic species onto the colloidal surface. It is also important to note that a steady state was not achieved during the time allotted for these experiments, and in turn will not be achieved within our dynamic on-chip detection scheme, which ultimately may effect signal reproducibility.

To determine the effect of pluronics in decreasing the adhesion of AgNPs to channel surfaces, samples representative of the channel side walls were investigated. Both the PDMS coated glass cover window and the C4 modified chip surfaces were soaked for 4 hours in a solution of rhodamine 6G in colloid of varying pluronic concentrations. These samples were then rinsed with deionized water and dried. Figure 5.3 shows the averaged SERS signal of a 200 μm x 200 μm portion of both the chip surface (Figure 5.3a) and cover window (Figure 5.3b) after this treatment. In both cases, as the pluronics concentration increased, the signal intensity decreased to the extent that we could assume there is minimal adhesion. This was also evident in bright field images (Figure 5.3a inset) taken of the chip surface at pluronic concentrations of 50 μg/ml (left) and 500 μg/mL (right). The optimal pluronic concentration required to inhibit adhesion varied by surface. While only 50 μg/mL pluronics was required to almost completely eliminate adhesion on the cover window, up to 500 μg/mL pluronics had the same effect on the C4 modified chip surface. This is counter to what we expected, as the PDMS surface is more hydrophobic than the C4 modified surface, and thus the hydrophilic PEO blocks exposed to solution and channel side walls should be more attracted to the more hydrophobic surface. This may be a result of the influence of Rhodamine dye, present in this experiment, on the association of the polymer coated AgNP with the surfaces.

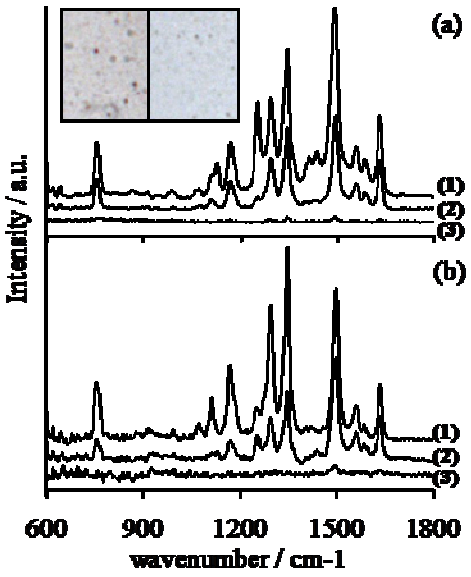

Figure 5.3 Study of the effect of the pluronic concentration on the sticking of AgNP's onto surfaces of the microfluidic chip. (a) C4 modified chip surface at AgNP pluronic complex concentrations of (1) 50 μg/mL, (2) 200 μg/mL, and (3) 500 μg/mL. Inset shows corresponding bright field images of 50 μg/mL(left) and 500 μg/mL (right) respectively. (b) PDMS coated cover windows at AgNP pluronic complex concentrations of (1) 3 μg/mL, (2) 10 μg/mL, and (3) 50 μg/mL. All spectra show the average signal of 5E-5 M R6G over a 200 μm x 200 μm region.

The small volume detection window and mixing time limitation provided by our microfluidic separation device could, unfortunately, result in a decreased signal in comparison to larger volume systems. To negate this effect within our system we aimed to increase the surface area of the reagent available to bind to the analyte. This was achieved by increasing the AgNP density per unit volume of colloid solution (see experimental section). Figure 5.4 depicts both the spectral signal of rhodamine 6G with increase in peak intensity (inset) produced when increasing the number of silver particles per unit volume (modified with a pluronic concentration of 50 μg/mL). As depicted, the signal intensity trends linearly with AgNP concentration, where a colloidal solution concentrated 6x would provide a signal 6 times greater than that of the conventionally prepared colloid.

5.4.2 Fluid dynamics

The design and fabrication of the pillar arrayed microfluidic devices was developed to meet the chromatographic lab on chip requirements for both enhanced separation efficiency and improved detection capabilities. As previously reported in the studies by the Desmet group [11] and our own research,[8] pillar arrayed separation channels have experimentally achieved chromatographic plate heights below 1 μm, while being capable of separating complex mixtures. [10] The design used for our current work additionally addresses the need for compatible detection methods performed in real time with minimal sample manipulation. As shown in Figure 5.1b, our design incorporates a simple diffusive mixing region that provides interaction between AgNPs and separated analytes. This interaction occurs downstream from the pillar array, thus after the separation channel, as not to interfere with the retention characteristics of sample analytes.

To characterize the mixing of the two streams, we used computational fluid

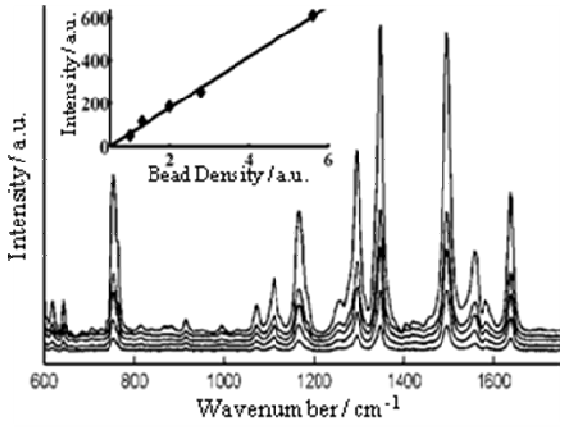

Figure 5.4 AgNP density study showing the increase of signal as a result of increasing the number of AgNPs per unit volume. The spectra of 5E-6 M R6G in AgNP pluronic complex concentrations of 50 μg/mL are plotted in descending order from 5.6x concentrated (top) to regularly prepared 1x concentrated silver colloid (bottom). Inset depicts the linear trend of peak 1495 cm-1 with increased AgNP concentration.

dynamics (CFD) and modeled the concentration and flow velocity profiles of two solutions in a confluent stream by using appropriate diffusion coefficients of the AgNPs and the analyte (Figure 5.5a,b). Each solution was assumed to be of full concentration (100 mmol/L) as they entered the channel from their respective inlets. The opposing stream was modeled as an aqueous solution of zero concentration (blue). The flow rate of the streams was driven by laminar inflow at pressures of around 0.005 psi, representative of the conditions experienced by our on chip experiments. As is demonstrated in Figure 5.5, the AgNP's, of a very small diffusion coefficient (5 x 10-8 cm^2 s^{-1}), mixes with the opposing stream to a small degree within then 2 mm long detection window. In contrast, the analyte, of a larger diffusion coefficient (3 x 10-6 cm^2 s^{-1}), diffuses into the opposing solution to a much greater extent, and assumes a uniform concentration profile after 2 mm. With this flow profile, and assuming that most analytes have a similar diffusion coefficient, finding a possible position for detection downstream from the detection reagent channel should be straightforward. It is also reasonable to assume that as the two streams diffusively mixed within the channel, signal would increase over time along the length of the detection window. However, as binding kinetics vary by analyte, finding an optimal position for detection may not be trivial.

Figure 5.5b depicts the velocity profile of the two mixing streams. The velocity of the flow from the pillar array channel is smaller than that of the reagent due to the increased pressure drop across the separation channel. However, as is shown, the velocity becomes uniform within 50 μm after the two channels converge. As a result, the mobile phase sample plug velocity increases to come into hydrodynamic equilibrium with the linear velocity of the detection reagent flow. This fluidic attribute is important to take into concern when

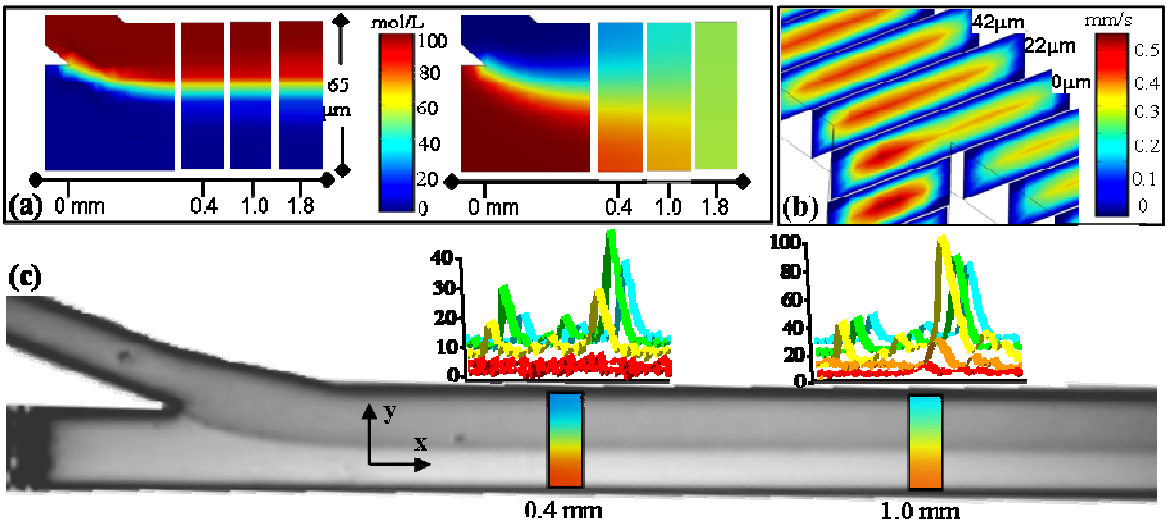

Figure 5.5 Study of the laminar flow diffusive mixing of the analyte and detection reagent introduced after the pillar array column. Computational fluid dynamic (CFD) modeling of the concentration profiles of (a) AgNPs (left) and the analyte (right) as they mix with an aqueous solution. (b) The velocity profiles of the two confluent fluid streams at their interface. (c) Bright field image of the detection channel during mixing experiments with the inset spectra corresponding to the signal of 5E-4 M R6G at representative locations downstream from the reagent inlet. See text for details.

comparing separation efficiency upstream and downstream from the reagent inlet, as the velocity of the band changes, yet the volume of the plug is relatively constant if dispersion does not occur.

To confirm that our microfluidic devices would behave in the manner demonstrated by fluidic modeling, we conducted similar on chip experiments using the constant flow of rhodamine 6G as our analyte, and pluronics modified AgNPs as the detection reagent. Figure 5.5c depicts a bright field image of the two streams mixing along the detection region. The dark region is demonstrative of the colloidal solution, and the light region is analyte flow. We collected SERS spectra at two different locations downstream for the reagent inlet. Spectra were produced by mapping a 60 μm (y axis) by 20 μm (x axis) area, collecting data in 4 μm increments and plotting the average signal along the y axis (inset Figure 5.5c). The colors of the spectra correspond to the location along the y axis in which it was collected. As is demonstrated, the signal is optimal at the interface of the two streams, and increases with increasing mixing time. As with the fluidic model, the colloid diffuses into the analyte stream to a small extent (see the transition from no signal in the two red spectra collected at 0.4 mm to small signal in red and orange spectra collected at 0.1 mm). Also in agreement with the fluidic modeling, the analyte diffusively mixes with the AgNP solution across the y axis. The intensities more than triple across the region of flow dominated by the colloid (yellow, blue, and green spectra).

5.4.3 Detection under chromatographic zonal conditions

Our CFD modeling and experimental studies of the fluidic interface created by the simple diffusion of the solutions shows a significant area in which ample mixing between AgNPs and analyte plugs could occur. Therefore, the implemented microfluidic devices

provide straightforward SERS detection and fingerprinting of sample plugs eluted from the on-chip separation column. One of the main advantages of SERS is the high sensitivity of the technique. This sensitivity is often dependent upon signal acquisition and signal generation times. To study the effect of these kinetic factors within our experimental design we collected SERS spectra of eluted sample plugs while varying the signal acquisition rate and the location of the detection zone.

The data collected for benzenethiol in Table 5.1 shows analytes of SERS data collected while varying the acquisition time from 0.1 second to 0.8 second acquisitions, and monitoring the intensity of the band at 1562 cm^{-1}. As the acquisition time increases, signal intensity at peak center, peak area, and the signal to noise ratio (SNR) increase, as expected. Traditional chromatographic detection schemes require a large number of data points for accurate mapping of Gaussian bands without peak distortion (broadening). In this work, however, the specificity of SERS spectral bands facilitates qualitative identification and quantitative determination via integrated spectral band area over time data, even when acquisition times are so large as to cause issues with less information rich detection schemes.

Increasing the mixing times of the streams will improve signal intensity, however it will also increase the diffusion dominated band dispersion. The data collected for rhodamine 6G in Table 5.1 shows the analysis of SERS data collected at different locations downstream from the reagent inlet. The spectra show the intensity of the peak at 1495 cm^{-1} over time, fit to a Gaussian curve. The dashed line shows the data points collected at a distance of 0.6 mm downstream, showing a high-quality agreement with the fit used to model the peaks. As the distance increases, thus mixing time increases, the signal intensifies and SNR improves. Plate heights transition from 1.4 μm at 0.1 mm downstream, 1.8 μm at 0.35 mm downstream

	Benzenethiol				Rhodamine 6G		
Distance (mm)	0.35	0.35	0.35		0.1	0.35	0.6
$t_{acquisition}$ (sec)	0.1	0.4	0.8		0.1	0.1	0.1
Date points	12	5	3		11	12	11
Peak intensity	18	64	148		19	75	85
Peak Area	33	165	436		31	147	208
SNR	19	33	72		6	12	28

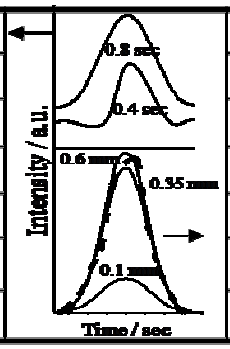

Table 5.1 Analysis of SERS data collected while varying experimental conditions. Inset spectra depict data collected for BT (top) and R6G (bottom).

and 2.3 μm at 0.6 mm downstream from the reagent inlet. This shows significantly more diffusion in the 2 mm long detection zone than in the 10 mm long separation channel.

To determine the ability of our system to identify components of a sample mixture without resolution of peaks we collected chromatographic SERS spectra of a mixture of benzenethiol and rhodamine 6G. Tests were completed using pure methanol as the mobile phase, thus creating non-retentive conditions. Figure 5.6a shows the intensity of representative peaks for both analytes over time. As expected, the peaks were not retained and eluted simultaneously. Additionally, both peaks have the same shoulder at approximately 20 seconds, which we believe is an artifact created by the limitations of our instrumental software, thus should not be present when using a more accurate instrumental system. Our instrument performs accurate acquisition rates down to 0.5 seconds per data point. However as this rate decreases, we have observed that the acquisition times vary from acquisition to acquisition, resulting in signal intensity fluctuations.

The inset chromatogram shows 3 consecutive profiles of rhodamine 6G collected by laser induced fluorescence (LIF) detection using an external 543 nm laser. LIF signals were collected immediately after the pillar array and upstream for the reagent inlet, yielding an average plate height of 1.2 μm. The plate height of rhodamine 6G in Figure 5.6a evaluated 0.5 mm downstream from the reagent inlet is 2 μm, a trend consistent with our previous analysis. Figure 5.6b shows the SERS spectra collected at peak center. The peaks used to model the chromatograms depicted in Figure 5.6a are denoted. Figures 5.6c and 5.6d are independent spectra collected for benzenethiol and rhodamine 5.6G, respectively.

While we recognize the temporal limitations of our design, it is also important to note that our absolute limit of detection is adequate. All data collected for Table 1 and Figure

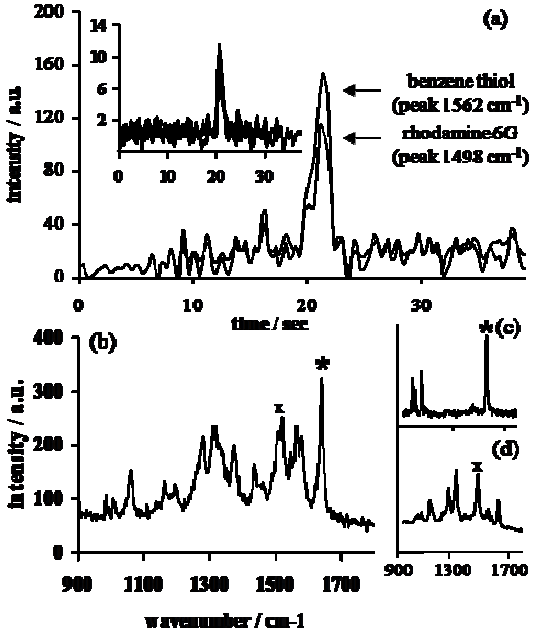

Figure 5.6 (a) Chromatograms of the analyte mixture at representative SERS peaks for 8E-5 M BT and 5E-4 M R6G collected 0.5 mm downstream. Inset shows laser induced fluorescence chromatograms collected 0.1 mm upstream (3 consecutive spectra). (b) SERS spectra at peak center (21.38 sec) with spectra of BT (c) R6G (d) collected for reference in static flow conditions. * Denotes peak at 1562 cm^{-1}, and ^{X} denotes peak at 1498 cm^{-1}.

6 corresponds to picoliter injection volumes, resulting in femtomole analyte amounts. Although this detection scheme is notably less sensitive that alternative LIF detection methods reported for microfluidic devices[50-52], we believe that the fact that SERS provides considerable spectral information justifies further studies toward making real-time microfluidic SERS devices. Additionally, higher laser power and fully optimized colloid and fluidic conditions may result in some improvement in sensitivity.

5.5 Conclusions

In this study, we implemented and evaluated a microfluidic separation chip that integrates a chromatographic separation column based on an ordered pillar array with a post-column passive mixer that enables efficient SERS detection. Our design is the first example of an on-chip format capable of performing pressure driven separations combined with real time SERS detection. The simple detection scheme utilizes diffusive mixing of AgNP solutions with the eluent stream in a laminar flow to induce SERS signals with minimal sample manipulation. Previous researchers have focused on creating complex micromixers for more complete mixing. However, they have not investigated these designs with regard to chromatographic efficiency, which is a critical figure of merit for separation systems. In our current design signal intensity is limited by the mixing kinetics within our 2 mm long detection zone, as signal increases with time, i.e. distance. Conversely, as time and distance of mixing increases, so does the diffusion based band broadening which detrimentally effects separation efficiency. Therefore there is a trade-off between sensitivity and efficiency, as plate heights increased from 1.2 μm upstream to 2.3 μm at 0.6 mm downstream from the reagent inlet. Future studies will focus on the incorporation of more complex mixing

features to determine if active mixing designs can improve sensitivity without significantly decreasing efficiency. On the other hand, the use of SERS instead of the more common LIF detection scheme affords the ability to simultaneously collect data from complex mixtures, without complete resolution of chromatographic bands, as SERS spectral features provide additional means to identify analyzed species.

5.6 Acknowledgments

A portion of this research was conducted at the Center for Nanophase Materials Sciences, which is sponsored at Oak Ridge National Laboratory by the Office of Basic Energy Sciences, U.S. Department of Energy

5.7 References

[1] F.E. Regnier, HRC-Journal of High Resolution Chromatography, 23 (2000) 19.
[2] B. He, F. Regnier, Journal of Pharmaceutical and Biomedical Analysis, 17 (1998) 925.
[3] M.R. Schure, R.S. Maier, D.M. Kroll, H.T. Davis, Journal of Chromatography A, 1031 (2004) 79.
[4] P. Gzil, N. Vervoort, G.V. Baron, G. Desmet, Analytical Chemistry, 75 (2003) 6244.
[5] J. De Smet, P. Gzil, N. Vervoort, H. Verelst, G.V. Baron, G. Desmet, Analytical Chemistry, 76 (2004) 3716.
[6] W. De Malsche, L. Zhang, J.O. De Beeck, J. Vangelooven, B. Majeed, G. Desmet, Journal of Separation Science, 33 (2010) 3613.
[7] H. Eghbali, V. Verdoold, L. Vankeerberghen, H. Gardeniers, G. Desmet, Analytical Chemistry, 81 (2009) 705.
[8] N.V. Lavrik, L.C. Taylor, M.J. Sepaniak, Lab on a Chip, 10 (2010) 1086.
[9] L.C. Taylor, N.V. Lavrik, M.J. Sepaniak, Analytical Chemistry, 82 (2010) 9549.
[10] H. Eghbali, S. Matthijs, V. Verdoold, H. Gardeniers, P. Cornelis, G. Desmet, Journal of Chromatography A, 1216 (2009) 8603.
[11] H. Eghbali, W. De Malsche, D. Clicq, H. Gardeniers, G. Desmet, Lc Gc Europe, 20 (2007) 208.

[12] M. Kato, M. Inaba, T. Tsukahara, K. Mawatari, A. Hibara, T. Kitamori, Analytical Chemistry, 82 (2010) 543.
[13] F. Detobel, H. Eghbali, S. De Bruyne, H. Terryn, H. Gardeniers, G. Desmet, Journal of Chromatography A, 1216 (2009) 7360.
[14] F. Detobel, S. De Bruyne, J. Vangelooven, W. De Malsche, T. Aerts, H. Terryn, H. Gardeniers, S. Eeltink, G. Desmet, Analytical Chemistry, 82 (2010) 7208.
[15] W. De Malsche, H. Gardeniers, G. Desmet, Analytical Chemistry, 80 (2008) 5391.
[16] W. De Malsche, D. Clicq, V. Verdoold, P. Gzil, G. Desmet, H. Gardeniers, Lab on a Chip, 7 (2007) 1705.
[17] O. Gustafsson, K.B. Mogensen, P.D. Ohlsson, Y. Liu, S.C. Jacobson, J.P. Kutter, Journal of Micromechanics and Microengineering, 18 (2008).
[18] K. Kneipp, H. Kneipp, I. I, R.R. Dasari, M.S. Feld, Chemical Reviews, 99 (1999) 2957.
[19] S.M. Nie, S.R. Emery, Science, 275 (1997) 1102.
[20] J. Abian, Journal of Mass Spectrometry, 34 (1999) 157.
[21] L. Callipo, P. Foglia, R. Gubbiotti, R. Samperi, A. Lagana, Analytical and Bioanalytical Chemistry, 394 (2009) 811.
[22] J. Hardouin, R. Joubert-Caron, M. Caron, Journal of Separation Science, 30 (2007) 1482.
[23] P. Thibault, M.H. Fortier, E. Bonneil, P. Goodley, Analytical Chemistry, 77 (2005) 1631.
[24] T.D. Lee, J. Xie, Y.N. Miao, J. Shih, Y.C. Tai, Analytical Chemistry, 77 (2005) 6947.
[25] J.M. Ramsey, I.M. Lazar, R.S. Ramsey, S. Sundberg, Analytical Chemistry, 71 (1999) 3627.
[26] A.G. Chambers, J.S. Mellors, W.H. Henley, J.M. Ramsey, Analytical Chemistry, 83 (2011) 842.
[27] J.S. Mellors, K. Jorabchi, L.M. Smith, J.M. Ramsey, Analytical Chemistry, 82 (2010) 967.
[28] R.M. Connatser, L.A. Riddle, M.J. Sepaniak, Journal of Separation Science, 27 (2004) 1545.
[29] I. White, J.K. Liu, D.L. DeVoe, Analytical Chemistry, 83 (2011) 2119.
[30] M. Kall, L.M. Tong, M. Righini, M.U. Gonzalez, R. Quidant, Lab on a Chip, 9 (2009) 193.
[31] P.D.I. Fletcher, S.J. Haswell, X.L. Zhang, Electrophoresis, 24 (2003) 3239.
[32] L.X. Quang, C. Lim, G.H. Seong, J. Choo, K.J. Do, S.K. Yoo, Lab on a Chip, 8 (2008) 2214.
[33] D. Erickson, Y.S. Huh, A.J. Chung, B. Cordovez, Lab on a Chip, 9 (2009) 433.
[34] J. Choo, S. Lee, J. Choi, L. Chen, B. Park, J.B. Kyong, G.H. Seong, Y. Lee, K.H. Shin, E.K. Lee, S.W. Joo, K.H. Lee, Analytica Chimica Acta, 590 (2007) 139.
[35] J. Parnell, R. Wilson, S.A. Bowden, J.M. Cooper, Analytical Chemistry, 82 (2010) 2119.
[36] M.J. Sepaniak, N.A. Abu-Hatab, J.F. John, J.M. Oran, Applied Spectroscopy, 61 (2007) 1116.
[37] J. Choo, T. Park, S. Lee, G.H. Seong, E.K. Lee, Y.S. Kim, W.H. Ji, S.Y. Hwang, D.G. Gweon, S. Lee, Lab on a Chip, 5 (2005) 437.

[38] J. Choo, K. Yea, S. Lee, J.B. Kyong, E.K. Lee, S.W. Joo, S. Lee, Analyst, 130 (2005) 1009.
[39] A.J. deMello, S.A. Leung, R.F. Winkle, R.C.R. Wootton, Analyst, 130 (2005) 46.
[40] D. Hanstorp, K. Ramser, J. Enger, M. Goksor, K. Logg, M. Kall, Lab on a Chip, 5 (2005) 431.
[41] J. Popp, K.K. Strelau, R. Kretschmer, R. Moller, W. Fritzsche, Analytical and Bioanalytical Chemistry, 396 (2010) 1381.
[42] W.F. Nirode, G.L. Devault, M.J. Sepaniak, Analytical Chemistry, 72 (2000) 1866.
[43] N. Leopold, B. Lendl, Analytical and Bioanalytical Chemistry, 396 (2010) 2341.
[44] R.M. Connatser, M. Cochran, R.J. Harrison, M.J. Sepaniak, Electrophoresis, 29 (2008) 1441.
[45] P.C. Lee, D. Meisel, Journal of Physical Chemistry, 86 (1982) 3391.
[46] T.W. Koo, S. Chan, L. Sun, X. Su, J.W. Zhang, A.A. Berlin, Applied Spectroscopy, 58 (2004) 1401.
[47] J. Popp, K.R. Strehle, D. Cialla, P. Rosch, T. Henkel, M. Kohler, Analytical Chemistry, 79 (2007) 1542.
[48] J. Choo, G. Wang, C. Lim, L. Chen, H. Chon, J. Hong, A.J. deMello, Analytical and Bioanalytical Chemistry, 394 (2009) 1827.
[49] T.I. Abdullin, O.V. Bondar, Y.G. Shtyrlin, M. Kahraman, M. Culha, Langmuir, 26 (2010) 5153.
[50] G. Ocvirk, E. Verpoorte, A. Manz, M. Grasserbauer, H.M. Widmer, Analytical Methods and Instrumentation, 2 (1995) 74.
[51] J.P. Fu, R.B. Schoch, A.L. Stevens, S.R. Tannenbaum, J.Y. Han, Nature Nanotechnology, 2 (2007) 121.
[52] J.C. Fister, S.C. Jacobson, L.M. Davis, J.M. Ramsey, Analytical Chemistry, 70 (1998) 431.

Chapter 6

Concluding Remarks

The use of microfluidic chip based separation systems for routine chemical analysis is still in its early stages. Multiple technological approaches toward creating these systems have shown promise as possible methods for device advancement. Theoretical studies suggest that very dense submicron pillar arrays could mimic separation beds and become suitable for high performance separation and analysis. The application of microfabrication processing techniques to create highly ordered and tunable features of nanoscale dimensions allow for the characteristic sizes of separation beds to decrease, establishing a footprint comparable to that of integrated circuits. Although theoretical modeling has pointed to the advantages of producing pillar array separation beds below 1 μm, current research indicates that the progression to submicron features in these systems is hindered by fundamental and practical limitations.

The complexity of generating reliable sealed 3-D structures suitable for miniaturized liquid phase separations has been highlighted in many studies. While several necessary advancements have been accomplished toward improving system fabrication, integration, and operation in pillar array and similar designs, for the most part miniaturized separation systems have yet to become a competitive alternative to traditional CE and HPLC system. This is understandable as fabrication technology has only recently been applied in this field. That being said, prototype analytical separation devices for laboratory research are necessary before the adaptation to a commercially viable product. With this consideration, advances must be made to make these systems more user friendly so that they may be subjected to repetitive testing.

In chapter 3, we presented an innovative streamlined fabrication process which yields robust high-aspect-ratio pillar array fluidic channels. The high integrity

implemented structures were stabilized with a capping layer of silicon oxide. This robust scaffold made possible the repeated use of the microfluidic chip, able to withstand the treatment of multiple processing steps and experimental iterations. Devices were sealed with a non-permanent bonding technique so that they could be subjected to extreme cleaning procedures between experimental runs. These systems performed in a manner which yielded plate heights below 1 μm as well as exhibited improved permeability, thereby decreasing pressure requirements for the system.

In addition to improving the mechanical stability of the system, the silicon oxide deposition in combination with the characteristic Bosch ridges created during etching increased the available surface area for stationary phase-mobile phase interaction. While this unique processing attribute has not been fully investigated, preliminary BET analysis suggests this may increase pillar surface area by 10x that of a normally smooth walled pillar. Future studies will focus on fully characterizing the pillar surfaces created by our processing sequence and investigate the capacity of the system.

While the science of modifying or coating conventional columns to impart stationary phase-mobile phase interaction has undergone vast improvements, minimal research has focused on surmounting the various challenges of functionalizing small volume micro or nanoscale microfluidic channels performing pressure driven partition based separations. This includes finding simple, high throughput approaches for functionalization and eliminating column blockage. Our initial studies indicate that the bonding technique employed created silicone contamination of the pillar surface. Although this is outcome is unsatisfactory, it importantly suggested that the high silanol content silicon oxide pillar sidewalls readily chemically bound to volatile species under

ambient temperatures and pressures. Using this revelation, we established a simple protocol for functionalizing pillar surfaces by either using vapor phase modification or by using dynamic modification to create a pseudo stationary phase. Both methods involve straightforward modification without forming occlusions. Further studies are being conducted to optimize these techniques.

Finally, recognizing the need for sensitive and information rich detection schemes compatible with chip based devices, we introduced design modifications to be able to introduce a reagent for detection purposes. While our preliminary results indicate that kinetic and temporal limitations may diminish the performance of our current design, future studies will focus on creating a more complex mixing geometry for more efficient and sensitive detection. Additionally, this same detection scheme will be studied to determine the applicability of DNA separations techniques using LIF induced detection methods.

It should be emphasized that this research provides proof of principle results showing the function of highly uniform pillar array microfluidic channels for improving the performance of chromatography. Fundamentally, chromatographic systems should be able to operate at velocities above those accessible by the current chip design. Therefore, for complete analytical utility alternative bonding techniques must be employed to ensure that pressure tolerances are not a factor in device operation. Chapter 1 describes some applicable bonding techniques found in literature, however implementing these bonding methods may not be trivial. We believe the increase in mechanical stability imposed by our unique processing sequence should improve the ability to successfully assemble high pressure resistant microfluidic separation devices; however, the topographical

characteristics, i.e. the smoothness, of the silicon oxide capping layer may be an impeding factor for some bonding techniques.

Furthermore, as was mentioned in Chapter 1, there is debate as to whether the theoretical developments proposed by the Desmet group suitably describe the flow and mass transport within pillar array systems. A recent study by Tallarek et. al.[1] suggests that with more defined and complete boundary conditions at channel walls, the resultant macroscopic confinement significantly alters the fluid dispersion within pillar systems. In contrast to typical random sphere packings where diffusive mixing is characterized by eddy diffusion, uniform pillar arrays do not function as a mechanical mixer and instead exhibit pseudo-diffusive behavior. Consequently, longitudinal dispersion grows quadratically with the velocity, and the plate height curves approach a linear velocity dependence as transverse dispersion becomes velocity-independent. Specifically, this study points to the limitations of Gidding's coupling theory to properly describe the nature of the transverse dispersion evident in plate height curves of pillar arrays. The Tallarek study was modeled for comparison with conventional random sphere packings using pillar diameters and channel width to pillar height ratios far larger than those experimentally used in our research. While the motivation behind our research was in essence to decrease the length of the diffusion paths in order to accelerate mass transfer, therefore improving efficiency, these new findings have significant impact on our future pillar and experimental design.

While our research has initially focused on the possibility of using pillar array microfluidic channels to perform traditional reverse phase chromatography, these designs are now being investigated as unconventional separation platforms. By incorporating the

use of additional established fabrication tools, specifically atomic layer deposition and electron beam lithography, we are able to convert from micro to nano dimension pillar diameter and pitch. This transition introduces nanoscale phenomena which can impart different modes of separation as the electric double layer becomes appreciable relative to the interpillar gap. For instance, the electrical potential and ion structure of an electrolyte generates a field in which oppositely charged counterions concentrate near the surface and co-ions migrate into the interior, thereby shielding bulk solutions from the surface charge. For nanoscale systems, this effect can modify the distribution of charged analytes within the roughly parabolic flow profile[2-4]. In addition to electrostatic-derived hydrodynamic separation mechanisms, pressure driven movement of the diffuse layer within the EDL can cause a streaming current and an accumulation of downstream charge[5-8]. The charge accumulation generates an opposing conduction current which can alter flow profiles and offers the possibility of producing streaming potential generated electrokinetic separations by ionic migration in pressure driven systems; i.e., even without applied potentials.

In addition to investigating these more complex separation processes, we are also exploring pillar array systems for planar chromatography as a potential new separation system which has fewer sealing and pressure related complications. Using advanced lithographic fabrication techniques we have created pillar array "forests" for 2-D spatial chromatography. Initial testing of these systems reveal that the increased uniformity and permeability of the pillar bed should exhibit significant merit and operational simplicity in a capillary action-driven, open mode of operation, potentially achieving performance significantly beyond traditional porous bed TLC media. Optimized pillar array systems

may eventually permit realization of high performance 2-D separations and imaging detection of biological and environmental samples, wherein complexity dictates higher dimensionality and peak capacity.

References

[1] A. Daneyko, S. Khirevich, A. Holtzel, A. Seidel-Morgenstern, U. Tallarek, J. Chromatogr. A, 1218 (2011) 8231.
[2] M. Kato, M. Inaba, T. Tsukahara, K. Mawatari, A. Hibara, T. Kitamori, Analytical Chemistry, 82 (2010) 543.
[3] X.Y. Wang, J.Z. Kang, S.L. Wang, J.J. Lu, S.R. Liu, J Chromatogr A, 1200 (2008) 108.
[4] X.Y. Wang, S.L. Wang, V. Veerappan, C.K. Byun, H. Nguyen, B. Gendhar, R.D. Allen, S.R. Liu, Analytical Chemistry, 80 (2008) 5583.
[5] X.C. Xuan, D. Sinton, Microfluid Nanofluid, 3 (2007) 723.
[6] X.C. Xuan, J Chromatogr A, 1187 (2008) 289.
[7] S. Das, S. Chakraborty, Langmuir, 25 (2009) 9863.
[8] Y.S. Choi, S.J. Kim, J Colloid Interf Sci, 333 (2009) 672.

Vita

Lisa C. Taylor was born in Bremerton, Washington, on August 8, 1980. She graduated from Wilbur High School in June of 1998, and attended college at the University of Washington and the University of North Texas, ultimately receiving her Bachelor's of Science degree in chemistry with a certificate in Biomedical Criminalistics from the latter in December of 2006. She is currently attending graduate school at the University of Tennessee, Knoxville, studying analytical chemistry under the direction of Dr. Michael J. Sepaniak. Her research centers on the miniaturization of separation methods by designing microrchitecture and fabrication processes that improve separation efficiency, with specific focus on microfluidic platforms for pressure-driven applications. In May 2012, she will graduate with her Doctor of Philosophy degree.